POST-TREATMENT ASSESSMENT OF HYDRAULIC FRACTURING WITH INTEGRATED MODELING OF NATURAL FRACTURE DISTRIBUTION

A Thesis

Submitted to the Graduate Faculty of the
Louisiana State University and
Agricultural and Mechanical College
in partial fulfillment of the
requirements for the degree of
Master of Science

in

The Craft & Hawkins Department of Petroleum Engineering

by
Ping Puyang
B.S., Louisiana State University, 2012
May 2015

Acknowledgements

I would like to thank my graduate advisor, Dr. Arash Dahi-Taleghani, for his enduring support and guidance on my research in the past three years. This work could not be achieved without his mentorship, and I owe him a debt of gratitude for every footstep I took thus far in my research and graduate study. I also wish to thank two other committee members, Dr. Juan Lorenzo and Dr. Bhaba R. Sarker, for serving as my committee members and providing constructive and valuable recommendations to the perfection of this work.

I also thank the LSU Department of Petroleum Engineering for offering me the opportunity to advance my knowledge and skills through their graduate program. In addition, credit also goes to all members at Geomechanics Research Group at Louisiana State University for their help, support and friendship during the past three years.

In the end, I would like to express my gratitude to my parents, who firmly supported my plan of pursuing higher education in United States and encouraged me at the time of hardship, depression and exhaustion during my graduate program.

Table of Contents

Acknowledgements ii

Abstract v

1. Introduction 1
   1.1 Introduction to Hydraulic Fracturing 1
   1.2 Monitoring and Evaluating Hydraulic Fracturing Treatments 5
   1.3 Research Motivation 13
   1.4 Research Objectives and Outline 16

2. Natural Fractures and Their Roles on Hydraulic Fracturing 18
   2.1 Natural Fractures 19
   2.2 Modeling Natural Fractures in Fractured Reservoirs 29
   2.3 Hydraulic Fracturing in Naturally Fractured Reservoirs 32
   2.4 Conclusion 37

3. Barnett Shale 38
   3.1 Geology and Development of the Barnett Shale 38
   3.2 Natural Fracture Distribution in Barnett Shale 45
   3.3 Well Configurations 47
   3.4 Fracturing Treatment History 49
   3.5 Net Pressure Matching 50
   3.6 Conclusion 52

4. Numerical Modeling and Determination of Fracture Network 53
   4.1 Microseismic Mapping in Hydraulic Fracturing 53
   4.2 Model Description and Mathematical Formulation 55
   4.3 Model Verification 64
   4.4 Field Application – Generating Natural Fracture Realizations 67
   4.5 Adaptive Spacing, Partial Network Refinement of Natural Fracture Gridding System 75
   4.6 Conclusion 79

5. Forward Modeling of Hydraulic Fracturing with Natural Fracture Distribution 81
   5.1 Preliminary Analysis 81
   5.2 StimPlan Simulation of Orthogonal Natural Fracture Realization 85
   5.3 StimPlan Simulation of Non-Orthogonal Natural Fracture Realization 90
   5.4 Estimation of Net Pressure Deviations and Results Discussion 92
   5.5 Conclusion 94

6. Numerical Simulation of Hydrocarbon Production with CMG 95
   6.1 Model Setup 95
   6.2 Simulation Results and Discussion 100
   6.3 Conclusion 104

7. Conclusions and Recommendation for Future Work.....105

References.....107

Vita.....113

Abstract

Hydraulic fracturing is the principal reservoir stimulation technique to improve production capacities of low permeability formations. On the other hand, through core and outcrop studies, advanced logging tools, microseismic fracture mapping and well testing analysis, it has been further revealed that many of the shale gas formations are naturally fractured. The presence of natural fractures and their interactions with hydraulic fractures must be taken into consideration while designing fracturing treatment. Although most natural fractures are cemented by precipitations during diagenesis, they may be reactivated during hydraulic fracturing and serve as weak paths for fluid flow and fracture growth.

However, current technologies are incapable of accurately estimating the distribution of natural fractures. Core and outcrop studies involve significant uncertainties in sampling and modeling of microfractures, and prediction of macrofracture properties based on biased observation might lead to erroneous estimation. Existing numerical modeling approach for naturally fractured reservoirs requires accurate details about natural fractures, which is often difficult or expensive to gather during hydraulic fracturing. Moreover, these numerical modeling usually does not incorporate post-treatment measured data, which could not reflect the actual reservoir characteristics.

This research proposes a multi-discipline data integration workflow to estimate the characteristics of natural fracture network based on formation evaluations, microseismic data, treatment history and production history. Least-square modeling is first conducted to find natural fracture gridding systems that result in smaller overall squared error between fracture networks and double couple microseismic events. Forward modeling that incorporates Discrete Fracture Network (DFN) is subsequently used to simulate hydraulic fracturing treatments, and the net

pressure responses from simulations and field measurements are quantitatively compared to determine the degree of match of natural fracture networks. Reservoir simulation tools are also used thereafter to simulate the production of hydrocarbon from such naturally fractured reservoirs, and the production history from simulations and the actual well will be compared to further evaluate the fitness of natural fracture realizations. This workflow is able to integrate scientific data from multiple aspects of the reservoir development process, and results will provide geologist and reservoir engineers an innovative assessment tool for evaluating and modeling naturally fractured reservoirs.

Chapter 1: Introduction

Hydraulic fracturing is an evolving technology that has been contributing to the oil and gas production in the United States since mid-1990s, several decades after its initial appearance in the middle of the last century (Hubbert and Willis, 1957). Massive hydraulic fracturing jobs have been conducted in the past two decades and significantly relieved the increasing energy needs from both developed and emerging economies (Montgomery and Smith, 2010). Meanwhile, concerns were raised by industry professionals and government regulatory agencies regarding the effectiveness of fracturing and possible hazards due to hydraulic fracturing (David, 2013). The fact that hydrocarbon-bearing reservoirs are seldom homogeneous in terms of their geomechanical properties further complicates the hydraulic fracturing design and post-job assessment. Specifically, the pre-existing natural fractures in some of these formations would interact with hydraulic fractures and inevitably impact the propagation, geometry and effectiveness of induced fractures (Dahi Taleghani and Olson, 2013). This chapter provides an overview of the hydraulic fracturing technology, including its history, principles, and common techniques for evaluating fracturing treatment such as pressure diagnostic, radioactive tracer techniques, and microseismic fracture mapping. Thereafter, the motivation, objectives and outlines of this research work will be covered. The subsequent introductory chapters of this thesis will also include an overview of the naturally fractured reservoirs, current approaches of modeling fractured reservoirs, current industry practices for assessing fracturing treatments, and identify the deficiencies with these post-treatment assessment techniques.

1.1 Introduction to Hydraulic Fracturing

Hydraulic fracturing is a well stimulation technique in which formation rock is cracked by excessive hydraulic pressure, and initiated fractures subsequently propagate and form high

permeable flow pathways (Smith, 2006). Continuous pumping of fracturing fluid enlarges the fracture volume and keeps the fracture propagating in the direction with smallest resistance or lead to maximum energy release. The idea of hydraulic fracturing initially came from acid stimulations by Dow Chemical Company in 1930s, during which it was discovered that by injecting fluid at a sufficiently large pressure, it is possible to improve the effectiveness of acid stimulation by cracking the formation surrounding the wellbore (Grebe and Stoesser, 1935). However, it was not until 1947 when the first commercial hydraulic fracturing treatment was performed in a gas well in Hugoton field, Kansas (Gidley et al, 1990). Since then, approximately 2.5 million fracturing treatments have been performed in the oil and gas industry worldwide as of 2010, and it has been estimated that currently 60% of the wells drilled are being fractured (Montgomery and Smith, 2010). Hydraulic fracturing not only improves the production rate of hydrocarbons, but also increases the ultimate recovery of producible oil and gas in extremely low permeability reservoirs (Ma et al, 2013). Fracturing technology have added 9 billion barrels of oil and more than 700 trillion cubic feet of natural gas to the hydrocarbon reserves in the United States, which are otherwise not accessible nor economical through conventional production technology (Friedrich and Milliken, 2013). Towards the end of 2012, the total proved natural gas reserve around the world reached 6614.1 trillion cubic feet (Tcf), whereas annual natural gas consumption has been constantly rising and reached approximately 116.5 Tcf in the same year (US Energy Information Administration, 2014). While the current proved reserve of natural gas worldwide could meet the world's energy needs for the next 50 years, the increasing demands for natural gas globally call for better enhanced oil recovery technologies to further exploit the hydrocarbon reserves and meet skyrocketing fossil fuel consumptions (BP Annual Energy Report, 2013). The United States Energy Information Administration (EIA) estimates that by

2020, the demand for natural gas in the United States is expected to reach 33 trillion cubic feet annually, and the total natural gas consumption worldwide will break 160 Tcf per year (US Energy Information Administration, 2014). A significant portion of this demand will have to be met by unconventional shale gas reservoirs – formations with ultra-low permeability that typically require hydraulic fracturing to establish economically viable production (Gomaa et al, 2014). While conventional production and stimulation techniques for low permeability reservoirs only reap a small portion of the reserve, hydraulic fracturing leads to both faster and more abounding hydrocarbon recovery.

Figure 1.1. Schematic of Hydraulic Fracturing

The first step in hydraulic fracturing is perforating the casing. A perforation gun is lowered to a targeted depth into the cased well and adjusted itself to a certain direction and inclination angle. A small explosive charge, similar to bullets firing from weapons, is then triggered with an electrical current. This creates perforated holes on both casing and formation, which simultaneously serves as the initiation point of hydraulic fracture and the outlet of hydrocarbons from the formation to the well. The beginning of a fracture treatment always starts

with pumping gels or fracture fluid only, also known as "pad volume", which is different from fracturing fluid carrying proppants. The logic behind this step is that fluid loss is extremely high near the fracture tip; therefore, pad is needed to break the formation, initiate the fracture, and generate sufficient fracture penetration and width that will allow subsequent proppant – laden fluid to enter the fracture and avoid having tip screenout (Economides and Nolte, 2000). In addition, similar fracture treatment without (or with small quantities of) proppant is also possible through acid fracturing, where fractures are generated by acid etching instead of excessive hydraulic pressure (Williams and Nierode, 1972).

Continued pumping of fracturing fluid maintains a high pressure in the fracture, and keeps the hydraulic fracture propagating in the direction of least resistance, which is usually perpendicular to the minimum horizontal stress of the formation. When the leakoff rate of fracture fluid no longer causes excessive dehydration, proppant is gradually introduced into the fracturing fluid with increasing concentrations and moves towards the fracture tip (Economides and Nolte, 2000); however, proppant concentration may also follow a complicated schedule, such as Schlumberger's proppant HiWAY technology, which could both lower proppant usage and increase production. For the duration of the treatment, fracture fluid is constantly escaping through the permeable fracture walls and network of natural fractures. As fractures propagate in the formation, larger leakoff area for fracturing fluid leads to an increasing fluid-loss rate. Therefore, the pump schedule must be engineered precisely such that the amount of fluid and pressure inside the fracture is constantly sufficient to maintain its propagation while refraining from complications such as uncontrolled height growth, screenout and irregular fracture pattern. The final stage of a treatment is also considered a "flush stage" except for treatments through slickwater, where gel breakers are pumped to "flush" the fracture and remove the gel remaining.

It also cleans the wellbore and the perforation, which would ideally leave a "clean" fracture with only proppants left (Economides and Nolte, 2000). Proppants remain inside the fracture to keep the fracture open; their strength must exceed the closure pressure of the formation in order to support the opening of hydraulic fractures (Economides and Nolte, 2000).

Vertical wells only have a limited area of contact with the reservoir – i.e. the height of the hydrocarbon bearing formation. As larger contact area is desired to faster produce a larger quantity of hydrocarbon reserves, horizontal wells are usually drilled in unconventional gas reservoirs to maximize the contact area between the well and the reserve (Al Haddad and Crafton, 1991). In addition, multiple stages of hydraulic fracturing can be done in horizontal wells, where treatments can be separately performed on multiple intervals in the horizontal section of the wellbore. To avoid fracturing undesired intervals and jeopardize the fracturing efficiency, "Plug and Perf" strategy is usually utilized in multistage fracturing to perforate and fracture each interval separately while other intervals are plugged to prevent fracturing fluid access (Economides and Nolte, 2000).

1.2 Monitoring and Evaluating Hydraulic Fracturing Treatments

The progress of hydraulic fracturing treatments can be monitored, recorded, and analyzed either real time or afterwards to evaluate the effectiveness of fracturing and the extent of induced fracture network. Techniques for monitoring and evaluating hydraulic fracturing range from simplest pressure and rate measurements or adding radioactive tracers during the treatment to sophisticated microseismic mapping approach. In addition, PLT log and distributed temperature logs are also utilized for determining the characteristics of the induced fractures such as their permeabilities, lengths and proppant placements (Hoffman et al, 2009; Wheaton et al, 2014).

Radioactive tracer technique provides direct and simple dynamic evaluation of stimulation and other tertiary recovery techniques (Kelldorf, 1970). This technique has been used in oilfields since 1970s to assess and monitor the progress of waterflooding, fluid flow, and fracture stimulation (William and McCarthy, 1987). In waterflooding and other injection process, radioactive tracer surveys are frequently conducted to evaluate the injection profile against the planned profile. In hydrocarbon production, radioactive tracer surveys are utilized to identify

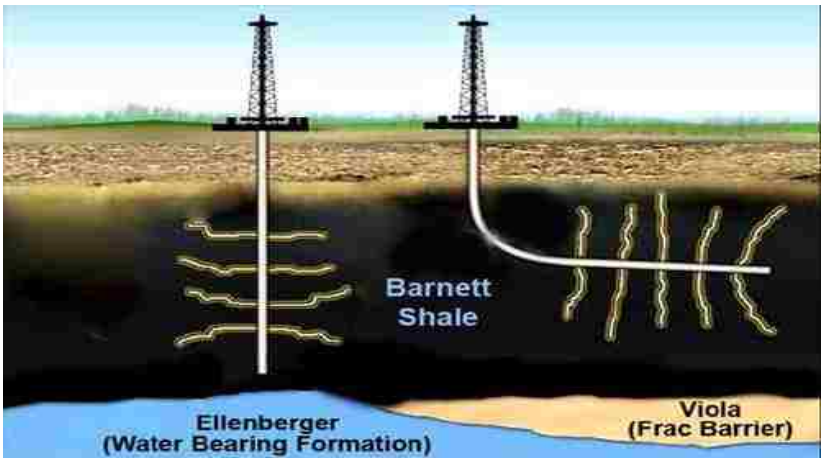

Figure 1.2. Multistage Fracturing in Vertical and Horizontal Wells in Barnett Shale. Horizontal wells maximize the contact area between the well and the reservoir.

issues such as water influx, channeling, and permeability damage (Flagg et al, 1955). Common practice of this technique in hydraulic fracturing is to tag the proppant with radioactive materials such as Iridium – 192, and survey their distributions after the treatment using conventional gamma ray logging tool (William and McCarthy, 1987). Evolving radioactive technology had allowed for multiple radioactive isotopes in this technique to eliminate the uncertainties of fluid and proppant placement during the logging. Williams and McCarthy (1987) had reported using up to four different radioactive isotopes in a single wellbore at Santa Fe Energy, including Antimony- 124, Scandium – 46, Iridium- 192, Silver -110 and Gold -198 in conventional

sandstone fracturing and acid fracturing. Through cased hole logging tool, they were able to evaluate the treatments with a single logging pass, and infer fracture information such as fracture height and proppant placement in the fracture. However, in hydraulic fracturing, this technique is only useful near the wellbore, and could only provide information regarding fracture heights. Tracers will quickly be removed once production starts, thus become less useful.

Measurement of pressure and pumping rate information during the treatment is another powerful tool to qualitatively and quantitatively estimate the formation properties and evaluate fracturing treatment such as fracture geometry and fracture height growth. Nolte and Smith (1979) proposed a pressure diagnostic technique for interpreting pressure responses during the fracture treatment, and identifying periods of fracture propagation with different modes for height growth. However, the limitation of Nolte-Smith analysis lays in that it couldn't deal with naturally fractured reservoirs because in such reservoirs, pressure response during the treatment can be significantly impacted by reactivating natural fracture networks. This methodology assumed constant injection rate and uniform fluid properties during the treatment, no boundary slippage in horizontal planes or horizontally propagating fractures is allowed (Nolte and Smith, 1979). To conduct pressure diagnostics, the net pressure at the bottomhole (the difference between the bottomhole pressure and the fracture closure pressure during the treatment) is plotted against the time with a log-log scale. Fracture growth behaviors can then be identified based on the slope of the curve (Figure 1.3). Nolte and Smith (1979) classified the fracture growth into four Modes. Under Mode I, the bottomhole net pressure is increasing with a slope between 1/8 and 1/4. This small positive slope indicates confined height growth and unrestricted extension of the fracture, where the neighboring layers provide good confinement against fracture height growth. Mode II behavior exhibits a nearly constant net pressure on the log - log

plot. This constant pressure regime is potentially the most important portion of the treatment because it usually preceded a drastic pressure increase (Mode III) or decrease (Mode IV). During this pressure regime, the rate of fracture extension is less than that of Mode I. On the other hand, larger fluid-loss and greater height growth lead to the constant pressure behavior in this Mode. In Mode III, net pressure versus time has a unit slope, which is greater than that of Mode I. Other conditions held constant, the steeper slope in Mode III signaled a significant changing in pressure. Nolte and Smith (1981) concluded that this rate of increase in net pressure is due to the limited fracture extension. With limited fracture growth and extension, relatively less fracturing fluid will be lost to the formation or near the fracture tip. Therefore, larger quantities of fracturing fluid inside the fracture lead to a higher increase in net pressure or alternatively fracture width.

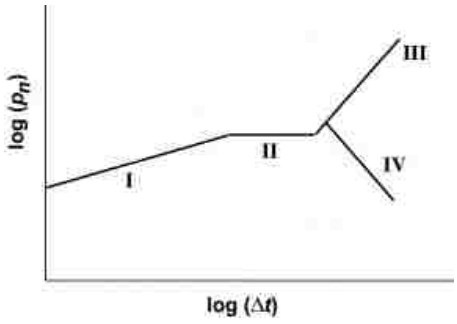

Figure 1.3. Four modes of fracture growth behavior in Nolte –Smith pressure diagnostic technique (Economides and Smith, 2000)

Mode IV has a negative slope towards the end of the treatment. This drastic decrease in net pressure is due to the rapid and unstable height growth of the fracture. According to the material balance equation during the fracturing treatment, a significant decrease in net pressure must be accompanied by higher fluid loss, larger fracture volume increase, or abrupt change in formation geomechanical properties. Nolte and Smith (1979) concluded that while all other scenarios leading to drastic pressure decrease seem unrealistic, a significant increase in fracture

height is the most probable cause for Mode IV pressure response. This significant height growth is often related to fracture growing into adjacent softer formations (Economides and Smith, 2000).

In addition to Nolte–Smith pressure diagnostic technique, pressure decline analysis and injection tests also assists engineers evaluating fracturing treatments and inferring formation properties (Economides and Smith, 2000). Typical tests include step rate test and shut-in decline test. Actual fracture treatment is usually preceded with a pre-frac test, or caliburation test, where a small volume of fracturing fluid is pumped into the formation to create a small fracture. After the pump is shut in, bottomhole pressure will decline to stabilize around the fracture closure pressure. According to the patterns of the pressure decline, parameters such as the fracture closure pressure, fluid efficiency, and formation geomechanical properties including Young's Modulus, fluid loss rate, and Poisson's ratio can be inferred from such analysis. (Economides and Smith, 1987). For example, a change in slope on the bottomhole pressure versus square of time plot indicates the fracture closure pressure of the formation. Shut in time and pumping time can be used to find the dimensionless closure time and further the efficiency of the mini frac test (Tinker et al, 1997). With assumed fracture geometry, fluid loss coefficient of the formation and the fracture length can be solved simultaneously with iterative approach (Economides and Smith, 2000). Closure pressure of the formation can also be found using step-rate injection test. In step rate test, individual injections are conducted in the same time interval with the same injection rate. Pressure responses from the step rate injection test could identify the closure pressure of the formation and the fracture extension pressure (Economides and Smith, 2000). Overall, simple measurements of pressure and injection rate during the stimulation treatment lead to valuable analysis regarding the fracturing job and the formation. In addition, hydraulic fracturing

in naturally fractured reservoirs can be simulated with numerical fracturing simulator such as StimPlan, GOHFER and Fracpro. Accurate modeling of the reservoir, formation and treatment allows for detailed interpretation and evaluation of the fracturing job, and net pressure responses from the simulation and treatment can serve as a benchmark for determining the accuracy of the modeling.

The progress of the fracture treatment may also be monitored real time with microseismic mapping technique. This technique is preferred over traditional fracturing assessment technologies such as tiltmeter analysis and borehole imaging logs because it's capable of observing the fracture extension and height growth in a timely manner, and problematic treatment strategy can be identified and corrected in its infancy. However, there are considerable uncertainties for the location of the microseismic events determined by this method, and data processing could also be lengthy. Microseismic mapping technique is based on the principle that the propagation of hydraulic fracture will crack the formation rock and generate mini – earthquake with magnitude below 3.0, also termed as microseismic events, which can be detected by sensitive seismic receivers (Vermylen and Zoback, 2011). Results from microseismic mapping could not only reveal information regarding the fracturing treatment such as induced fracture height, length, and locations, but also affect the location, orientation, and spacing of the future wells (Hulsey et al, 2011). Compared with other traditional fracturing monitoring or evaluation tools, microseismic mapping allows for more direct visualization of the induced fracture network, and could also assist operators in avoiding legal issues related to illegal fracture trespassing in some jurisdictions in United States (Hall and Dahi Taleghani, 2014).

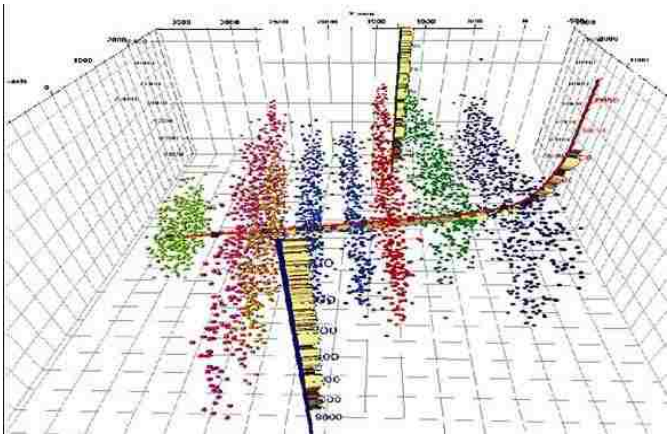

Figure 1.4. Microseismic fracture mapping reveal the development of the hydraulic fractures along their paths of propagation.

Arrays of seismic receivers are placed either on the surface or downhole in neighboring offset wells to monitor and locate the microseismic events during the treatment. Typical receivers used in microseismic fracture mapping include geophones and accelerometers, both of which are simple harmonic oscillators consist of a suspended proof mass connected with a damped spring. Accelerometers are sensitive for low frequency waves below 5 Hz while geophones are sensitive to seismic waves between 5 Hz to 200 Hz (Hon et al., 2008). Due to the fact that microseismic events generated during hydraulic fracturing are usually above 10Hz in frequency, geophones are considered more sensitive and appropriate in microseismic fracture mapping. Despite the valuable information gathered from microseismic fracture mapping, the limitation of this technique lies in its inaccuracy. Detected microseismic events can contain "noise" information, which are events irrelevant to fracture propagation. On the other hand, the determination of microseismic event locations involves considerable amount of uncertainty. Thornton and Eisner (2011) has reported that at a depth of 7000 ft, average measurement errors for 85 microseismic events in X, Y, and Z direction were 76 ft, 106 ft and 116 ft, respectively. To avoid uncertainties in microseismic fracture mapping, the signal to noise ratio (SNR) can be

used to filter the events prior to evaluation. A larger SNR ratio indicates that the location of an event has a higher level of confidence (Thornton and Eisner, 2011).

It is also noteworthy that not all detected microseismic events are related to fracture tip propagation. Both fracture propagation and interactions between natural fractures and hydraulic fractures will generate microseismic events. While the location of these events is the fundamental piece of information in treatment evaluation, the moment tensor of the event can be used to identify the origin and characteristic of the event. Moment tensor identifies the radiation pattern of seismic energy from the epicenter of the event, which relates to the failure mode of the medium. Fracture tip propagation in the formation is considered as Mode I failure, which generates pure tensile moment tensor, or Compensated Linear Vector Dipole (CLVD). On the other hand, interactions between natural fractures and hydraulic fractures lead to Mode II or Mode III failure, which contains shear component in its moment tensor (Baig and Prince, 2010). By calculating and identifying shear component with microseismic events, it's possible to determine whether the event is from fracture tip propagation or from the interaction between fractures.

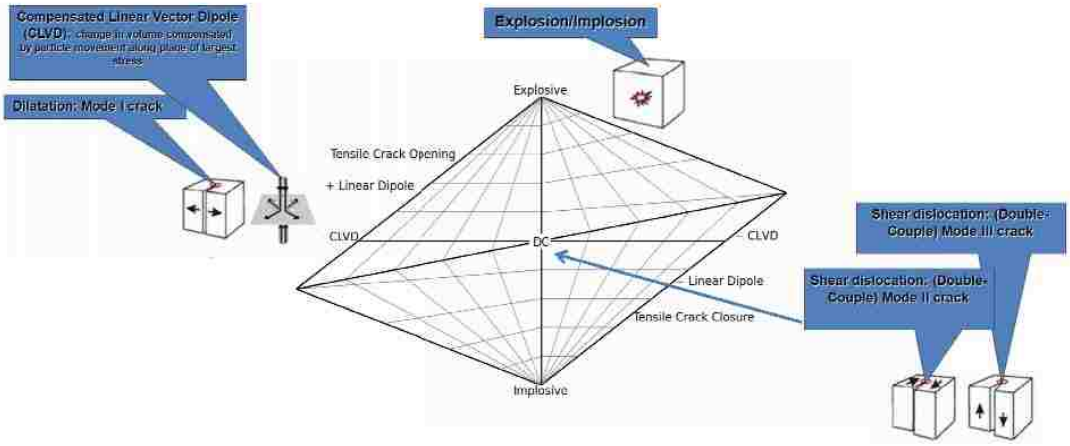

Figure 1.5: Moment tensor of the microseismic event can identify failure mode in the medium. (Baig and Prince, 2010).

1.3 Research Motivation

The economic values of hydraulic fracturing are mainly attributed to production enhancement; specifically, hydraulic fracturing leads to both increased hydrocarbon production rate and larger quantities of producible hydrocarbon. With the biggest proven natural gas reserve in the world, Russia adopted hydraulic fracturing technology for production enhancement purpose in mid 1990s, and significantly boosted their gas production and domestic economy by exporting natural gas to neighboring countries (Pongratz et al, 2008). It was also reported that after focusing on production technologies enhancement in late 1990s, oil production in Russia had another spike to reach more than 9MM BOPD, nearly 45% up from a prior nosedive in oil production in mid 1990s (Pongratz et al, 2008). Mile et al. (2008) also recorded a nearly 90% spike in long-term gas production in Bakken Shale Formation in North Dakota. On the other hand, hydraulic fracturing technology is constantly evolving and renewing itself with relentless research efforts from both industries and scholars around the world. Pongratz et al (2008) reported that from 1995 to 2005, the improving hydraulic fracturing technology had increased the hydrocarbon production by an average of 30%. Clearly, oil and gas industry is a heavily technology-driven industry; technologies used in production enhancement must be constantly evolving and updating to adapt innovations in design, operation and modeling. This demands a diligent research on the possible innovation and improvement in modeling and assessment of hydraulic fracturing. Accurate prediction and evaluation of hydraulic fracturing treatments will allow for more reliable prediction of reservoir performance and reservoir decline analysis for reservoir engineers.

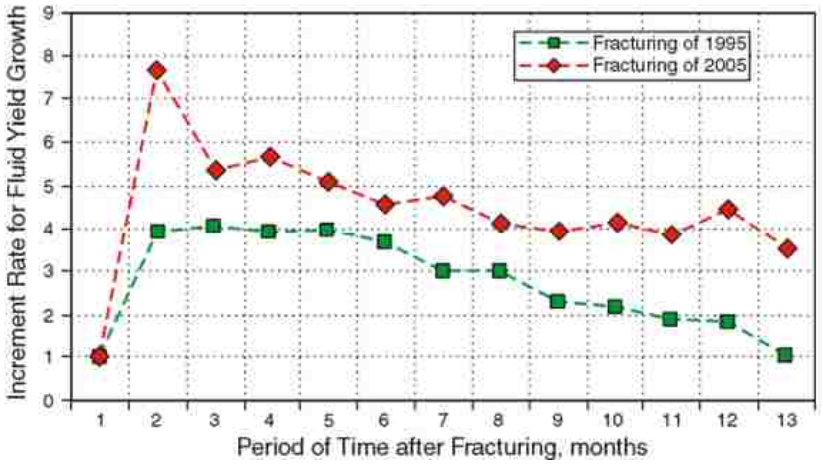

Figure 1.6: Hydrocarbon Production in Fractured Reservoirs in 1995 and 2005.

Hydraulic fracturing also received attention especially in natural gas production because it also increases the rate of recovery, which is usually desired during the high demand season. A contrasting difference between oil production and gas production lies that while produced oil can be stored, transported and refined with relatively low cost and limited facility requirement, produced natural gas are usually sold locally or exported through pipelines instead of having them stored and transported over a long duration. Moreover, natural gas prices are constantly fluctuating seasonally, which makes natural gas storage both risky and costly. It was reported that most natural gas producers in Texas, United States has stopped producing excessive natural gas because facilities that store natural gas are more costly than the profit from natural gas itself, and operating gas-producing field in the long run is also costly to operators. Moreover, natural gas is traded through future contracts in the U.S financial market. Future price of natural gas has contango for most of the time (i.e. the price for a later contract is higher than an expiring contract). However, during the season with high natural gas demand, or during natural disasters in which natural gas production is negatively impacted, future prices of natural gas might also experience backwardation, the exact opposite of contango. Therefore, hydraulic fracturing

technology may leads to faster gas production in such periods and generates more revenue to the company. Warpinski (1991) has observed that the gas production rate in low permeability sand Piceance basin and Greater Green River basin increased from around 250 MMscf/day to 450 - 500 MMscf/day after the fracturing treatment. A thorough understanding of hydraulic fracturing treatment and its evaluation could also lead to better control in fracturing design and consequently the rate of gas production.

Current industry practices in assessing and modeling hydraulic fracturing treatments relied on simplified fracture and fluid flow models, which could only provide approximated descriptions regarding the actual fracture geometry. For instance, common assumptions in fracturing modeling include homogeneous formation properties and limited fracture growth in vertical direction; these assumptions are likely to be erroneous in unconventional gas reservoirs where material properties and fracture development can be quite complicated (Valencia et al, 2005). Moreover, current analysis and design of hydraulic fracturing tend to rely on only one single source of information, such as microseismic data, pressure diagnostics, tilemeter analysis, and radioactive tracer technique. While most of the current evaluation tools and technologies yield satisfactory analysis and design of hydraulic fracturing, uncertainties are constantly exist in the source of information, which inevitably leads to less-than-perfect design and analysis. Therefore, the integrated modeling approach in this research could fill this gap by combing different source of data. This integrated modeling methodology will incorporate information including geological background, pressure response, microseismic data, mathematical optimization, numerical simulation, and production analysis; it will provide an integrated workflow to assess fracture treatment and yield a reliable geometry of natural fractures. Issues such as formation heterogeneity and uncertainties in data source will also be addressed.

1.4 Research Objectives and Outline

This research aims at assessing the hydraulic fracturing treatments in naturally fractured reservoirs and predicting the geometry of natural fractures by developing an evaluation workflow that integrates different source of information. The objectives of this research are:

1) Review characteristics of naturally fracture reservoirs including the origin, classification and natural fracture distribution in such fractured reservoirs. Discuss the challenges and considerations for hydraulic fracturing in naturally fractured reservoirs. Overview the current modeling techniques for naturally fractured reservoirs and their advantages and limitations. In addition, an overview of Barnett Shale will be included, in which the geology, hydrocarbon production, hydraulic fracturing and natural fracture characteristics in Barnett Shale will be reviewed.
2) Using optimization tool in MatLab and least square modeling technique to incorporate double-couple microseismic events and find different natural fracture geometries, including the spacing in 2D direction and the location of the network. Both orthogonal and non-orthogonal geometry will be considered. This optimization algorithm will generate different natural fracture realizations with smaller overall distance square between microseismic points and adjacent fracture grids.
3) Conduct forward-modeling of fracturing treatments with Discrete Fracture Network (DFN) with numerical hydraulic fracturing simulator StimPlan. Quantatively comparie the net pressure responses from the treatment and simulation to determine the fitness of each natural fracture geometry.
4) Use numerical simulators such as CMG to build reservoir models that incorporates hydraulic fractures and natural fractures. Compare the hydrocarbon production from unstimulated

reservoirs, naturally fractured reservoirs and hydraulically fractured reservoirs, and discuss the impact of hydraulic fracturing in naturally fractured reservoirs.

The outline of this thesis is organized as follows. Chapter 2 will provide an overview of the field-of-research, including well locations, geological background, treatment history, and microseismic mapping results. Chapter 3 will cover the role and properties of natural fractures in hydraulic fracturing, including their history, classification, properties, and their interaction with hydraulic fractures. Chapter 4 will present the least square modeling for estimating natural fracture realizations based on microseismic events locations. Chapter 5 will focus on forward modeling with StimPlan, and Chapter 6 will present results from production simulation using CMG, which considers different natural fracture geometries. Chapter 7 will conclude the thesis and provide recommendations for future work.

Chapter 2: Natural Fractures and Their Roles on Hydraulic Fracturing

By studying core and outcrops on one side and observing well testing and production behavior on the other side, it has been revealed that many of the unconventional hydrocarbon resources such as Marcellus Shale (Pommer et al, 2013), Barnett Shale (Patel et al, 2013), EagleFord Shale (Fan et al, 2011), Antrim Shale (Hopkins et al, 1995), Woodford Shale (Gupta et al, 2013) and San Juan Tight Sand (Ouenes et al, 1998) are naturally fractured. This chapter will discuss the origins and distribution of natural fractures and how natural fractures affect hydraulic fracturing. The presence of natural fractures in hydrocarbon bearing reservoirs profoundly impacts the propagation of hydraulic fractures and the overall efficiency of fracturing treatment; thus oil and gas industry consider natural fractures as a double-edge sword to hydrocarbon production. On one hand, although natural fractures are mostly fully cemented by diagenetic materials, open and debonded natural fractures may still serve as highly permeable paths for oil and gas flow, which leads to enhanced productivity of the well. On the other hand, however, hydraulic fractures' interaction with natural fractures may form complex fracture networks (Warpinski and Teufel 1987), which may lead to extra leakoff of fracturing fluid (Potluri et al, 2005), or cause early screenout at fracture tip or near the wellbore (Cipolla et al, 2010) and therefore impacts the efficiency of hydraulic fracturing. Overall, these complications make treatment design more challenging and stimulation results more unpredictable. In most petroleum engineering applications especially reservoir engineering studies, natural fracture distributions are considered as fully random phenomena. We will show that the distribution of natural fractures is not fully random. Due to limited access to the subsurface, core and outcrop studies as well as numerical modeling have been the primary tools to model the distributions of natural fracture in the reservoir, as will be reviewed in this chapter.

2.1 Natural Fractures

Core and outcrop studies have revealed the presence of abundant natural fractures in many hydrocarbon reservoirs (Gale et al, 2007; Dahi Taleghani et al, 2014; Papazis, 2005). Typical size of natural fractures ranges from a few millimeters to several thousand meters (Dahi Taleghani et al, 2014), and they significantly impact the processes happening inside earth's crust like fluid flow and fracture growth regardless of their dimensions. Although the hydraulic conductivity of natural fracture system is low due to the occluding cements that precipitated during the diagenesis processes (Gale et al, 2007; Dahi Taleghani et al, 2014), sealed natural fractures may be reactivated thermally (Dahi Taleghani et al, 2014) or by excessive pressure during hydraulic fracturing (Potluri et al, 2005) and hence serve as potential paths for fluid flow or fracture growth.

Natural fractures are caused by brittle failures in rock (Pollard and Aydin, 1988; Shah et al, 2013; Langenbruch and Shapiro, 2014). Pollard and Aydin (1988) defined joints as those fractures with field evidence of opening displacements, and reviewed different theories on the origins of jointing. Over the past century, there had been heated debate on the origin of joints. Pioneer geologists held contrasting perspectives regarding the origin and mechanism of jointed structures in rocks. For example, Becker (1893) and Van Hise (1896) argued that the joints in rocks were mainly caused by tensile or compressive stresses. Woodworth (1896) believed that joints were secondary features caused by later shear displacements on some of the joint planes. Sheldon (1912) studied the structural geology of the Finger Lakes region of the upstate New York and gathered abundant field data on joint orientations. Based on geometric relationships between joints, faults and regional folds, she concluded that the joints in this region were formed due to folding in the early stages of the Appalachian folding. Nickelsen and Hough (1967)

repudiated the conjugate shear fracture concept of jointing by concluding that joints are characterized by plumose structures and opening displacements against the surface of joints. They also developed the idea of a fundamental joint system that includes two sets of unequal joints, which consists of a set of systematic continuous joints and another set of nonsystematic joints approximately perpendicular to the first set. Engelder (1980) studied regional joints in the Appalachian Pleateau and inferred the paleostress field in this region. Based on the plumose structures, calcite filling and lack of shear displacements in joints, he concluded that these joints were extensional fractured formed in a principal stress plane during Alleghanian orogeny. Although there is barely consensus about the origin of natural fractures, it has been widely accepted that natural fractures are formed due to changes in stress field, such as folding (Sheldon, 1912) or abnormally pore pressure such as excessive fluid pressure during hydraulic fracturing (Engelder and Lacazette, 1990). Moreover, change in reservoir stress field during hydraulic fracturing is the primary cause for the reactivation of cemented natural fractures. Vermylen (2011) summarized three causes of stress change in the reservoir during hydraulic fracturing. The first cause is the dilation of tensile fractures, particularly the dilation of main hydraulic fracture planes. The second source of stress change can be attributed to the poroelastic effects when fracturing fluid enters the reservoir and increases the reservoir pore pressure. Lastly, the initiation and propagation of hydraulic fractures itself also lead to formation stress change.

Griffith (1921) developed mechanistic relationships for fracture shape, material properties and energy needed for fracture propagation based on an energy criterion. From fracture mechanics' point of view, fractures will open and propagate in the direction that confronts least resistance. Accordingly, conventional wisdom holds that fractures will align with

the current maximum horizontal stress. However, misaligned natural fractures have been observed where the direction of natural fracture sets misaligned with that of maximum in-situ stress. Laubach et al (2004) concluded that natural fractures would not necessarily parallel to the direction of the current maximum in-situ stress due to the fact that paleostress field may experience significant direction change due to geological events, such as folding and faulting. In other words, rather than the present-day stress field, the direction of in-situ stress during the formation of natural fractures determines their orientation. Therefore, natural fractures discovered at present time are not necessarily orientated in the direction of maximum in-situ stress.

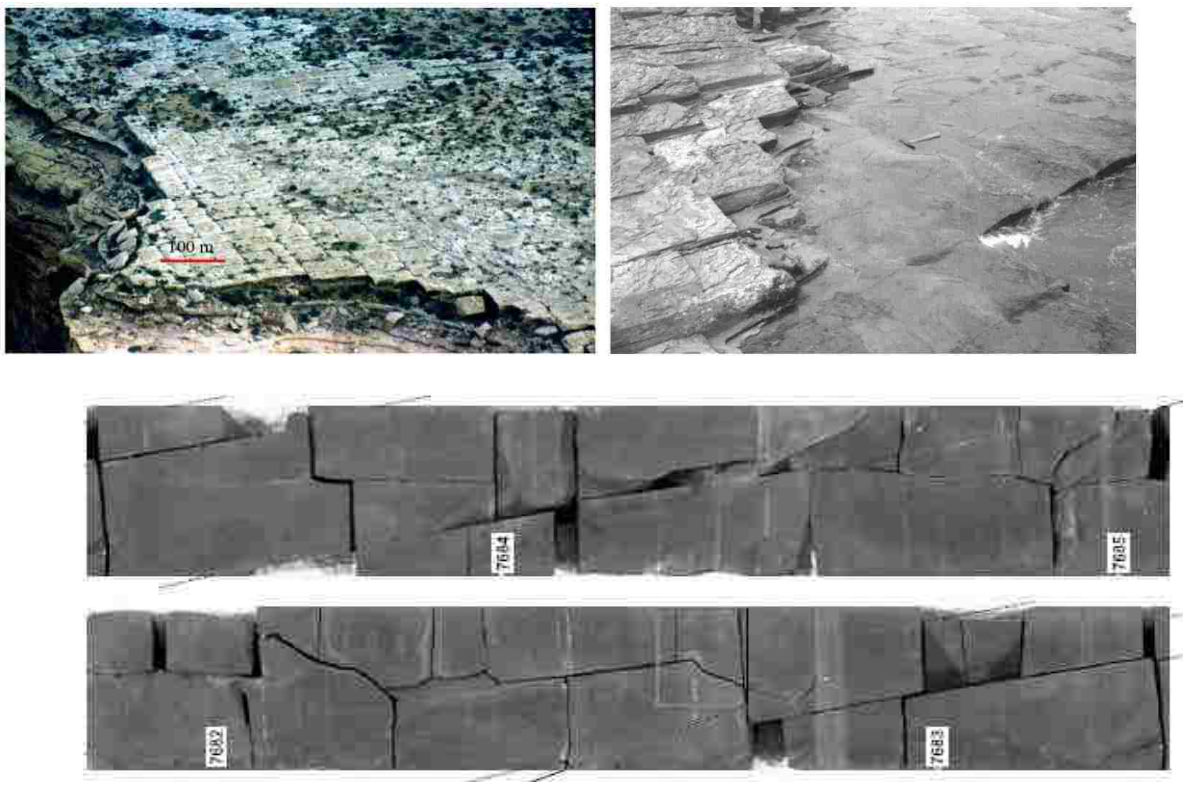

Figure 2.1. Core and outcrop studies showed the presence of natural fractures at different length scales (Photo adapted from Gale et al, 2007; Nelson, 2001 and Anupam, 2010)

Natural fractures can be classified based on their forming mechanisms. Stearns and Friedman (1972) had broadly categorized natural fracture systems into regional fractures and structure - related fractures. While this classification approach is usually ambiguous due to the high degree of heterogeneity in subsurface, they further revised their classification scheme to categorize natural fractures into 1) Tectonic Fractures, 2) Regional Fractures, and 3) Contractional Fractures. Although most natural fractures are related to stress-related rock failures, this classification scheme allows for more accurate description for the origin of natural fractures. In this research, it has been assumed that natural fractures expand over the majority of the reservoir, which could be considered as regional fractures. Regional fractures are natural fracture systems that were developed over a large area, which relatively little change in fracture patterns, fracture orientations, and fracture spacing (Stearns and Friedman, 1972). Physiological provinces such as Colorado Plateau, Uinta Basin and Piceance Creek are all examples of formations with regional fractures (Nelson, 2001), in which natural fracture systems were developed with the unit of miles. Figure 2.3 below is an example of a regional fracture system in Southeastern Utah. It can be observed from the areal view that natural fractures are predominantly aligning in the vertical direction, while spacing between visible major fractures is nearly constant (Nelson, 2001).

Core and outcrop studies have shown consistent natural fracture length, spacing and aperture distribution in fractured reservoirs, such as Barnett Shale (Gale et al, 2007) and Marcellus Shale (Pommer et al, 2013; Gale et al, 2014). Successful design of hydraulic fracturing treatments requires accurate information regarding the distribution of major natural fractures because they may impact the growth of hydraulic fractures (Potluri et al, 2005; Dahi Taleghani et al, 2013; Dahi Taleghani and Olson, 2014). Since it is not possible to accurately

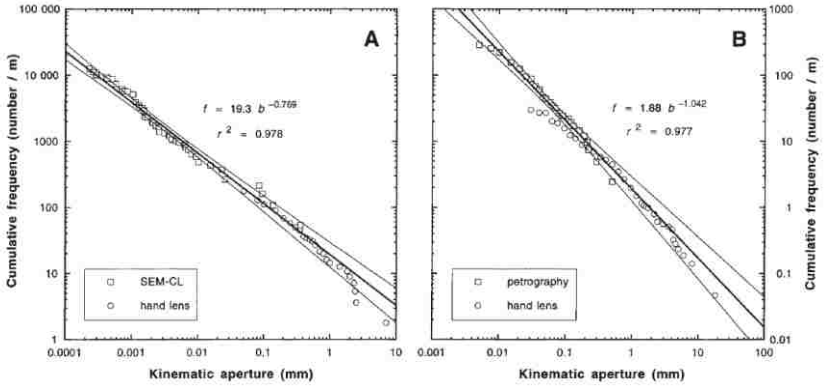

Figure 2.2. Aperture population analysis from Marrett et al (1999) exhibited nearly-perfect straight-line relationship, which implies power-law scaling between fracture intensity and aperture.

Figure 2.3. A vast area of regional fracture in a Jurassic Navajo sandstone in southeastern Utah. (Adapted from Nelson 2001)

determine distributions of all major natural fractures in subsurface with seismic tool or logging tool, we can use natural fracture distributions derived from core and outcrop studies to predict the geometries of major natural fractures in fractured reservoirs. Marrett et al (1999) conducted field measurement and collected data sets from natural fractures and extension fractures in Marble Falls Limestone and Ozona Sandstone. The population analysis on fracture kinematic aperture exhibited nearly-perfect straight-line relationship on a log-log scale with coefficients of determination around 0.98. Through regression analysis, they found that these data sets exhibit

simple power-law scaling relationship regardless of the rock type or movement mode. Ortega et al (2006) conducted field measurements of natural fracture intensity in Sierra Madre Oriental formation in northeastern Mexico. By normalizing fracture intensity at different volumes of rock, they proposed a scale-independent approach that explicitly accounts for variation of fracture intensity due to fracture size variation. Moreover, they also observed power-law scaling between average fracture spacing and fracture aperture. Gale et al (2014) studied cores and outcrops from 18 shale formations around the world and compared their observations with published descriptions of these formations (Figure 2.7). Their analysis revealed log-normal distribution of fracture apertures and power-law relationship between fracture aperture and average fracture spacing in nearly all cases. Friedman and McKiernan (1995) performed statistical analysis of fracture spacing for outcrops in Austin Chalk, and concluded that fracture spacing distribution had an increasing concave-down cumulative frequency histogram, which corresponds to a log-normal distribution of fracture spacing (Figure 2.6). On the other hand, Olson (2003) studied the scaling of fracture aperture and fracture length, and concluded that fracture aperture-to-length scaling can be either linear or to the ½ power. Therefore, these findings can assist us in modeling fracture lengths in fractured reservoirs. Kumar et al (1997) used NMR Imaging tool to measure the aperture in rock fractures, and the results showed a normal-distribution pattern of fracture apertures. However, natural fracture recorded by logging tools may also include drilling-induced fractures that intersect with the wellbore. Heffer and Bevan (1990) also studied the scaling relationships in natural fractures, in which they measured the lengths of natural fractures in a sandstone outcrop in the Gulf of Suez. Fracture length frequency distribution initially showed a nearly log-normal distribution, and later on they concluded that due to the imperfect resolution of the viewing technique, the results of fracture lengths were somehow distorted, and they further

concluded that the lengths of the natural fractures generally follow a power-law distribution with an exponent close to -3.

Based on results from core and outcrop studies, the geometries of natural fracture networks can be generated stochastically with mathematical tools. In this approach, geostatistics will first be utilized to investigate spatially distributed geological variables, in which average fracture azimuth, fracture spacing, fracture length and their variance are primary parameters for natural fracture distribution. These properties are stochastically determined using probability distributions specified by the user when generating random natural fracture systems. Below, we demonstrate the stochastic generation of natural fracture system with MATLAB based on single perturbation of fracture spacing, fracture length, and fracture azimuth. As it's observed below, a greater variance (Figure 2.3a) led to larger discrepancies in in fracture length, while relatively smaller variance in fracture azimuth and spacing (Figure 2.3b and 2.3c) led to relative uniform fracture distribution.

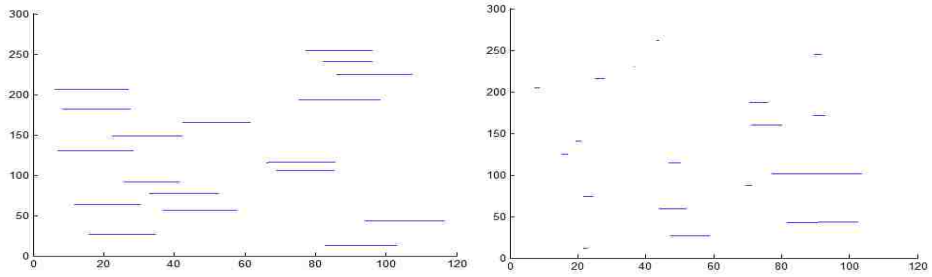

Figure 2.4a. Stochastic generation of natural fracture system with single perturbation of fracture length

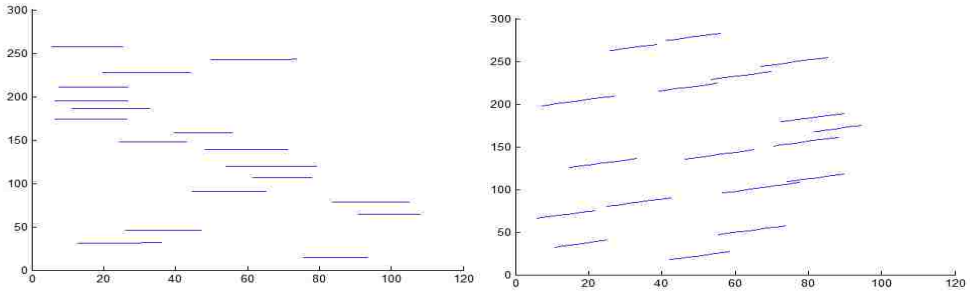

Figure 2.4b. Natural fracture system based on single variable perturbation of fracture azimuth

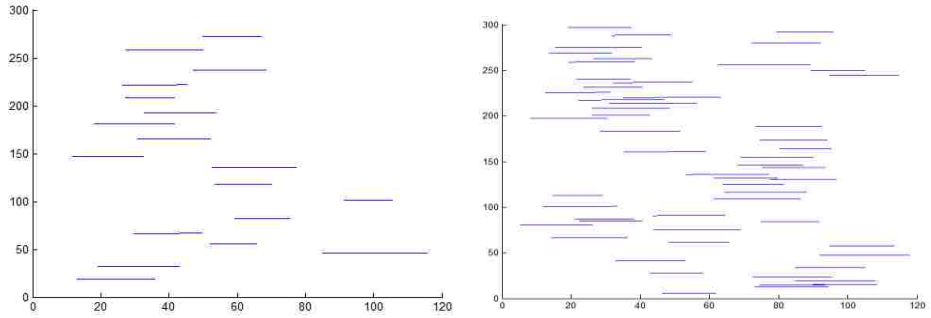

Figure 2.4c. Natural fractures generated based on single variable perturbation of fracture spacing

Based on the concept of subcritical crack index proposed by Olson (1993), we can also generate a cluster of natural fractures, as known as fracture swarm. Subcritical crack index (SCI) describes the degree of clustering for natural fractures. With a higher subcritical fracture growth index, fracture lengths will be distributed in a more skewed log-normal pattern. Formations with large SCI will have clustered fractures with very small spacing, while fractures will growth in a more scattered pattern with intermediate or low SCI. In Figure 2.5, we demonstrate the fracture swarms generated from an algorithm of fracture growth with different SCI. The principle of this algorithm is the likelihood that each piece of fracture grows is proportional to its current length to the n^{th} power, where n is the subcritical fracture growth index. Therefore, the larger the subcritical fracture growth index, the more rapidly that the longer fractures will grow. This algorithm first generate a random set of small fracture pieces with equal lengths; thereafter, it will run a number of iterations, in which the sum of the fracture lengths to the power of n will be calculated, where n is the subcritical fracture growth index. A random threshold will then be established, which will subsequently be examined against each piece of fractures. If the fracture lengths to the power of n exceed the threshold, that fracture will grow in this time step. This procedure is repeated for a sufficient number of times until the desired pattern of fracture clustering is observed. Olson (1993) concluded that with low values of SCI (below 20),

computed natural fracture patterns exhibit small spacing relative to bed thickness. At high values (above 80), fractures are spatially arranged in widely spaced clusters. Intermediate values (20 – 80) result in more regular fracture spacing that is roughly proportional to layer thickness.

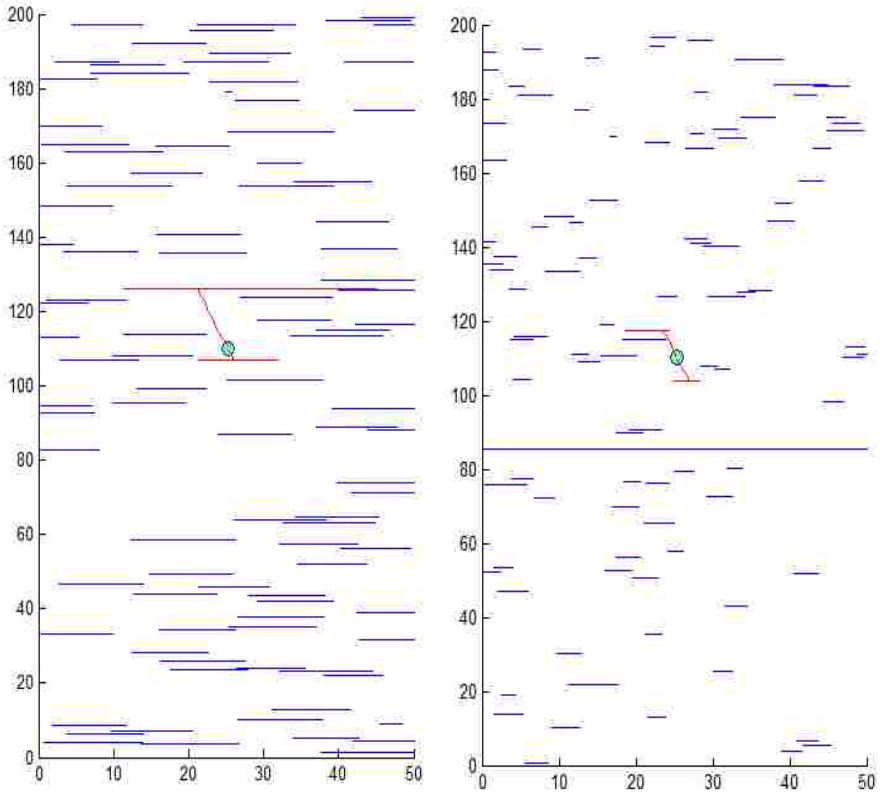

Figure 2.5. Fracture swarms generated by considering contrasting subcritical crack index. Larger n led to wide spaced fracture clusters while smaller n led to fractures with relatively similar length and spacing

Overall, the distribution of natural fractures in hydrocarbon bearing formation significantly impacts the growth of hydraulic fractures (Dahi Taleghani and Olson, 2013; Jeffrey et al, 2009) and permeability of the reservoir (Huang et al, 2011; Cho et al, 2012). It is possible to predict properties and distributions of macrofractures based on observations of microfractures from core and outcrop studies. However, significant uncertainties exist in sampling and modeling for these microfractures, and prediction of macrofracture properties based on biased observation might lead to erroneous conclusion. An integrated modeling that incorporates large-scale

mapping results could significantly reduce the uncertainties in modeling naturally fractured reservoirs.

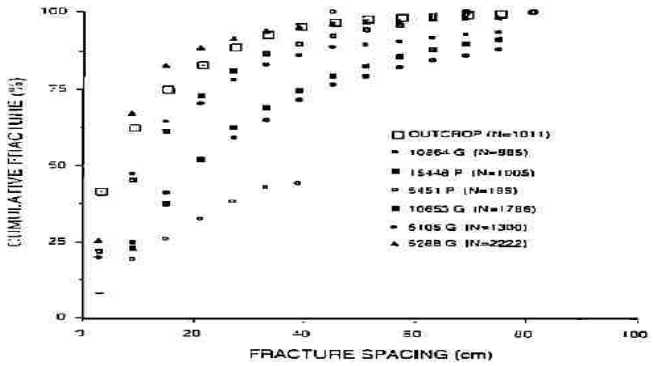

Figure 2.6. Outcrop studies of fracture spacing in Texas Austin Chalk exhibited log- normal distribution pattern (Friedman and McKiernan 1995)

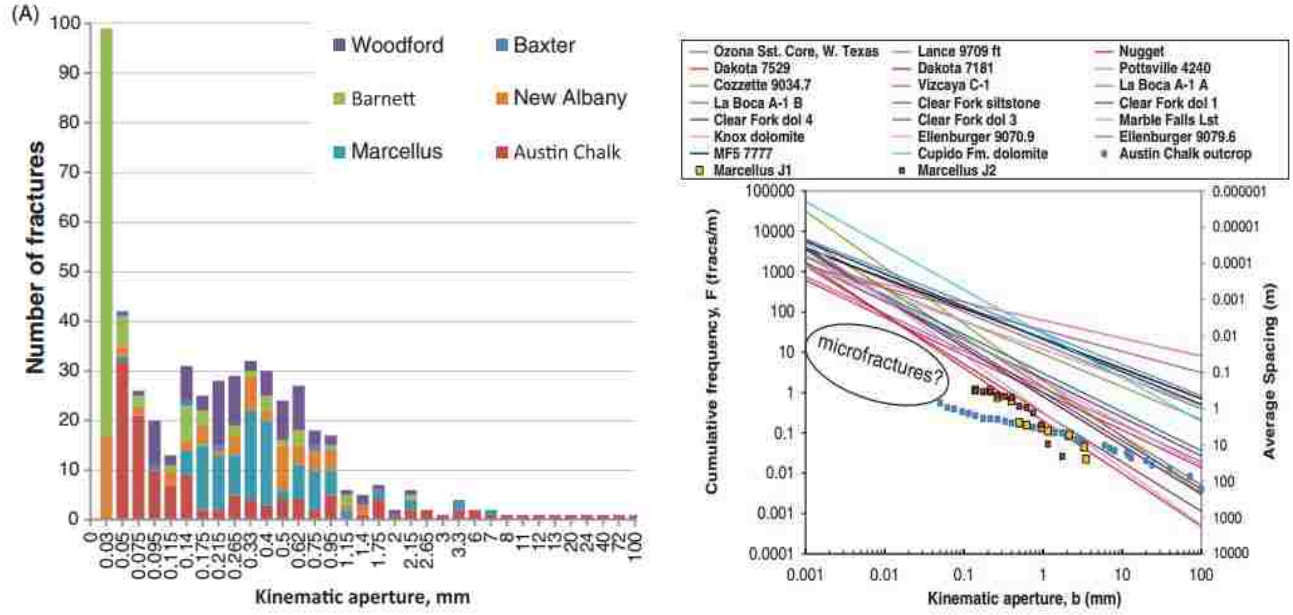

Figure 2.7. Observations of natural fractures from 18 shale formations showed log-normal distributions of fracture kinematic aperture and power-law scaling of fracture aperture and spacing. (Gale et al, 2014)

2.2 Modeling Natural Fractures in Fractured Reservoirs

In addition to core studies and outcrop measurements, advanced logging tools such as FMI (Fullbore Formation Micro-Imager) and EMI (Electro Micro-Imaging) could assist in determining the presence of natural fractures and their properties. However, direct observation of natural fractures with logging tool may include drilling induced fractures and is thus not always accurate. Due to the limited access to the subsurface formation, it is not possible to have direct observations of macrofractures and directly measure their distributions and properties. Numerical modeling instead could help us to generate natural fracture realizations for fracture geometry in the subsurface. This modeling can be solely based on statistical properties of natural fractures observed from outcrop and core studies or mechanical properties of rock. A set of mathematically equivalent natural fracture networks could be developed that incorporates average properties of observed natural fractures in outcrops, and fracture mechanics based models could also generate possible natural fracture geometries. The results of numerical modeling could provide insightful observations regarding the characteristics of fractured reservoirs.

Olson (1993) and Olson (2004) modeled the fracture growth and clustering in naturally-fractured reservoirs, and studied the effect of subcritical crack growth indices on fracture growth (Figure 2.8). His simulation results showed that as the subcritical crack growth index increases, fracture lengths will be distributed in a more skewed log-normal pattern. He also concluded that the fracture spacing and other fracture patterns can be controlled by the subcritical crack index (SCI) n. A large SCI will generate clustered fractures with very small spacing, while fractures will growth in a more scattered pattern with intermediate or low SCI. With low values of SCI (below 20), computed natural fracture patterns exhibit small spacing relative to bed thickness. At

high values (above 80), fractures are spatially arranged in widely spaced clusters. Intermediate values (20 –80) result in more regular fracture spacing that is roughly proportional to layer thickness. He also concluded that normal distribution will be suitable for fracture spacing, as bed thickness does not vary wildly within a small region of the formation. However, this modeling technique only considered one set of clustered natural fractures in a single direction, which is not consistent with core and outcrop studies that two or more sets of intersecting natural fractures are common in naturally fractured reservoirs, such as in Olson and Pollard, 1988; Gale et al, 2007; Gale et al 2014.

Olson et al (2009) presented an analysis approach that incorporates fracture mechanics and diagenesis processes to predict fracture network geometry, fracture aperture distribution and preservation. They used poroelastic stress calculations combined with fracture mechanics criteria to model a tight gas sandstone formation in Texas. Their results showed that pore pressures substantially below the overburden stress and small extensional strains can create fracture network with considerable flow capacity. However, their approach could not predict the natural fracture geometry based on any data retrieved from hydraulic fracturing treatment or microseismic data, which could not be useful in post-treatment assessment of natural fracture distribution.

Zhao (2013) presented a semi-analytical modeling approach to simulate natural fracture network system in heterogeneous tight formations. He used source and sink function method (SSM), or integrated transformation method (ITM) and proposed a pseudo-fracture body concept to study the pressure drop and fluid influx around natural fractures and compute natural fracture geometry in the pseudo-fracture body. However, this technique requires detailed fluid flow and pressure drop information of the natural fracture, which is impossible to obtain during hydraulic

treatment. Moreover, this modeling approach did not consider any field measurement data, which may lead to incomplete or inaccurate natural fracture geometry.

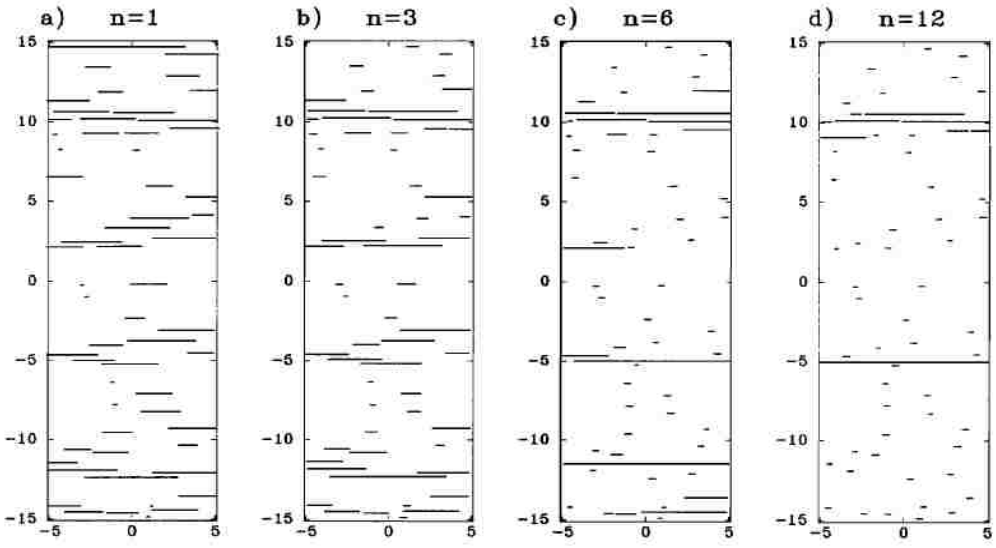

Figure 2.8. Subcritical Crack Indices determines the degree of clustering in fractured reservoirs; a large SCI value indicates greater fracture clustering (Olson 1993)

In conclusion, direct observation of fractured reservoirs is not feasible due to the limited access to the subsurface, and core and outcrop sampling may lead to biased observation and inaccurate estimation of macrofractures in fractured reservoir. Existing numerical modeling of naturally fractured reservoirs requires accurate details about natural fractures, which is often difficult or expensive to gather during hydraulic fracturing. Moreover, these numerical modeling usually does not incorporate post-treatment measured data, which could not reflect the actual situation and heterogeneity of the fractured reservoir being studied. Therefore, the multi-disciplinary data integration workflow we propose in this research could fill this gap by integrating a multitude of scientific data from hydraulic fracturing, geological study and engineering calculations.

2.3 Hydraulic Fracturing in Naturally Fractured Reservoirs

Due to the ultra-low permeability of unconventional reservoirs, their resources cannot be economically recovered without resorting to reservoir stimulations such as hydraulic fracturing. The main objective of reservoir stimulation is to improve the conductivity of the formation by hydraulic fracturing, and attempt to establish better connection between the wellbore and the pre-existing natural fracture network (Hart Energy Publishing, 2007). Although naturally fractured, formation conductivity of the natural fracture network is usually low due to the fact that most of these fractures are cemented by precipitations during the digenesis process (Gale et al, 2007; Dahi Taleghani et al, 2014). However, by reactivating these cemented fractures, pre-existing natural fracture system may still serve as weak paths for hydrocarbon flow, and consequently benefit hydrocarbon production from naturally fractured reservoirs.

Hydraulic fracturing in fractured low permeability reservoirs is facing additional challenges compared to fracturing in conventional reservoirs. Reactivated natural fractures may serve as extra flow paths for fracturing fluid during the treatment, thus hydraulic fracturing in fractured reservoirs is usually accompanied with unusually high leakoff rate (Valko and Economide, 1999). In addition, excessive fracturing fluid loss also causes early screenouts, which has been documented by Massaras and Mcnealy (2012). Barree (1998) and Britt et al (1994) have concluded that the leakoff rate in fractured reservoirs is primarily controlled by net pressure during the treatment and fracturing fluid rheological properties. Therefore, by reducing net pressures and varying fracturing fluid properties, excessive fluid leakoff rate in fractured reservoirs can be alleviated.

Core and outcrop studies and field data has also revealed that in naturally fractured reservoirs, induced hydraulic fractures are likely to develop in complicated manners and form complex fracture network. Murphy and Fehler (1986) reported that microseismic mapping results in fracturing treatments at Fenton Hill, New Mexico showed a broadened cloud of microseismic events in the direction of minimum in-situ stress, which indicated that induced fractures was developing in a network pattern. Pollard et al. (1975) and Delaney and Pollard (1981) have also documented that induced fractures were developed with branching and segmentation in naturally fractured reservoirs. Sato et al. (1998) assessed the treatment history of a hydraulic fracturing job in Minami-Nagoka gas field, and concluded that the development of multi-stranded hydraulic fractures was responsible for early screenout during the treatment. Hopkins et al (1998) also reported that during hydraulic fracturing in Antrim shale formation in Michigan, the microseismic mapping results showed that cloud of microseismic events was distributed within 50 ft of the induced fracture tip. They concluded that complex geometry of induced fractures is mainly caused by the pre-existing natural fracture network in Antrim shale.

Interactions between natural fractures and induced hydraulic fractures have been extensively studied through lab experiments and numerical simulation, and various criterions about fracture interactions were also proposed through these studies. Laboratory studies in early years concluded that fracture interactions were mainly affected by the weakness of the rock matrix. For example, Lammont and Jessen (1963) conducted lab experiments with triaxial compression on all samples, and observed that induced fractures were more likely to cross over natural fractures at a large angle of intersection. They further concluded that the location of the exit point in natural fractures was largely controlled by some particular weakness in the rock matrix. Similar experiment done by Blanton (1982) investigated the effect of differential stress

and angle of interaction on the propagation of hydraulic fractures, and he concluded that both low differential stress and low angle of intersection lead to fracture diversion, while high angle of intersection and differential stress cause induced fractures to cross over natural fractures. Jeffery et al. (2009) conducted mineback field experiments and examined the growth of hydraulic fractures through a network of natural fractures. They observed that the induced fractures tend to develop in a much complicated pattern due to diversion of the progressing hydraulic fracture into natural fractures, or simply the reactivation of these fractures (Warpinski and Teufel, 1987, Olson and Dahi Taleghani, 2009). This complexity can either be suppressed or utilized in some extent to benefit the reservoir productivity (Cipolla et al, 2010).

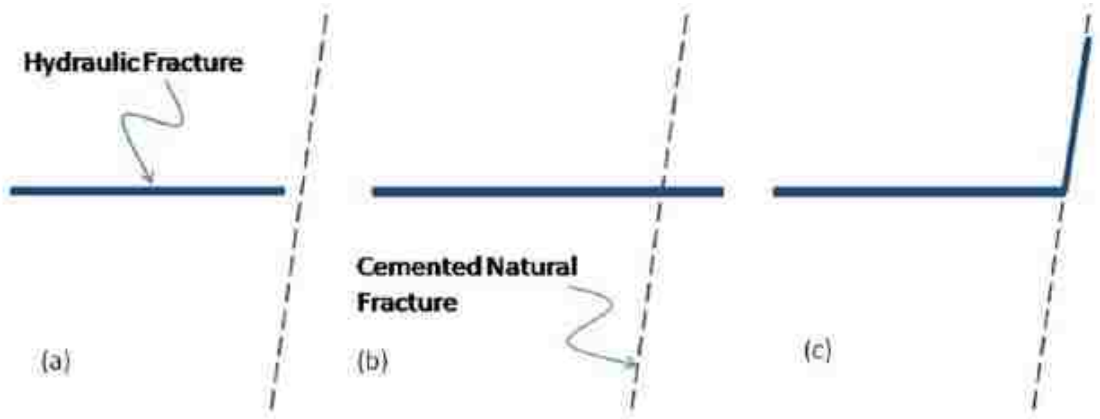

Figure 2.9. Possible interactions between natural fracture and hydraulic fractures. a) Approaching hydraulic fracture exerts tensile stress on sealed natural fractures and reopens the cemented natural fractures. b) Hydraulic fracture can cross over the natural fracture and keep propagating in the original direction if their ratio of energy release rate is above the threshold. c) At low intersection angles, hydraulic fracture will be diverted into the natural fracture, and consequently natural fracture will be extended. (Dahi Taleghani 2009, Dahi Taleghani et al, 2013)

In addition to experimental studies, numerical modeling is also useful in verifying the interaction between fractures. Wilson and Witherspoon (1974) used Boundary Element Methods (BEM) to simulate the steady state fluid flow in rigid networks of planar fractures. Carter et al. (2000) and Bouchard et al. (2000) used Finite Element Method (FEM) with re-meshing strategies

to model fracture growth in naturally fractured reservoirs. Zhang and Jeffery (2008) used a two-dimensional boundary element model that coupled elastic deformation and fluid flow to study the reactivation and termination of fluid driven fractures. They concluded that with large contrasts in formation modulus or toughness, fracture containments are likely to occur across the formation interface. Dahi Taleghani (2009) used an Extended Finite Element Method (XFEM) to address two-dimensional static and quasi-static problems. Crack propagations in strong and weak quasi-static form were described by deriving the governing equations from XFEM. By decomposing the displacement field into continuous and discontinuous parts, XFEM can approximate the behavior of hydraulic fractures and its interaction with natural fractures in a naturally fractured reservoir without any need for remeshing the problem for each increment of fracture propagation. Xu et al. (2010) proposed a semi-analytical pseudo 3-D fracturing simulator to simulate the growth of hydraulic fracture networks (HFN) in the grid of equally-spaced natural fractures. The wiremesh model assumes a growing symmetric elliptical front for the development of induced fracture network. However, the assumption of symmetric induced fractures is sometimes proved to be unrealistic by microseismic mapping of hydraulic fracturing. Dahi Taleghani and Olson (2013) extended the numerical analysis of fracture interaction to the case of cemented natural fractures. These fractures can be influential on geometric development of hydraulic fractures, which consequently affects the resultant gas production. They examined different scenarios of fracture interactions using an eXtended Finite Element Method (XFEM) numerical scheme that considers the fluid flow in the hydraulic fracture networks as well as the rock deformation. Dahi Taleghani and Gonzales (2014) used cohesive element approach to model fracture propagation in naturally fractured reservoirs. This technique limits the path of fracture propagation to predefined routes. In fractured reservoirs, this modeling technique will

place cohesive elements through the network of natural fractures, thus makes it possible to track the evolution of induced fracture network.

Based on Griffith's energy criterion, Dahi Taleghani (2009) discussed three possibilities exist (Figure 2.9) when a propagating hydraulic fracture intersects with a natural fracture. Induced hydraulic fractures may cross over natural fractures and keep their original directions of propagation, if their energy release rate is greater than a certain threshold determined by geomechanical factors and angle of intersection; hydraulic fractures may also completely divert into the natural fracture system if the energy release rate is smaller than the aforementioned threshold. Lastly, since propagating hydraulic fractures will exert traction on cemented natural fractures, reactivation of cemented natural fractures may occur if the infilling cement's strength is inadequate compared to the traction force. Similar models developed by Dahi-Taleghani and Olson (2011) reached the same fracture interaction criterion.

Interaction between natural fractures and induced hydraulic fractures is an important design consideration in planning fracturing treatment. Therefore, to implement these considerations in fracturing design, it's crucial to know the approximate geometry and location of the natural fracture system. Although outcrop and core studies provide a general picture about the natural fracture system in hydrocarbon bearing formation in a small scale, large scale experimental study on natural fracture system is not possible due to the limited access to the subsurface formation, and exact location or distribution of natural fractures are impossible to obtain with current formation evaluation technology. Therefore, the workflow we propose in research fills this gap by integrating the locations of large shear-type microseismic events to build a grid that resembles the geometry of natural fracture system in the subsurface.

2.4 Conclusion

In this chapter, we discussed the origins and characteristics of natural fractures in fractured reservoirs. We've also discussed the role of natural fractures in hydraulic fracturing, and showed that the presence of natural fractures profoundly impacts the fracture growth and overall success of hydraulic fracturing. Moreover, we've overviewed different modeling approaches for fractured reservoirs and concluded that they are not sufficient in combining numerical modeling capacity with post treatment measured data. In the next chapter, an overview of Barnett Shale, the formation that our case study will be based upon, will be conducted. The history, development and characteristics of Barnett Shale will be reviewed, and natural fracture distribution in Barnett Shale will also be reviewed in the next chapter.

Chapter 3: Barnett Shale

As a major shale gas play in North America, the Mississippian Barnett Shale formation covers some 5,000 square miles over 24 counties in Fort Worth basin in northern Texas. A horizontal well named P1 has been drilled in northeastern Barnett Shale in Denton County, Texas, and modeling and analysis of hydraulic fracturing and natural fracture distribution will be conducted on this well in this research. In this chapter, the geological background of Barnett Shale will first be reviewed, including its history, development, geological and geomechanical properties and natural fracture distribution. Thereafter, an overview will be provided on the Well P1, including the well information, perforation design, and treatment information. Net pressure matching without considering the presence of natural fractures will also be included by using a numerical fracturing simulator StimPlan to predict unknown major reservoir geomechanical properties that are not available through project data.

3.1 Geology and Development of the Barnett Shale

The Mississippian Barnett Shale in the Fort Worth Basin is the largest shale gas play in Texas and the third largest in the continental U.S. with an estimated reserve over 40 Tcf (United States Energy Information Administration, 2014). Gas wells located in the productive portion of the Barnett Shale in the Fort Worth basin are designated as the Newark East Field by the Texas Railroad Commission. The Fort Worth Basin was formed during the Paleozoic Ouachita orogeny, in which the basin was formed due to the collision of Laurissia and Gondwana (Bruner and Smosner, 2011). The Fort Worth Basin is described geologically as a "shallow, asymmetric formation" where the Barnett Shale is surrounded by the Ouachita Thrust-fold Belt and the Muenster Arch to the east and the Bend Arch to the west (Hayden and Pursell, 2005). Barnett Shale covers some 5000 square miles (13,000 km^2) over 24 counties surrounding this area. The

productive region of the field has depths ranging from 4000 ft in the west to 8500 ft in the east, and the net pay thicknesses of the formation vary between 200 ft and 500 ft (Zhao et al, 2007). The Barnett Shale is Mississippian in age and its stratigraphic description indicated that it is a dense, organic rich, black siliceous shale (Bruner and Smosner, 2011). The top of the Barnett Shale is estimated to be found at approximately a highest depth of 6500 feet to a low of about 8,500 feet (Hayden and Pursell). Figure 3.1 shows the stratigraphy of the Fort Worth Basin and the relative location of the Barnett Shale formation. The horizontal section of the well P1 was drilled in lower Barnett Shale formation, which was adjacent by Viola Limestone formation in the bottom.

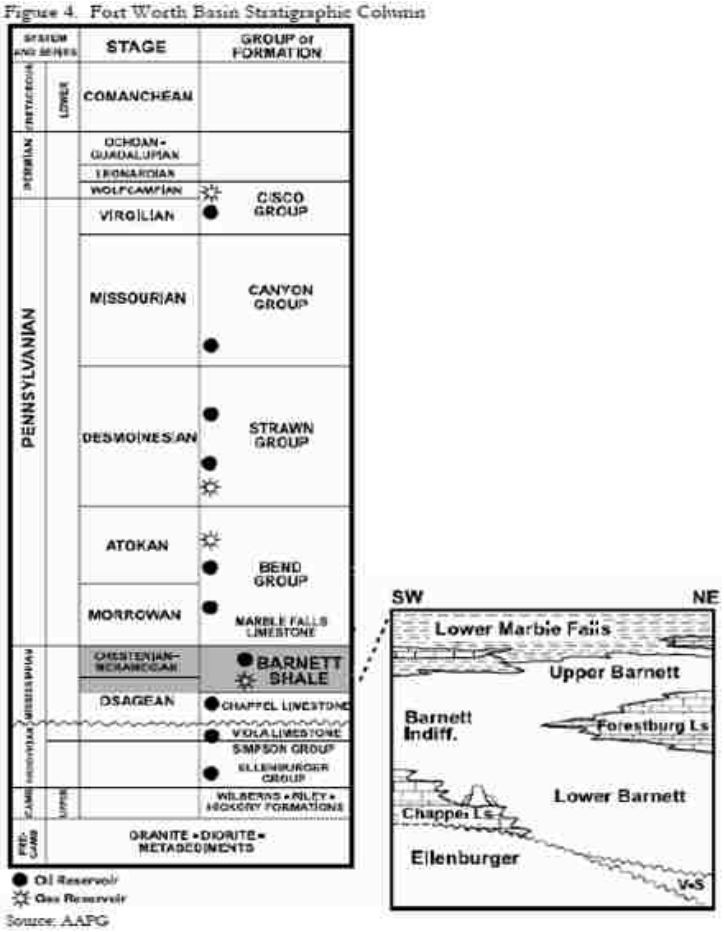

Figure 3.1. Geological Layering in Fort Worth Basin (Hayden and Pursell, 2005).

As an unconventional shale reservoir, Barnett Shale is characterized by its low porosity and permeability. Studies have shown that the average porosity in Barnett Shale is between 3% - 5 %, and its average permeability is around 0.01 md (Hart Energy Publishing, 2007). Gale et al (2007) conducted core studies on four vertical core samples from Barnett shale and estimated that the static Young's Modulus of Barnett shale is approximately 33 GPa, and the subcritical crack growth index in Barnett shale is as high as 109-326. Hill (1992) also estimated that the range of Poisson's ratio in Barnett shale is between 0.2 and 0.3. Hydrocarbon production from Barnett Shale has been heavily relied on hydraulic fracturing and other enhanced recovery techniques, such as CO_2 sequestration (Vermylen, 2011). As a fined-grained sedimentary rock, shale contains free and absorbed gas at the surface of the rock's organic mineral. Depending on the targeted gas type, the objective of stimulation may aim at producing free gas by improving the flow capacity of the formation, or produce released absorbed gas after free gas depletion by injecting CO_2, which will be preferentially absorbed by organic material.

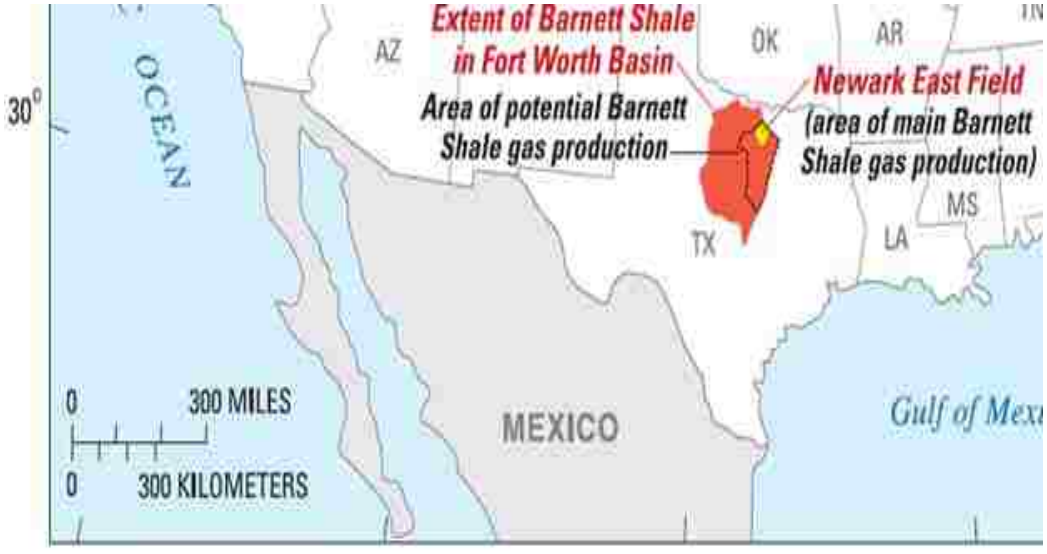

Figure 3.2. Barnett Shale in northern Texas. Main gas production zone in Barnett Shale is designated as Neward East Field, which is located in northeastern Barnett Shale. (Texas Railroad Commission,2012)

The average lateral length of horizontal wells in Barnett Shale is about 4000 feet. The wells are usually stimulated in 4-8 stages with 4 perforation clusters, with an average of 400 feet of span between each stage, and treating pressure is usually around 4000 psi. Average induced fracture is about 500 ft and average fluid efficiency is around 40% (Maxwell et al, 2002; McKeon, 2014). Cross-linked Gel (XLG) was originally used as a common fracturing fluid in Barnett Shale, and later on Slick Water Fracs (SWF) became common fracturing fluid, which requires much lower concentration of proppants because of the large volume of water, high pump rate (over 100 bbl/min) and less friction due to the addition of friction reducer (Grieser et al, 2008). Average amount of water need for stimulating a well is estimated to be around 3.5 million gallon (Ewing, 2008), and the average amount of proppants used per well is between 50,000 lbm to 200,000 lbm (Grieser et al, 2008). Refrac operations are also common in Barnett Shale and bring enhanced reservoir performance. Refrac operation is usually needed when recovery had declined to non-economic rates and other restimulation options are neither available nor feasible. The objective of refract is to enhance the productivity of the depleted reservoir by reorientation of fractures, enlarged fracture geometry, improved pay zone coverage, increased fracture conductivity, and restored fracture conductivity due to complications such as proppant embedment, fines plugging and gel degradation (Vincent, 2010). Cipolla et al (2008) reported that after a refract operation, the estimated stimulated reservoir volume (SRV) increased from 0.43 billion cubic feet to 1.45 billion cubic feet based on a case study in a Barnett Shale reservoir.

Hydraulic fracturing in Barnett Shale is also facing challenges. Uncontrolled fracture height growth may extend to the adjacent formations of Barnett Shale - Marble Falls limestone on the top and Viola Limestone at the bottom, both of which are hydrocarbon-rich reservoirs

(Evans, 1984; Petrichor Energy, 2014). Uncontrolled extension of hydraulic fractures may divert fracturing fluid into underground water aquifer and result in contamination, for which microseismic mapping could be used to monitor fracture growth in the subsurface (Hall and Dahi Taleghani, 2014). In addition to microseismic mapping, tiltmeters are also used in hydraulic fracture monitoring in Barnett Shale. Tiltmeters use sensitive electrolyte sensors to detect small changes in inclination angle between two orthogonal directions, which can be as accurate as nano-radians (Pandurangan et al, 2014). Hydraulic fractures generate tiny deformations in the surrounding rock and therefore cause changes in inclination angles at earth's surface. However, tiltmeters usually have small radius of investigation and are not useful in large scale fracture mapping (Wright et al, 1998).

Moreover, water flowback renders huge amount of flowback water, which may contain clays, chemical additives, dissolved metal ions and total dissolved solids (Vidic, 2010). Vazquez et al (2014) have estimated that up to 50% of fracturing fluid pumped into the formation is flowed back as the well starts production. Huang et al (2005) also reported that in 2002, almost 3.8 million barrels of water was produced for oil and gas drilling, and over 90% of the produced water was disposed at an average cost of $1 - $4 per barrel. The flowback water is sometimes reused in subsequently treatment, or it may be disposed responsibly after being processed at frac water treatment plant (Vidic, 2010). Moreover, the huge amount of water needed in Barnett Shale requires companies to obtain water rights from the State of Texas in order to drain water from natural resources. However, water usage by oil and gas production is still lower than civilian water usage.

Barnett Shale was first discovered and developed by Mitchell Energy in 1981 (Martineau, 2007). Over the next 15 years, Barnett Shale was developed in small capacity, with only less

than 400 wells drilled in this region. With the emergence of hydraulic fracturing, hydrocarbon production activities from Barnett Shale started to spike in late 1990s. Nowadays, Barnett Shale is considered as a major source of natural gas production in continental U.S. According to Texas Rail Road Commission, as of January 2012 there were approximately 16,000 gas wells producing in Barnett Shale, while the total number of permitted locations reached 2,457. Currently, Barnett Shale is the third most productive shale gas formation in the United States, behind the Marcellus Shale and Haynesville Shale. Natural gas production from Barnett Shale accounts for 31% of total gas production in Texas, and contributes to approximately 6.8% of all the natural gas production in the United States (US EIA, 2011). As of the end of 2014, there are approximately 19,000 oil and gas leases in the Newark East Field (Barnett Shale) held by 211 companies. The top three lease holders are Devon Energy, EOG Resources, and XTO Energy. The top three oil producers in Barnett Shale are EOG Resources, Canan Operating, and Rife Energy Operating. The top three gas producers are Devon Energy, Chesapeake Operating, and XTO Energy. The top three liquid gas producers are EOG Resources, Devon Energy, and Burlington Resources. Overall, the top five producers in the Newark East Field (Barnett Shale) are Devon Energy Production, Chesapeake Operating, XTO Energy, Quicksilver Resources, and Burlington Resources (Texas Railroad Commission, 2014). Production history of the field (Figure 3.2) showed that there has been a steep increase in the gas production from 2002 with 1,000 MCF/D to 2009 with 5,300 MCF/D. There has also been a steady increase in the oil and condensate production from 2002 with 5,000 BBL/D to mid-2010 with 10,000 BBL/D. In 2011 there was a sharp increase to 30,000 BBL/D. However, the production has been on a decline trend since mid-2011 (Powell Shale Digest, 2012).

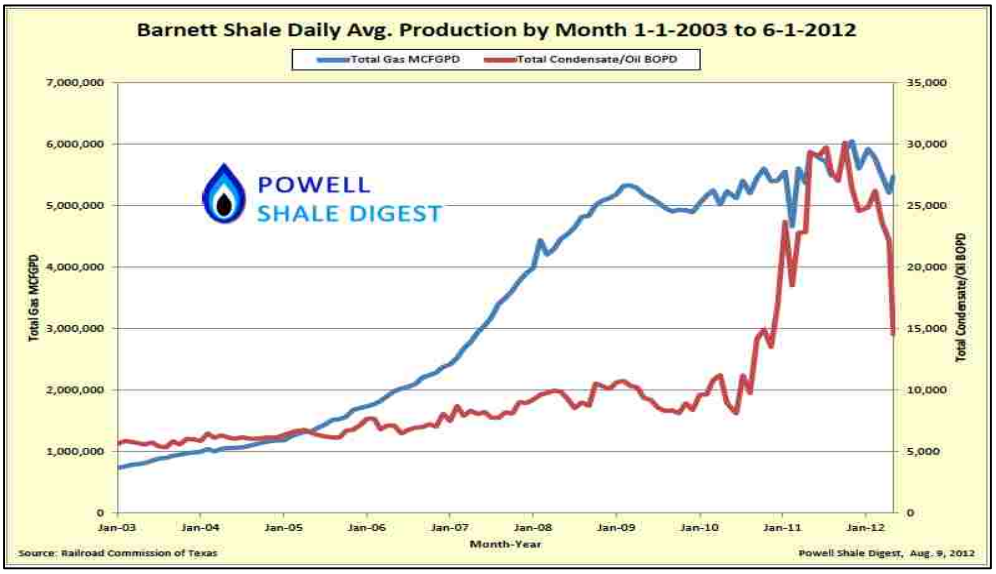

Figure 3.3. Barnett Shale daily average production for gas and condensate/oil production (Powell Shale Digest, 2012)

Figure 3.4. Active rigs in Barnett Shale as of September, 2014 (Texas Railroad Commission)

3.2 Natural Fracture Distributions in Barnett Shale

Both core studies and microseismic mapping have confirmed the presence of abundant cemented natural fractures in Barnett Shale. Fisher et al (2004) analyzed the microseismic mapping results from hydraulic fracturing treatments in Fort Worth Basin, and observed clusters of microseismic events along the fracture path (Figure 3.5). They concluded that in their case study, propagating hydraulic fractures clearly interacted with natural fractures. Moreover, they observed that induced fractures grow in a complicated network pattern in Barnett Shale with major fracture growth in at least two orientations. Warpinski et al (2005) also analyzed the mapping results of 2 test cases of hydraulic fracturing in Barnett Shale, and observed that induced fractures were developing in a large areal extent along the fracture path (Figure 3.6).

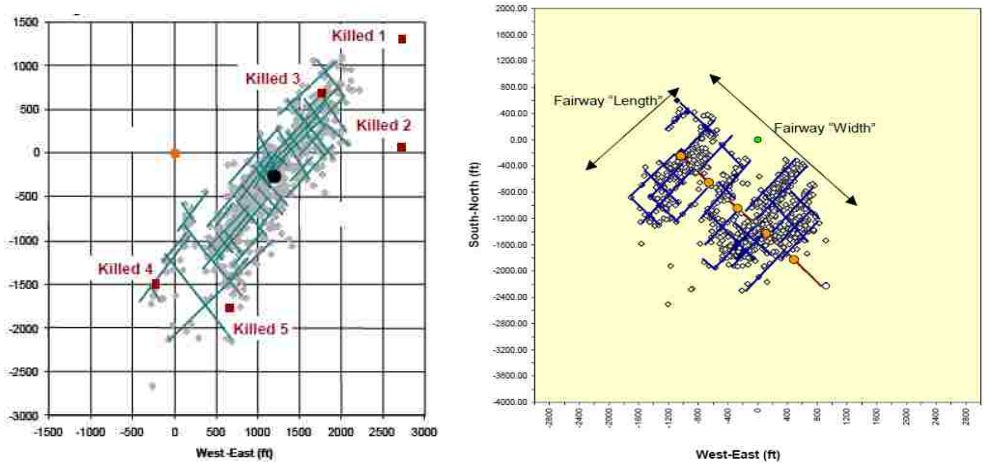

Figure 3.5. Microseismic Mapping in Barnett Shale showed the growth of fractures in a complex network pattern in two directions. (Fisher et al, 2004)

Gale et al (2007) conducted core studies on 4 vertical core samples from Barnett Shale. Through calculating the subcritical crack index of core samples, they concluded that the high subcritical crack index indicates that large open fractures exist in clusters spaced several hundred feet apart in Barnett Shale. Moreover, one of the core samples, T.P.Sim, showed oriented natural

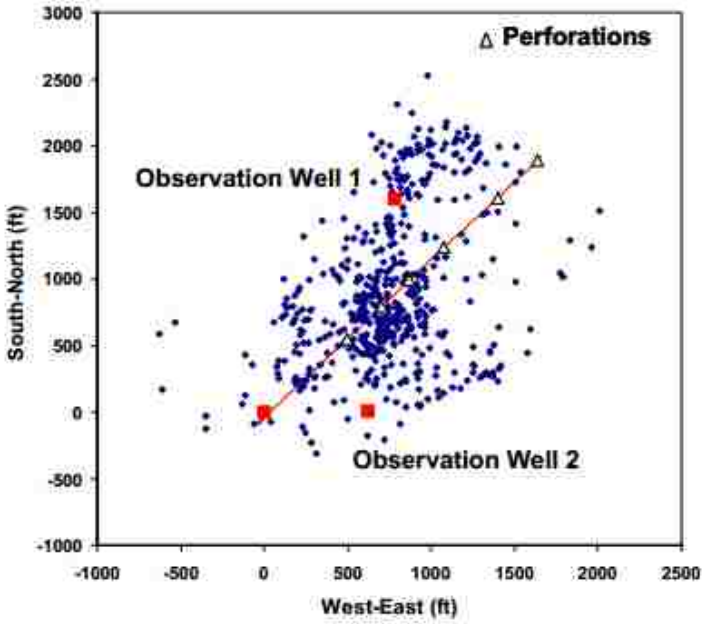

Figure 3.6. Microseismic Mapping in Warpinski et al (2005) showed a large areal network pattern of fracture growth in Barnett Shale

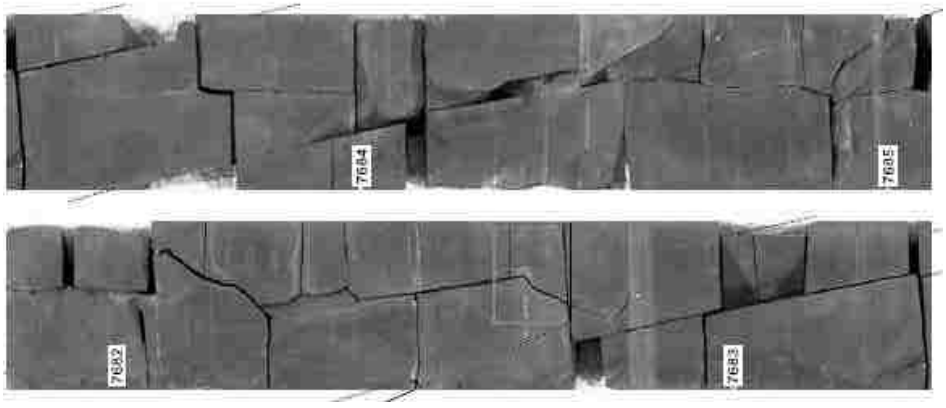

Figure 3.7.Barnett core samples showed oriented natural fractures intersecting at approximately 80^{o} (From Gale et al 2007)

fractures intersecting at approximately 80^{o} (Figure 3.7). Natural fractures tend to predominantly develop in the S_{Hmax} direction, but natural fractures orthogonal to present day S_{Hmax} can also be developed due to the fact that stress field may rotate during the long geological history of the formation, as discussed by Laubach et al (2004).

We propose to model natural fractures in this research as regionally developed natural fracture networks based on above results. Although natural fracture exists in different scales with lengths from microns to kilometers and with apertures from 0.1mm to 10 mm, here we are mainly interested in natural fractures with lengths and apertures comparable with those of hydraulic fractures. Thus, we ignore those small natural fractures here even if they could impact the growth of induced fractures and fluid flow. The scaling attributes of natural fractures (Marrett et al, 1999) indicates that fracture size is inversely proportional to its frequency, as it's documented by Papazis (2005) (Figure 3.8). Therefore, our modeling of natural fractures in Barnett Shale only considers natural fractures with comparable size of hydraulic fractures. Clustered natural fractures in Barnett Shale will be modeled as evenly spaced natural fracture with properties similar to the major natural fractures in the cluster.

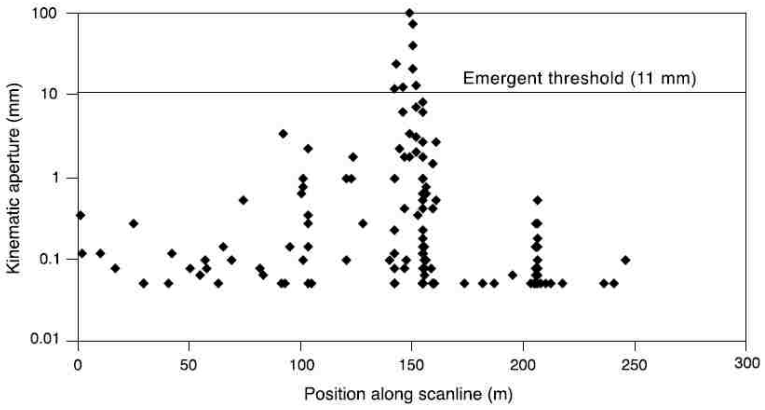

Figure 3.8. Fracture apertures in Barnett Shale showed widely spaced clusters along the scanline (Papazis 2005)

3.3 Well Configurations

Well P1 was one of the four wells drilled in this field. It was drilled vertically to a TVD of 8,531.4 ft and started the horizontal portion with an 8.33^{o}/100' dogleg rate. The well was drilled

up to a MD of 11,813.8 ft at a TVD of 8,660 ft. The horizontal section of the wellbore entirely lies within the lower Barnett formation, which is adjacent to Viola Limestone formation at the bottom. In addition to Well P1, three additional wells (Well P2, P3 and a monitoring well) were drilled in proximity of Well P1 with similar configurations. However, the monitoring well was a vertical well. Fracturing treatment in Well P1 was horizontally monitored from Well P2. Figure 3.9 below shows the configuration of four wells in the field.

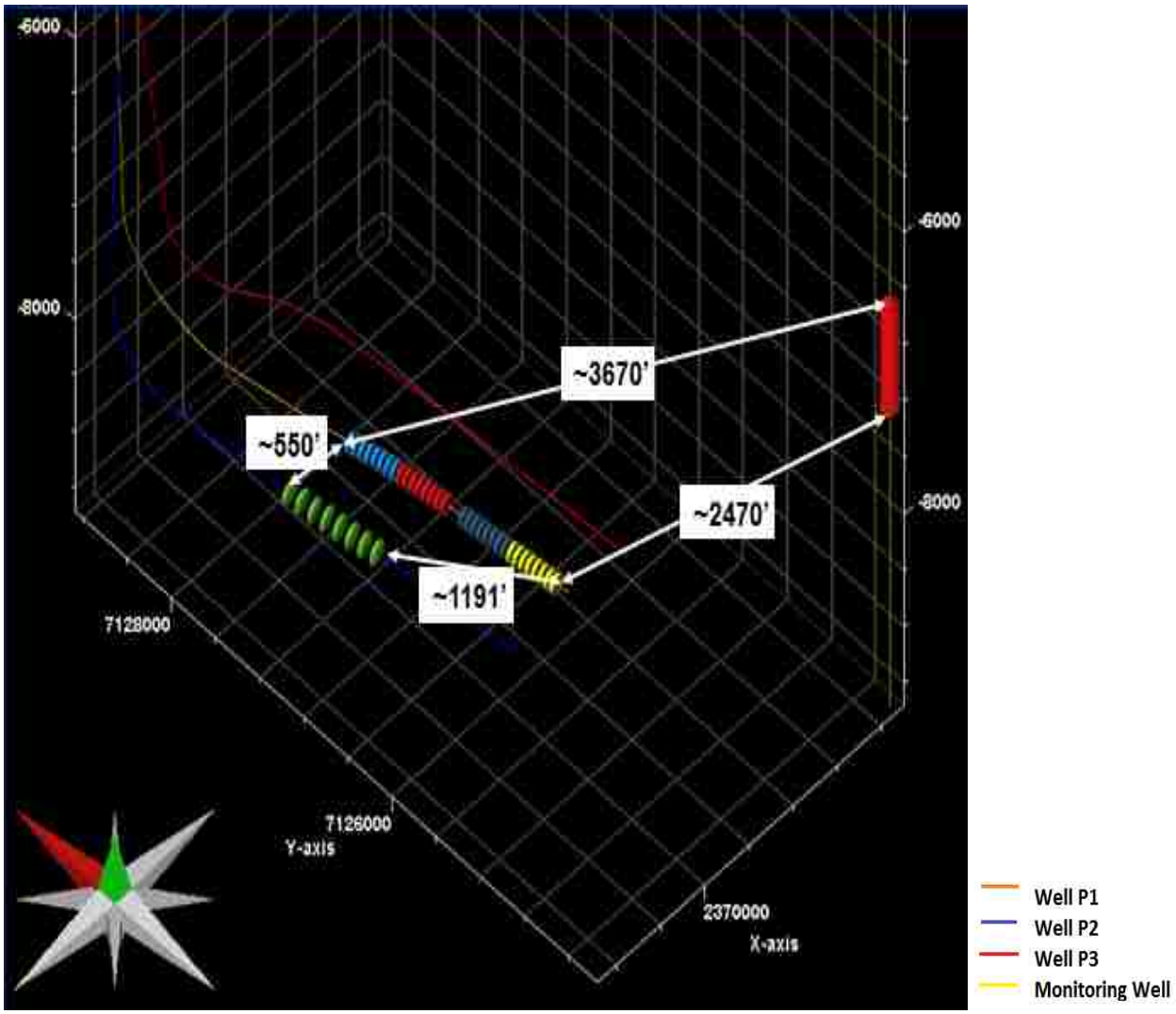

Figure 3.9. Well configurations in the field. Four stages of fracturing treatment were conducted in Well P1 (orange), and they were monitored from Well P2 (blue).

3.4 Fracturing Treatment History

The hydraulic fracturing treatment in Well P1 had four fracturing stages. Each perforation stage spans 350 ft in the horizontal section of the wellbore, and the perforation clusters contains 5 shots per foot at a 60^{o} phase angle. Fracturing fluid used in the treatment was slickwater, mixed with 100 Mesh Premium and 40/70 Ottawa Sand as proppants. The bottomhole pressure response, pumping rate and proppant concentration were provided by the operator, and were selectively demonstrated below. It's noteworthy that the Stage 3 of the well

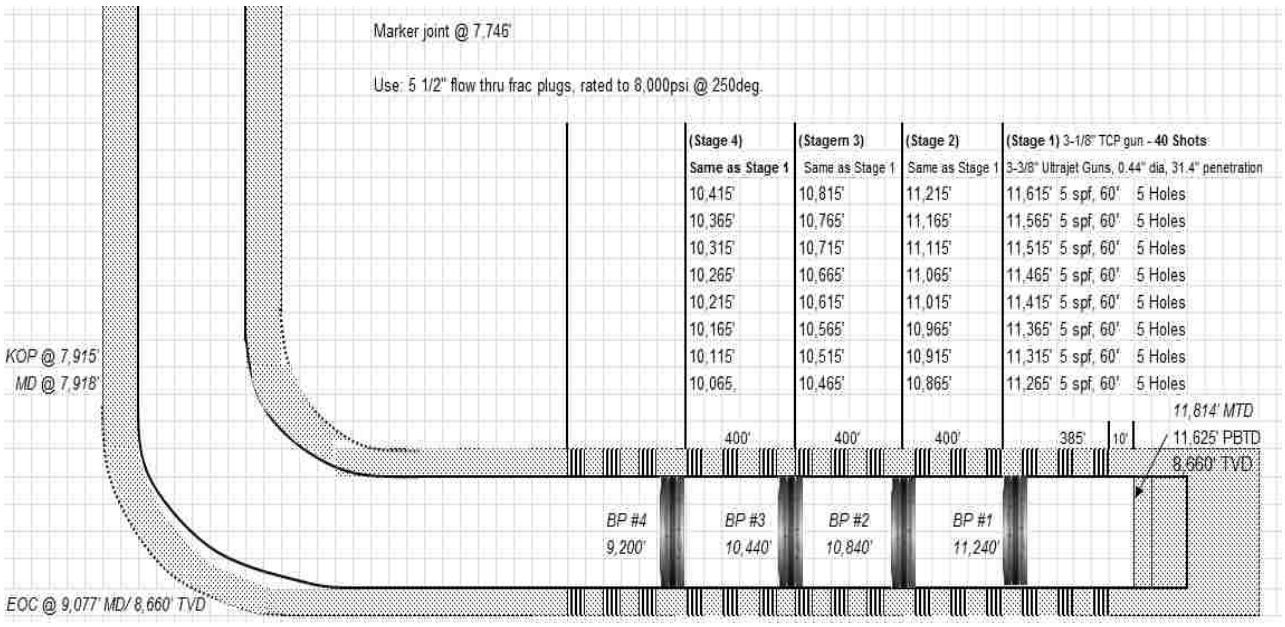

Figure 3.10. Perforation design for Well P1. There were a total of four fracturing stages for Well P1

contained an incorrect column of data and was missing bottom hole pressure history. Therefore, we will skip this stage and work on Stages 1,2 and 4. It has also been observed that the proppant was pumped in between different pumping stages. Rather than continuous adding proppant, this schedule allow for adequate time for proppant transporting by fracturing fluid and avoid screenouts while maintaining the same design objective for the treatment.

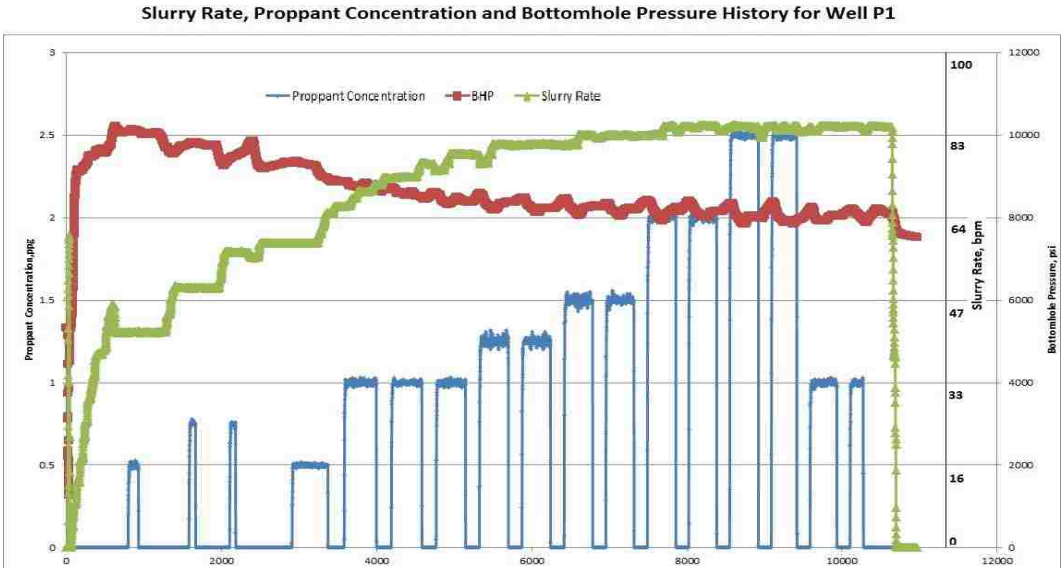

Figure 3.11. Botto hole pressure history, slurry rate and proppant concentration for stage 1, Well P1

3.5 Net Pressure Matching

Due to the fact that information provided by the operator was extremely limited, a number of other reservoir and well information is instrumental to the successful modeling of hydraulic fracturing and production. Information provided by the operator includes well survey, drilling report, well logs, treatment information, and microseismic monitoring data. On the other hand, information pertaining to the reservoir is quite limited. Among those unknown parameters, reservoir geomechanical properties, such as formation Young's Modulus, fluid loss coefficient, formation toughness, and Poisson's ratio must be determined in order to successfully model fracturing treatments. In this research, we used a numerical fracture simulator – StimPlan to build hydraulic fracturing models and perform net pressure matching based on the bottomhole pressure history from the treatment data. Parameters inferred from history matching will be used in subsequent chapters for building accurate models for forward modeling. Simulations that

consider Discrete Fracture Network (DFN), or networks of natural fractures, will be implemented in Chapter 5 of this thesis.

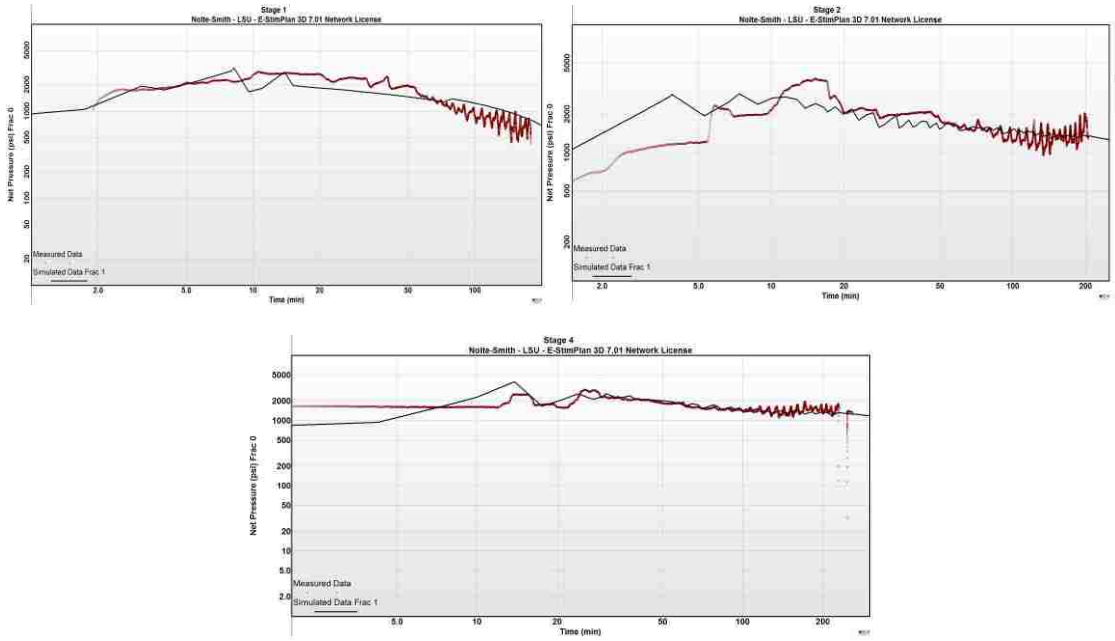

Figure 3.12. StimPlan net pressure matching for all three stages of Well P1

Table 3.1. Estimated Formation Geomechanical Properties

Formation Geomechanical Property	**Estimation**
Fluid Loss Coefficient	0.0015 ft/sqrt min
Young's Modulus	3.5 MM psi
Poisson's Ratio	0.33
Fracture Toughness	80,000
Stress Difference	3408 psi
Stress Gradient	0.65 psi/ft

Net pressure matching has shown close matches between simulated net pressure and measured net pressure. As it will be discussed in Chapter 5, the closure pressure of the formation has been estimated to be around 7400 psi. Based on this estimation, we have calculated the net

pressure responses from measured data, and conducted net pressure matching in StimPlan. The obtained formation geomechanical properties have been listed above, and will be used as the basis of forward modeling in subsequent chapters.

3.6 Conclusion

In this chapter, we have had an overview of the Barnett Shale, including its history, development, geological and geomechanical properties and natural fracture distribution. We have also proposed to model natural fractures in Barnett Shale as a network of natural fractures with properties similar to those of clustered natural fractures. In addition, the background information of Well P1 has also been introduced, including the well information, perforation design, and treatment information. In the next chapter, we will use microseismic data from the treatments to find the optimal representation of natural fracture networks.

Chapter 4: Numerical Modeling and Determination of Fracture Network

Despite huge capital investment on hydraulic fracturing treatments, there is no technology available for direct observation of fracture growth or geometry. Widespread lab measurements have shown that pre-existing natural fractures may profoundly impact the propagation of hydraulic fractures in the reservoirs. As discussed earlier, microseismic monitoring has been utilized widely to qualitatively locate fractures. Intersection of hydraulic fracture with natural fractures may generate string of double-couple microseismic events, which can be used as basis for fractures mapping. In this chapter, an optimization model is proposed to estimate the geometry of natural fracture network based on the location of double-couple events. This algorithm utilizes least overall squared error to estimate the natural fracture geometry based on the location of all microseismic events. Mathematical formulations will be proposed for both orthogonal and non-orthogonal natural fracture networks; corresponding models are validated with a set of hypothetical points, and thereafter the actual microseismic data from are imported into the model to produce a group of possible natural fracture realizations.

4.1 Microseismic Mapping in Hydraulic Fracturing

Microseismic mapping has been used to visualize the growth and geometries of hydraulic fractures. Techniques for monitoring and evaluating hydraulic fracturing range from the simplest pressure and rate measurements during the treatment to sophisticated microseismic mapping approach. Microseismic monitoring technique is preferred over traditional fracturing assessment technologies such as tiltmeter analysis and borehole imaging logs because of its capability of observing the fracture extension and height growth with direct visualization. Microseismic mapping technique is based on the principle that the propagation of hydraulic fracture will crack the formation rock and generate mini–earthquake with magnitude above -3 (Vermylen

and Zoback, 2011), also known as microseismic events, which can be detected by sensitive seismic receivers Results from microseismic mapping could not only reveal information regarding the fracturing treatment such as induced fracture height, length, and locations, but also affect the location, orientation, and spacing of future wells (Hulsey et al, 2011). Moreover, knowing the geometry and lateral extent of the induced fracture network also help operators to avoid legal issues related to fracture extension, such as unauthorized fracture trespassing into neighboring properties, which constitute illegal operation in some jurisdictions in United States (Hall and Dahi-Taleghani, 2014).

In microseismic mapping, arrays of seismic receivers are placed either on the surface or in neighboring offset wells in order to monitor and locate the microseismic events during the treatment. Typical receivers used in microseismic mapping include geophones and accelerometers, both of which are simple harmonic oscillators consist of a suspended proof mass connected with a damped spring. Accelerometers are sensitive for low frequency waves below 5 Hz, while geophones are sensitive to seismic waves between 5 Hz to 200 Hz (Hon et al., 2008). Due to the fact that microseismic events generated during hydraulic fracturing are usually above 10Hz in frequency, geophones are considered more sensitive and appropriate in microseismic fracture mapping. Despite the valuable information gathered from microseismic fracture mapping, the limitation of this technique lies in its inaccuracy. Detected microseismic events can contain "noise" information, which are events irrelevant to fracture propagation. On the other hand, the determination of microseismic event locations involves considerable amount of uncertainty. Maxwell (2009) conducted sensitivity analysis and used Monte Carlo simulations to estimate the measurement error of microseismic event location in Barnett Shale. In all cases, minor perturbations in velocity model, arrival time and directions lead to more than 200 ft

deviations (Maxwell, 2009). Thornton and Eisner (2011) has reported that at a depth of 7000 ft, average measurement errors for 85 microseismic events in X, Y, and Z direction were 76 ft, 106 ft and 116 ft, respectively. To avoid uncertainties in microseismic fracture mapping, the signal to noise ratio (SNR) can be used to filter the events prior to evaluation. A larger SNR ratio indicates that the location of an event has a higher level of confidence (Thornton and Eisner, 2011).

It is also important to note that not all detected microseismic events are related to fracture interaction. Both fracture propagation and interactions between natural fractures and hydraulic fractures will generate microseismic events. While microseismic mapping records the location of all events from fracture propagations and interactions, the moment tensor of the event can be used to identify the origin and characteristic of the event. Moment tensor identifies the radiation pattern of seismic energy from the epicenter of the event, which relates to the failure mode of the medium. Fracture tip propagation in the formation is considered as Mode I failure, which generates pure tensile moment tensor, or Compensated Linear Vector Dipole (CLVD). On the other hand, interactions between natural fractures and hydraulic fractures lead to Mode II or Mode III failure and generate double-couple microseismic events, or shear type events, which contains shear component in its moment tensor (Baig and Prince, 2010). By calculating and identifying shear component of the microseismic events, it's possible to determine whether the event is from fracture tip propagation or from the interaction between fractures.

4.2 Model Description and Mathematical Formulation

The model assumes that all microseismic events are located inside a hydrocarbon bearing reservoir, for which curvature along its length may be ignored as the reservoir only spans a tiny part on the earth. Moreover, this research primarily investigates the natural fracture distribution

in the x-y plane, thus our model doesn't take into account the vertical locations (depths) of the microseismic events. Therefore in this model, all microseismic events are distributed on a flat surface, which may be considered as the top-view of the rectangular reservoir. Each microseismic events will be assigned a coordinate (x,y) with respect to the origin (0,0), which may be selected to be the location of the wellbore. The optimized natural fracture network is more than likely to not passing through the origin (0,0), and the relative location of the natural fracture network with respect to the origin can be described by measuring the distance from the origin to the nearest natural fractures in positive x and y direction. It is also noteworthy that the origin and the overall coordinate system of the model can be selected arbitrarily, and corresponding microseismic event coordinates may be adjusted by transforming their original coordinates during microseismic monitoring.

The principle of least squares is used to evaluate the degree of fitness of natural fracture realizations in this model. In addition to propagating hydraulic fractures, interactions between induced hydraulic fractures and pre-existing natural fractures also generate microseismic events. Although both will be monitored and recorded with microseismic mapping technique, shear type, or double couple microseismic events, can be distinguished from those induced by propagating hydraulic fractures, or CLVD events. Therefore, the geometry of natural fracture network can be inferred by observing these shear type microseismic events only. The mathematical modeling procedure therefore attempts to generate and evaluate natural fracture realizations based on the location of shear type microseismic events; in other words, it was assumed that large magnitude of shear events will occur at the intersection of hydraulic fractures with natural fractures. Here, the minimum distance between a microseismic event and surrounding natural fractures is defined as the smallest perpendicular distance between the point and four sides of the grid block around

that point (Figure 4.1). Accordingly, the criteria of evaluating the fitness of natural fracture realizations will be the total minimum distance squares of all microseismic events, which is the sum of minimum squared distances for all microseismic points. Moreover, an additional constraint in our model is that it is necessary to set a minimum distance between fracture grids in the model, which is consistent with outcrop studies for statistical properties of natural fractures. Theoretically, total squared distance for all microseismic events can be infinitely small if the natural fracture spacing is infinitely reduced. If every microseismic event has a piece of natural fracture passing through, the total squared distance will become zero. However, this scenario is unrealistic in both hydraulic fracturing and natural fracture distribution pattern, and inherent uncertainties involved in locating microseismic events also make total squared distance assumption unrealistic with excessively small fracture spacing. Therefore, we need to set constraints that regulate the spacing of fracture grids within a reasonable range. Thus, the objective of this chapter is to develop a mathematical model to configure the natural fracture realization that will have minimum total squared distance between microseismic event points and their adjacent grids while subject to the minimum distance constraint between the natural fracture grids.

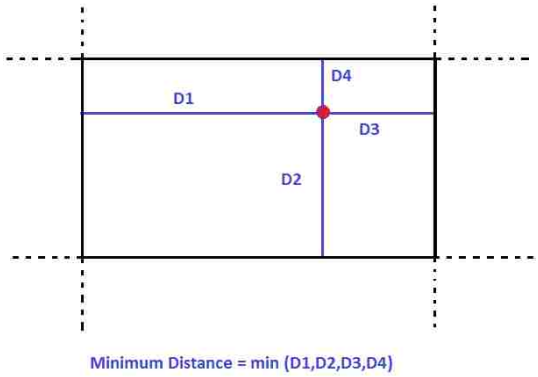

Figure 4.1. The concept of minimum distance, the smallest perpendicular distances bwteen the microseismic point and four adjacent grids (smallest of D1, D2, D3 and D4)

In the following section, we will derive mathematical formulations for calculating the minimum total distance square for both orthogonal and non-orthogonal natural fracture configurations. These will be the basis for developing objective functions for conducting optimization in MatLab Optimization GUI Toolbox.

Orthogonal Natural Fracture Network

We propose the following nomenclature for model description and constraining equalities/inequalities:

Input Variables:

- (x_i, y_i) : The coordinate of the i^{th} microseismic events
- (d_{xmin}, d_{ymin}): Minimum distances of neighboring natural fracture in x and y direction

Output (Decision) Variables:

- (d_x,d_y): Optimal spacing between vertical and horizontal natural fractures in positive x and y direction
- (Δ_x, Δ_y): Relative Displacement - Distance from (0,0) to the nearest natural fractures in positive x and y direction

Suppose there is a microseismic point (x_i, y_i) locating in a rectangle formed by four pieces of natural fractures (as shown in Figure 4.1), then the nearest 2 vertical fractures surrounding this point will pass through

$$\left((\Delta_x + \left\lfloor \frac{x_i - \Delta_x}{d_x} \right\rfloor d_x, 0\right) \text{ and } \left(\Delta_x + \left\lceil \frac{x_i - \Delta_x}{d_x} \right\rceil d_x, 0\right), \tag{4.1}$$

in which $\lfloor\ \rfloor$ and $\lceil\ \rceil$ indicate floor and ceil operation; i.e. the greatest integer smaller than a certain number and the smallest integer greater than a certain number. Similarly, the nearest 2 horizontal fractures surrounding this microseismic point will be intersecting the vertical axis at:

$$\left(0, \Delta_y + \left\lfloor \frac{y_i - \Delta_y}{d_y} \right\rfloor d_y\right) \text{and } \left(0, \Delta_y + \left\lceil \frac{y_i - \Delta_y}{d_y} \right\rceil d_y\right) \tag{4.2}$$

By inferring the nearest natural fractures that enclose the microseismic point (x_i, y_i) in the form of a parallelogram, we will be able to calculate the smallest distance between this point and the surrounding natural fractures. Therefore, the perpendicular distances between a microseismic point and its 2 nearest vertical fractures will be:

$$\left| x_i - \Delta_x - \left\lfloor \frac{x_i - \Delta_x}{d_x} \right\rfloor d_x \right|, \tag{4.3}$$

and

$$\left| \Delta_x + \left\lceil \frac{x_i - \Delta_x}{d_x} \right\rceil d_x - x_i \right| \tag{4.4}$$

where the absolute sign above eliminates the possibility of having negative distance. Similarly, the perpendicular distances between a microseismic event and its nearest 2 horizontal fractures will be:

$$\left| y_i - \Delta_y - \left\lfloor \frac{y_i - \Delta_y}{d_y} \right\rfloor d_y \right| \tag{4.5}$$

and

$$\left| \Delta_y + \left\lceil \frac{y_i - \Delta_y}{d_y} \right\rceil d_y - y_i \right| \tag{4.6}$$

Given the locations of all microseismic events in our model, we can now formulate our least-square optimization problem and its constraining equalities/inequalities according to the formulations above. The objective function in this optimization problem is to calculate and minimize Z, the sum of the minimum distance square for all microseismic events:

$$\begin{aligned} Z = Min \sum_{i=1}^{n} Min \Bigg(& \left| x_i - \Delta_x - \left\lfloor \frac{x_i - \Delta_x}{d_x} \right\rfloor d_x \right|^2, \quad \left| \Delta_x + \left\lceil \frac{x_i - \Delta_x}{d_x} \right\rceil d_x - x_i \right|^2, \\ & \left| y_i - \Delta_y - \left\lfloor \frac{y_i - \Delta_y}{d_y} \right\rfloor d_y \right|^2, \left| \Delta_y + \left\lceil \frac{y_i - \Delta_y}{d_y} \right\rceil d_y - y_i \right|^2 \Bigg) \end{aligned} \tag{4.7}$$

Subject to the following constraints:

1. Minimum spacing constraints:

$$d_x \geq d_{x\min}, d_y \geq d_{y\min} \tag{4.8}$$

2. Relative displacement constraints:

$$\Delta_x < d_x, \ \Delta_y < d_y \tag{4.9}$$

3. Non-negative constraints:

$$d_x, d_y, \Delta_x, \Delta_y \geq 0 \tag{4.10}$$

Non - Orthogonal Natural Fracture Network

We propose the following nomenclature for model description and constraining equalities/inequalities (Figure 4.3):

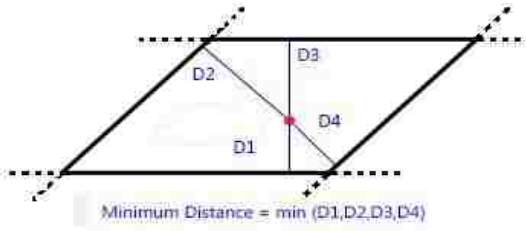

Figure 4.2. Minimum distance in a non-orthogonal natural fracture grid is the perpendicular distance from the point to four adjacent grids.

Input Variables:

- (x_i, y_i) : The coordinate of the ith microseismic events
- (d_{xmin}, d_{ymin}): Minimum distances of neighboring natural fracture in x and y direction

Output (Decision) Variables:

- (d_x,d_y): Optimal spacing between vertical and horizontal natural fractures in positive x and y direction
- (Δ_x, Δ_y): Distance from (0,0) to the nearest natural fractures in positive x and y direction
- (ϑ_x, ϑ_y): Angle between horizontal (vertical) natural fractures and positive x (y) direction

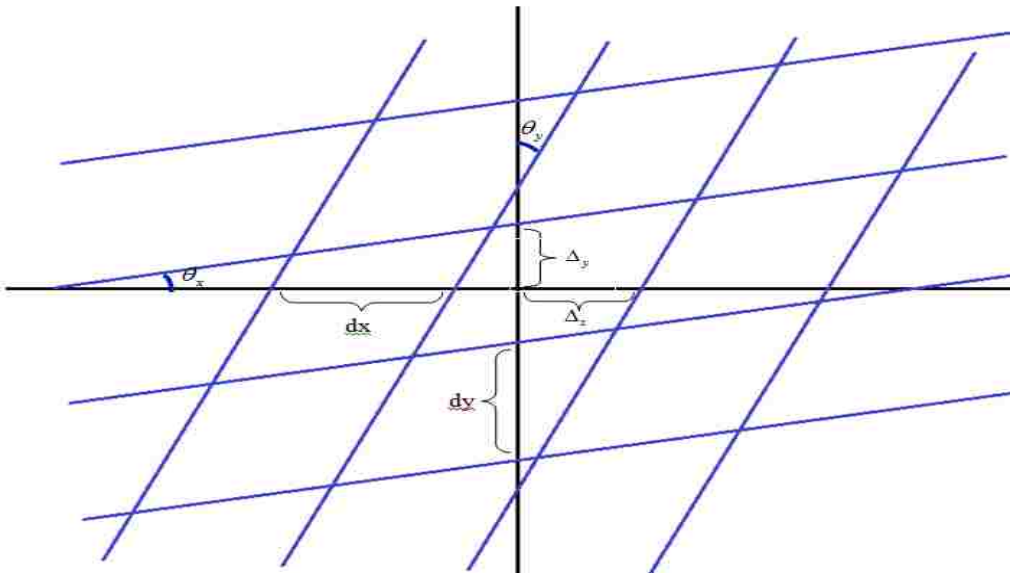

Figure 4.3. Optimal natural fracture configuration and decision (output) variables

Suppose there is a microseismic point (x_i, y_i) locating in a parallelogram formed by four pieces of natural fractures (as shown in Figure 4.2 and Figure 4.3), then the nearest 2 vertical fractures surrounding this point will pass through

$$\left(\Delta_x + \left\lfloor \frac{x_i - y_i \tan \vartheta_y - \Delta_x}{d_x} \right\rfloor d_x, 0\right) \text{ and } \left(\Delta_x + \left\lceil \frac{x_i - y_i \tan \vartheta_y - \Delta_x}{d_x} \right\rceil d_x, 0\right), \qquad (4.11)$$

in which $\lfloor\ \rfloor$ ($\lceil\ \rceil$) indicates floor (ceil) operation; i.e., the greatest integer smaller than a certain number and the smallest integer greater than a certain number. Similarly, the nearest 2 horizontal fractures surrounding this microseismic point will be intersecting the vertical axis at:

$$\left(0, \Delta_y + \left\lfloor \frac{y_i - x_i \tan \theta_x - \Delta_y}{d_y} \right\rfloor d_y\right) \text{and} \left(0, \Delta_y + \left\lceil \frac{y_i - x_i \tan \theta_x - \Delta_y}{d_y} \right\rceil d_y\right) \qquad (4.12)$$

By inferring the nearest natural fractures that enclose the microseismic point (x_i, y_i) in the form of a parallelogram, we will be able to calculate the smallest distance between this point

and the surrounding natural fractures. Therefore, the perpendicular distances between a microseismic point and its 2 nearest vertical fractures will be:

$$\left| x_i - y_i \tan \vartheta_y - \Delta_x - \left\lfloor \frac{x_i - y_i \tan \vartheta_y - \Delta_x}{d_x} \right\rfloor d_x \right| \cos \vartheta_y \tag{4.13}$$

and

$$\left| \Delta_x + \left\lceil \frac{x_i - y_i \tan \vartheta_y - \Delta_x}{d_x} \right\rceil d_x - x_i + y_i \tan \vartheta_y \right| \cos \vartheta_y \tag{4.14}$$

where the absolute sign in the formulation eliminates the possibility of having negative distance. Similarly, the perpendicular distances between a microseismic event and its nearest 2 horizontal fractures will be:

$$\left| y_i - x_i \tan \theta_x - \Delta_y - \left\lfloor \frac{y_i - x_i \tan \theta_x - \Delta_y}{d_y} \right\rfloor d_y \right| \cos \vartheta_x \tag{4.15}$$

and

$$\left| \Delta_y + \left\lceil \frac{y_i - x_i \tan \theta_x - \Delta_y}{d_y} \right\rceil d_y - y_i + x_i \tan \theta_x \right| \cos \vartheta_x \tag{4.16}$$

Given the locations of all microseismic events in our model, we can now formulate our least-square optimization problem and its constraining equalities/inequalities according to the formulations above. The objective function in this optimization problem is to calculate and minimize Z, the sum of the minimum distance square for all microseismic events:

$$Z = Min \sum_{i=1}^{n} Min \left(\left| x_i - y_i \tan \vartheta_y - \Delta_x - \left\lfloor \frac{x_i - y_i \tan \vartheta_y - \Delta_x}{d_x} \right\rfloor d_x \right|^2 \cos^2 \vartheta_y , \right.$$
$$\left| \Delta_x + \left\lceil \frac{x_i - y_i \tan \vartheta_y - \Delta_x}{d_x} \right\rceil d_x - x_i + y_i \tan \vartheta_y \right|^2 \cos^2 \vartheta_y ,$$
$$\left| y_i - x_i \tan \theta_x - \Delta_y - \left\lfloor \frac{y_i - x_i \tan \theta_x - \Delta_y}{d_y} \right\rfloor d_y \right|^2 \cos^2 \vartheta_x ,$$
$$\left. \left| \Delta_y + \left\lceil \frac{y_i - x_i \tan \theta_x - \Delta_y}{d_y} \right\rceil d_y - y_i + x_i \tan \theta_x \right|^2 \cos^2 \vartheta_x \right) \quad (4.17)$$

Subject to the following constraints:

1. Minimum spacing constraints:
$$d_x \geq d_{x\min}, d_y \geq d_{y\min} \quad (4.18)$$
2. Relative displacement constraints:
$$\Delta_x < d_x, \ \Delta_y < d_y \quad (4.19)$$
3. Non-negative constraints:
$$d_x, d_y, \Delta_x, \Delta_y \geq 0 \quad (4.20)$$
4. Limitation of Angles – 45^o maximum in both directions:
$$-45^o < \vartheta_x, \vartheta_y < 45^o \quad (4.21)$$

4.3 Model Verification

A simple set of data was imported into the model to verify its correctness and applicability. Six points were randomly selected to verify the model proposed above and validate the applicability of the optimization procedure, and ϑ_x , ϑ_y were also pre-set to 0 in order to verify the model under simplest condition. In other words, we are considering orthogonal fracture network for this test case. In this base case, distance between neighboring grids was arbitrarily set to 5 in both directions, and a set of orthogonal grids were arbitrarily set to be passing through the origin (i.e. $\Delta x = \Delta y = 0$). Calculations based on the formulations above

resulted in a total minimum distance square of 15. This result will be verified against the subsequent optimization model, which should theoretically generate smaller or equal total distance square value.

Table 4.1. Total Distance Square Calculation for Base Case

Point #	xi	yi	d_x	d_y	Δx	Δy	Distance Left	Distance Right	Distance Lower	Distance Upper	Distance Square
			5	5	0	0					
1	9	16					4	1	1	4	1
2	18	13					3	2	3	2	4
3	7	9					2	3	4	1	1
4	2	3					2	3	3	2	4
5	13	17					3	2	2	3	4
6	16	8					1	4	3	2	1
										Sum	15

The optimization procedure was conducted in MatLab Optimization GUI Toolbox. An objective function was developed based on the equations in the previous chapter. Results from the optimization showed that the total distance square can be drastically reduced to only 0.2 by setting d_x, d_y, Δ_x, and Δ_y to 5.4, 8, 1.9 and 0, respectively. In order to stay closely consistent with the base case, the minimum grid spacing in this optimization was held at 5 in both directions.

For the next model verification, a set of four points forming a parallelogram is being tested. Theoretically, the optimal non-orthogonal natural fracture network should pass through these four points by forming a parallelogram (Figure 4.6). Through optimization in MatLab, it was accurately calculated that d_x,d_y, Δx, Δy, ϑ_x, ϑ_y should be 1,1,1,1,45 and 0 respectively in order to achieve a minimized total distance square of 0, as demonstrated in Figure 4.7. Therefore, it has been ascertained that our optimization model would correctly minimize the total distance square for non-orthogonal natural fracture realizations.

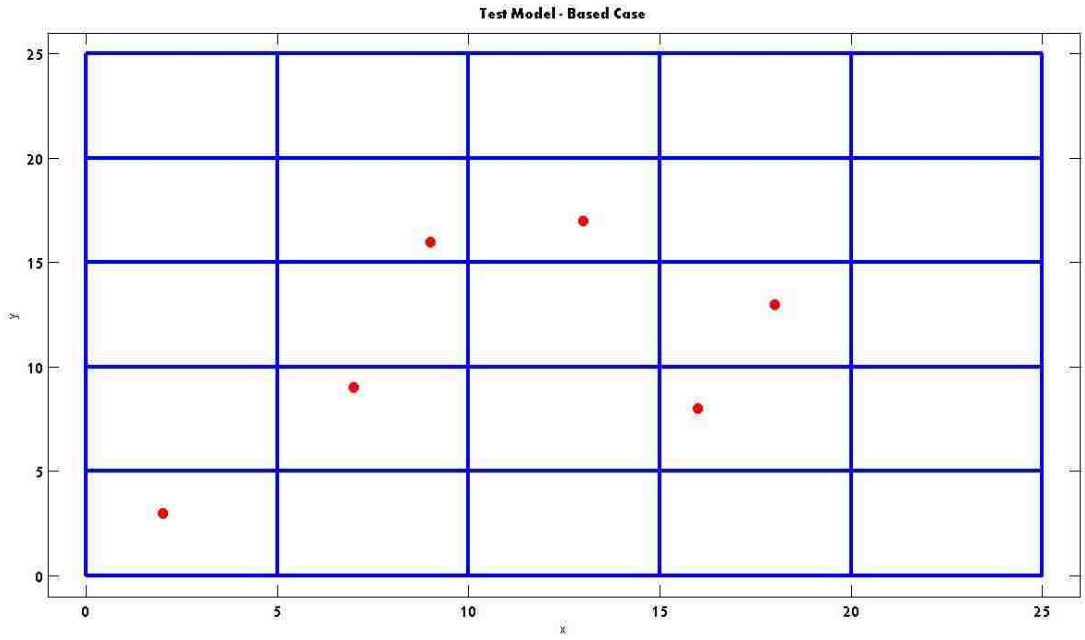

Figure 4.4. Fracture realization for model verification – base case

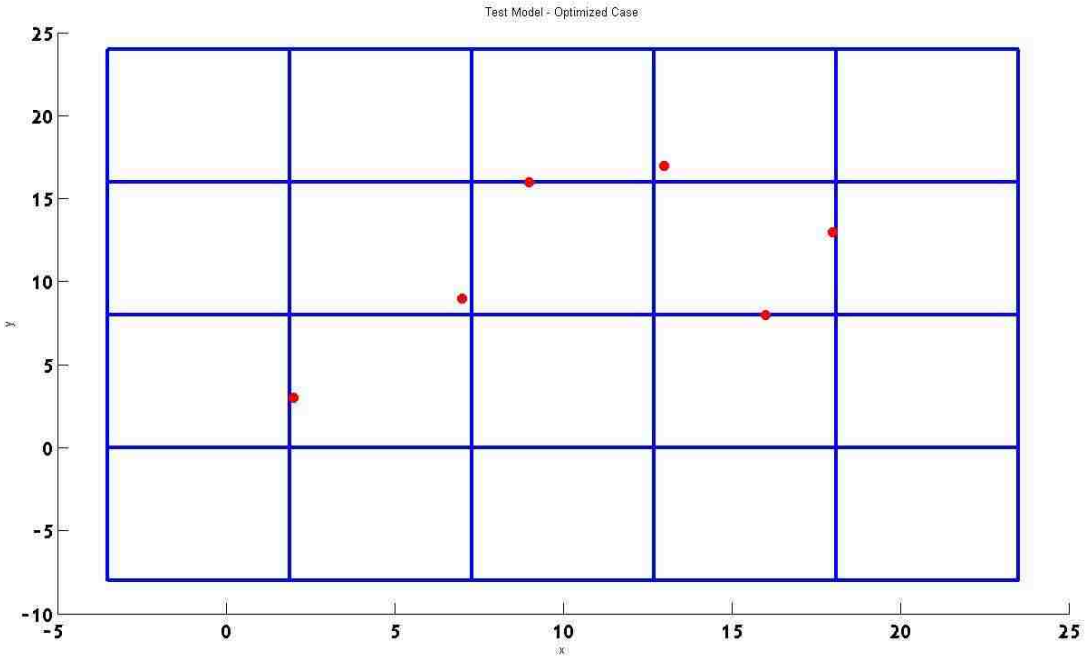

Figure 4.5. Fracture realization for model verification – optimized case

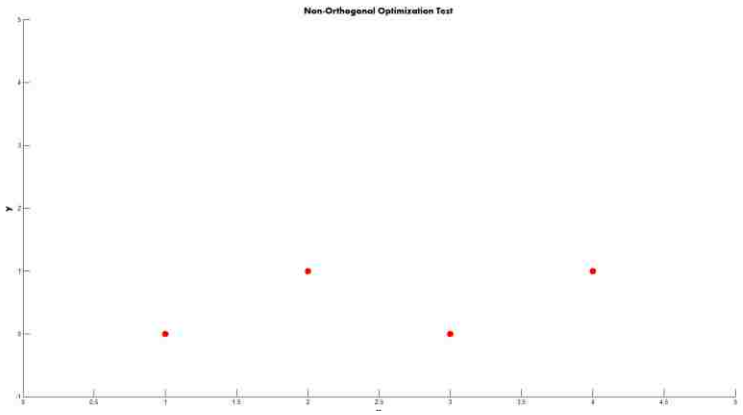

Figure 4.6. Four points forming a parallelogram in non-orthogonal optimization test

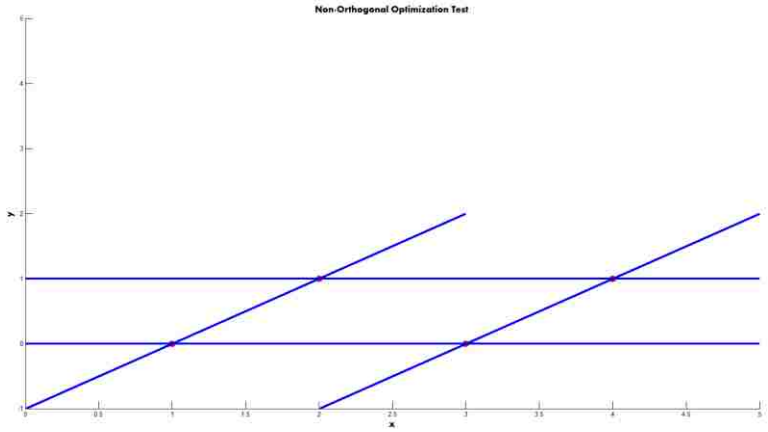

Figure 4.7. Result for non-orthogonal optimization test

4.4 Field Application – Generating Natural Fracture Realizations

The microseismic data for treatment stages 1 – 4 of Well P1 was preprocessed prior to conducting least-square modeling for generating natural fracture realization. Only shear-type microseismic events (or double couple microseismic events), which are related to interactions between natural fractures and hydraulic fractures, were retained. Moreover, signal to noise ratio (SNR) and Noise Level information was used to remove those events with high levels of uncertainty. Only those events with a SNR above 3.5 and a noise level below 300 were kept for

least square modeling. After pre-processing, there were a total number of 1,585 microseismic events, or approximately 72% of the original number of events; these events will subsequently be used in least-square optimization to generate natural fracture realizations.

We first attempt to generate an orthogonal natural fracture realization based on a minimum natural fracture spacing of 50 ft. This minimum natural fracture spacing value was selected by considering the fact that that formation height of this formation is approximately 400 ft and that the area over which microseismic events spanned is approximately 1,300 ft by 2,500 ft, and uncertainties in locating microseismic events are generally greater than 50 ft (Maxwell, 2009; Dahi Taleghani and Lorenzo, 2011). Therefore, 50 ft minimum fracture spacing ensures that the natural fracture realization we built bears sufficient resolution and is representative of the major formation characteristic.

The optimization was performed using MatLab Optimization GUI tool. Objective function was first developed according to the equations in the previous chapter, and constraints were also specified based on the rule of thumb for output parameters listed. It is also noteworthy that MatLab Optimization tool has 4 built-in optimization algorithms – Interior Point, SQP, Active Set and Trust region reflective. In order to obtain the best solution possible, all four algorithms will be used to select the best results. It has been observed through the optimization process that the Trust Region Reflective method is always more reliable in finding the optimal objective function values. This method uses Constraint Nonlinear Minimization (fmincon) option to find the smallest function value of the objective function. Trust region reflective is an algorithm that approximates a quadratic surface model to iteratively solve for optimization objective functions within the trust region (Yuan, 2000).

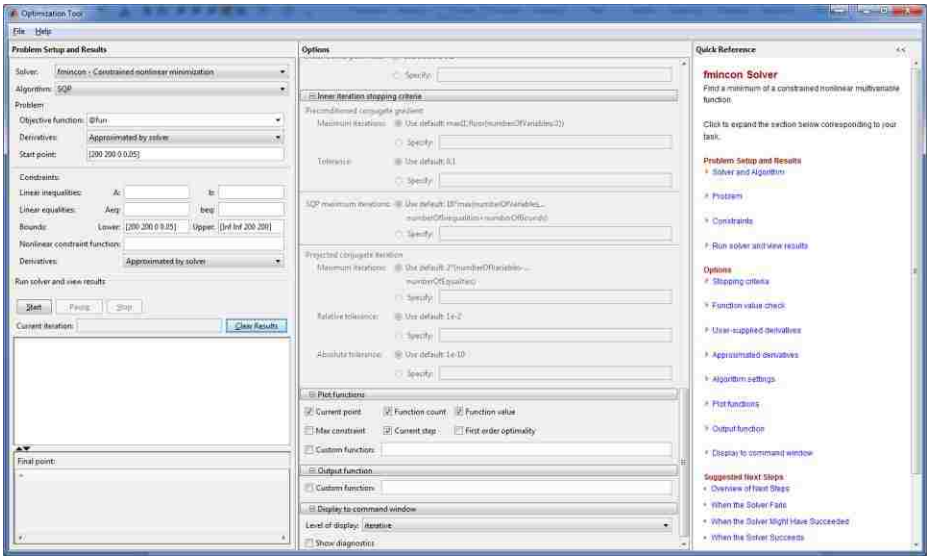

Figure 4.8. Model setup in MatLab optimization GUI toolbox

Results from optimization showed that the optimum natural fracture realization would result in a total minimum distance square of 0.158×10^{6} with d_x,d_y, Δx and Δy values listed below. It has been expected that the total minimum distance square will be reduced if fracture spacing is decreased, as microseismic points will generally get closer to its surrounding grids. Therefore, we expect that the optimized fracture spacing around the minimum fracture spacing value specified. Below in Table 4.2, the fracture spacing in north-south and east-west directions, as well as their orientations with respect to north-south and east-west directions, are presented in a table format with an accuracy of 3 decimal places. This information will allow for accurate modeling of natural fracture geometries in subsequent forward modeling of hydraulic fracturing and numerical simulation of hydrocarbon production within this naturally fractured reservoir.

Table 4.2. Optimization Results for Orthogonal Natural Fracture Realization

dx	**dy**	**Δx**	**Δy**
50.086 ft	50.018 ft	39.425 ft	23.976 ft

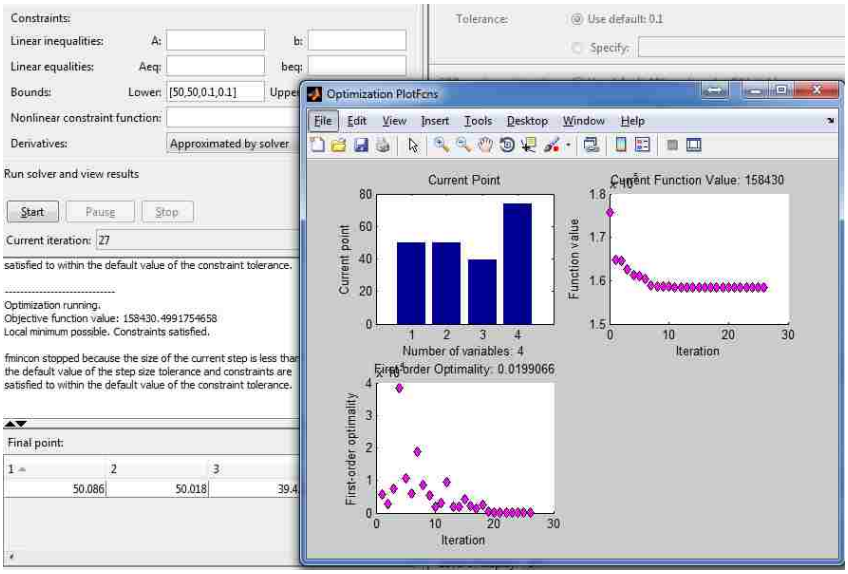

Figure 4.9. Optimization in MatLab GUI for orthogonal natural fracture realization

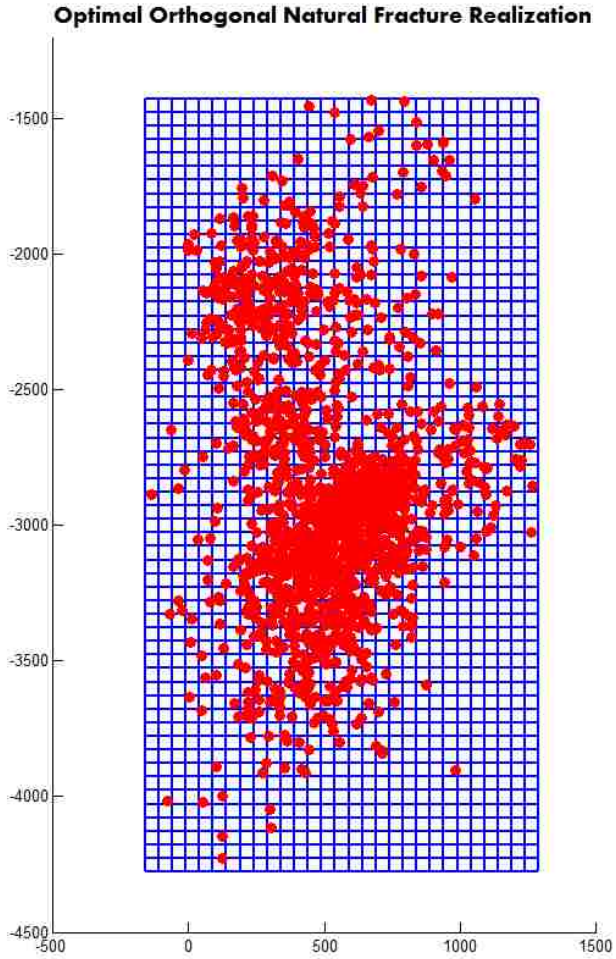

Figure 4.10. Optimized orthogonal natural fracture realization

Next, we attempt to generate an optimized non-orthogonal natural fracture realization based on the same 50 ft minimum fracture spacing requirement. Theoretically, since the condition of the fracture angle is relaxed, this non-orthogonal realization should result in a smaller or equal total minimum distance square compared to that of the orthogonal realization. Similar objective function was developed according to the formulations in 4.2, and the MatLab Optimization GUI obtained the following optimized natural fracture configuration. The total minimum distance square in this case was 0.085×10^6, a 46.2 % reduction from that of the orthogonal natural fracture realization.

Table 4.3. Optimization Results for Non - Orthogonal Natural Fracture Realization

$\mathbf{d_x}$	$\mathbf{d_y}$	$\Delta\mathbf{x}$	$\Delta\mathbf{y}$	θ_x	θ_y
50	55.541	2.154	33.712	0	-44.809

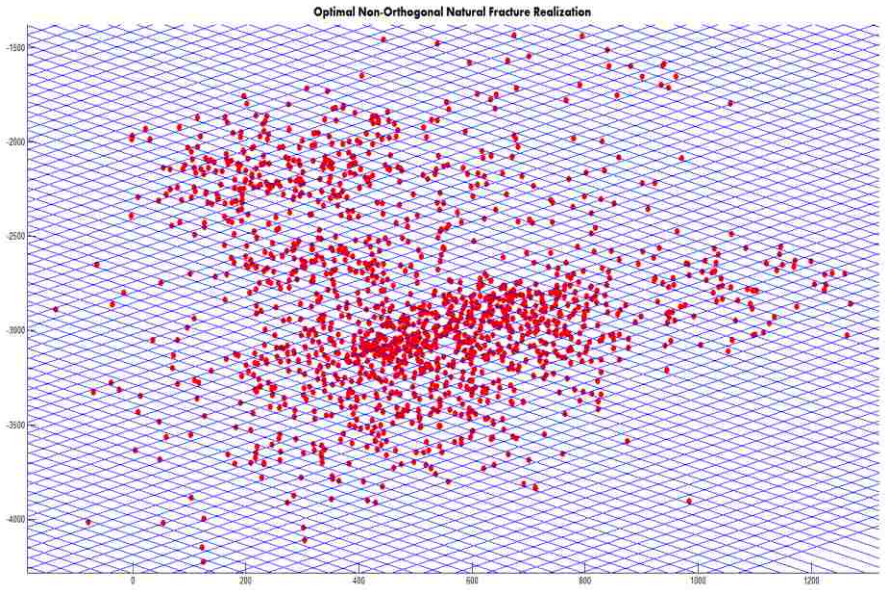

Figure 4.11. Optimized non-orthogonal natural fracture realization

It can be observed from field observation and outcrop studies that natural fractures are usually intersecting at a certain angle, such as 60° and 90°. Our optimization model previously proposed can be modified to produce such natural fracture realizations in which natural fractures are intersecting at a certain angle. However, by constraining the intersecting angle of the natural fractures, the objective of minimizing the total distance square could not be achieved. Under the same minimum fracture spacing requirement, the resulting total distance square will be greater or equal to that obtained from less-restrictive optimization in which natural fractures can be intersected at any angle.

By setting $\theta_x = -\theta_y$, we will be able to construct and optimize a natural fracture realization in which natural fractures are intersecting at 90°. This can be done by simply modifying the objective function in the previous example and let $\theta_x = -\theta_y$. Through the same optimization process, a "rotated" orthogonal natural fracture realization is established as shown in Table 4.4 and Figure 4.12 below. The minimized total distance square is 0.107×10^6, a 32.2% decrease from the first orthogonal case and 20.5 % increase from the second non-orthogonal case. Therefore, we can conclude that by relaxing one or more constraints in least square natural fracture modeling, it's possible to reach more reliable optimization results. Adding additional constraints to the problem, on the other hand, will lead to less optimal objective function value

Table 4.4: Optimization Results for 90° Intersecting Natural Fracture Realization

$\mathbf{d_x}$	$\mathbf{d_y}$	$\Delta\mathbf{x}$	$\Delta\mathbf{y}$	θ_x	θ_y
58.591	59.967	1.311	0.728	44.482	-44.482

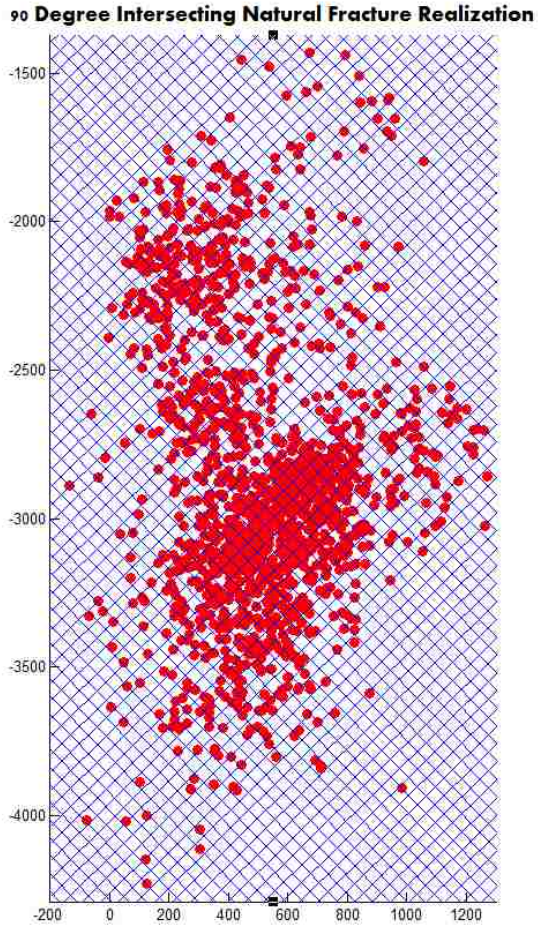

Figure 4.12. Optimized 90^o intersecting non-orthogonal natural fracture realization (graph scale adjusted to better show perpendicularity)

We may also generate natural fracture realizations in which natural fractures could be intersecting at any specific angle. This can be done by setting an additional constraint between θ_x and θ_y. However, due to this additional constraint, we would expect a higher optimized total distance square than that of the optimized case with no constraints on θ_x and θ_y. Below, we construct a natural fracture realization in which natural fractures are intersecting at 60^o. This can be easily done by modifying our previously developed objective function such that $\theta_y = 30^o - \theta_x$

. The optimized distance square in this case is 0.135×10^6, a 16.45% decrease from the first orthogonal case and 37.03% increase from the second non-orthogonal case.

Table 4.5. Optimization Results for 90° Intersecting Natural Fracture Realization

$\mathbf{d_x}$	$\mathbf{d_y}$	$\Delta\mathbf{x}$	$\Delta\mathbf{y}$	θ_x	θ_y
50.676	56.983	0.002	0	-45	75

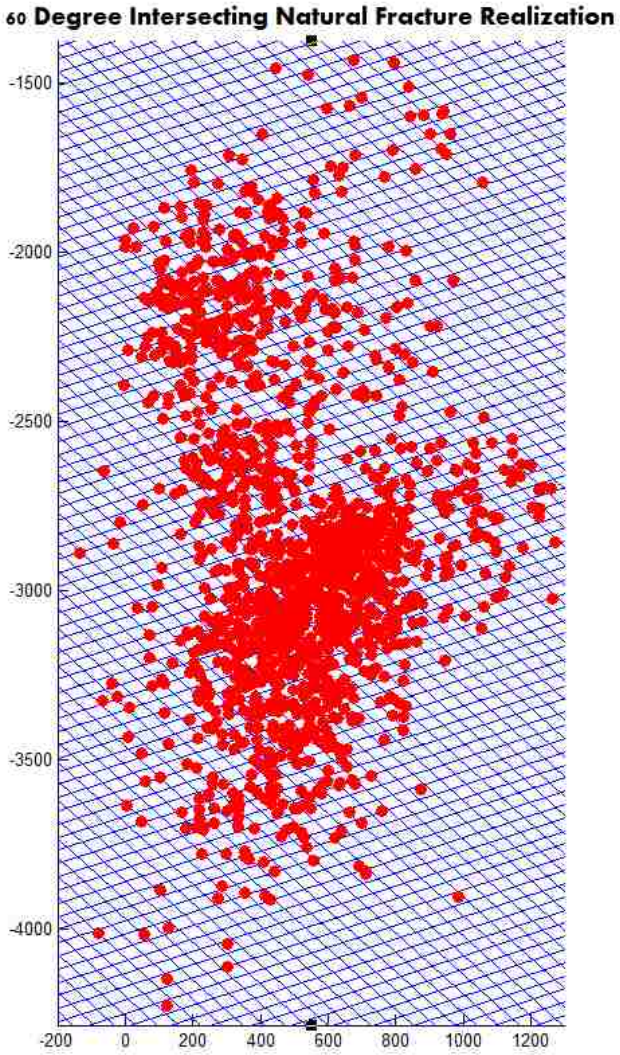

Figure 4.13. Optimized 60° intersecting non-orthogonal natural fracture realization

4.5 Adaptive Spacing and Partial Network Refinement of Fracture Gridding System

In this section, we present two algorithms to more precisely model the distribution of natural fractures based on the location of double-couple microseismic events. It has been observed from the microseismic map that the majority of recorded microseismic events are clustered in the center of the wellbore. Due to the high treatment pressure near the wellbore, minor cemented natural fractures are more likely to be reactivated together with major cemented natural fractures. On the other hand, as distance from the wellbore becomes larger, a much smaller number of cemented natural fractures could be reactivated due to much smaller treating pressure. Therefore, an adaptive spacing algorithm can be developed to account for clustered microseismic events. Clustered microseismic events are first sorted out from non-clustered events, and least square optimization algorithm described before was performed on both sets of microseismic events with a smaller spacing in clustered events. This adaptive spacing algorithm could more accurately model natural fracture reactivation near the wellbore, and overall squared error for this adaptive spacing optimization can be significantly reduced. Orthogonal adaptive spacing algorithm generated an overall squared error of 0.038×10^{6}, which is significantly smaller than the overall squared error for uniform spacing orthogonal natural fracture realization (Figure 4.14). Similarly, algorithms for optimizing non-orthogonal gridding system have been developed based on the same formulations. Optimization results showed that non-orthogonal adaptive spacing algorithm also generated a much smaller overall squared error of 0.021×10^{6} (Figure 4.15). Overall, these further improvements in modeling natural fracture distributions could more accurately describe the characteristics of natural fractures and lead to more reliable modeling and simulation outcomes.

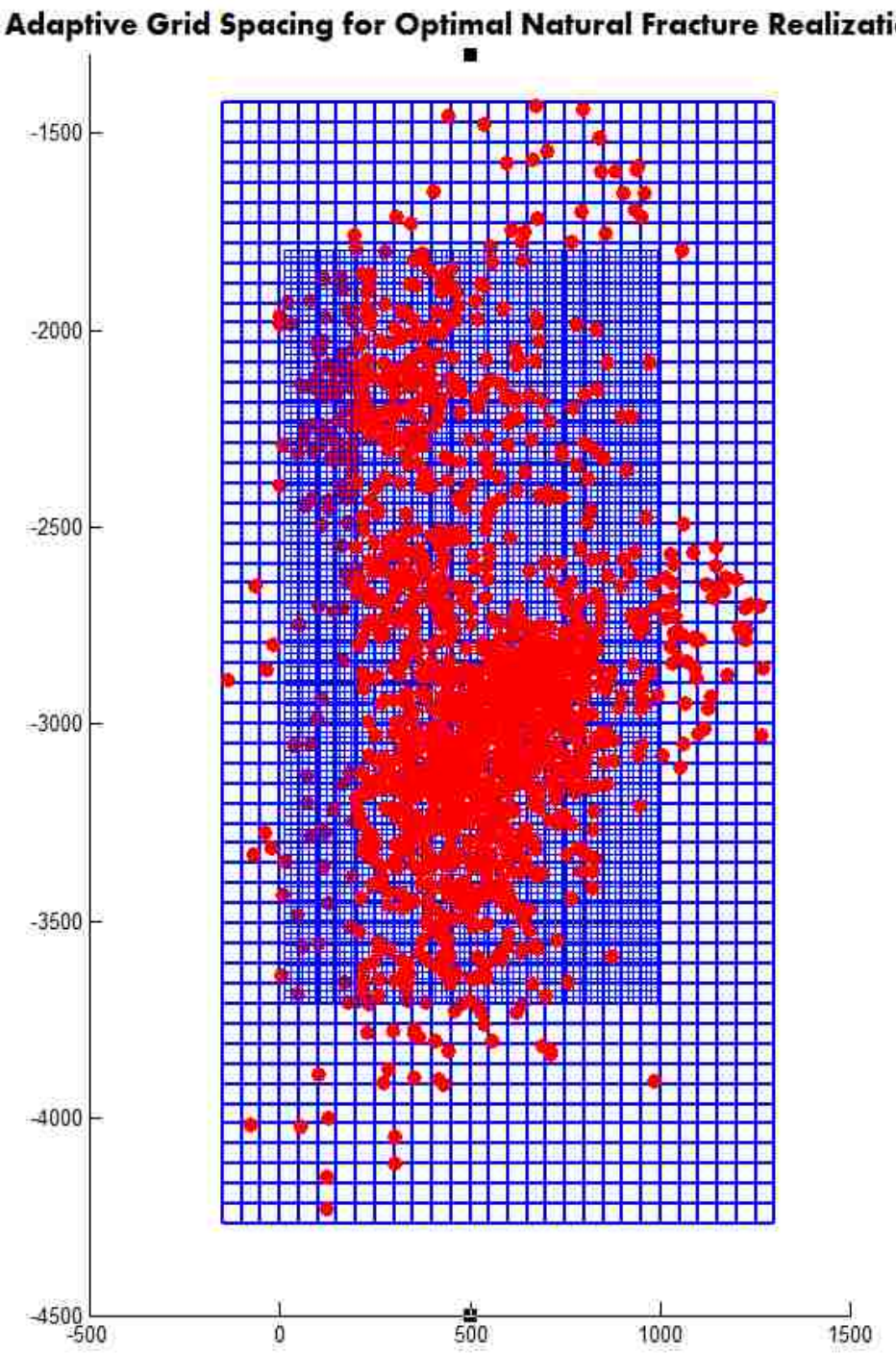

Figure 4.14. Adaptive spacing algorithm generates finer gridding system around clustered microseismic events and result in much smaller overall squared error.

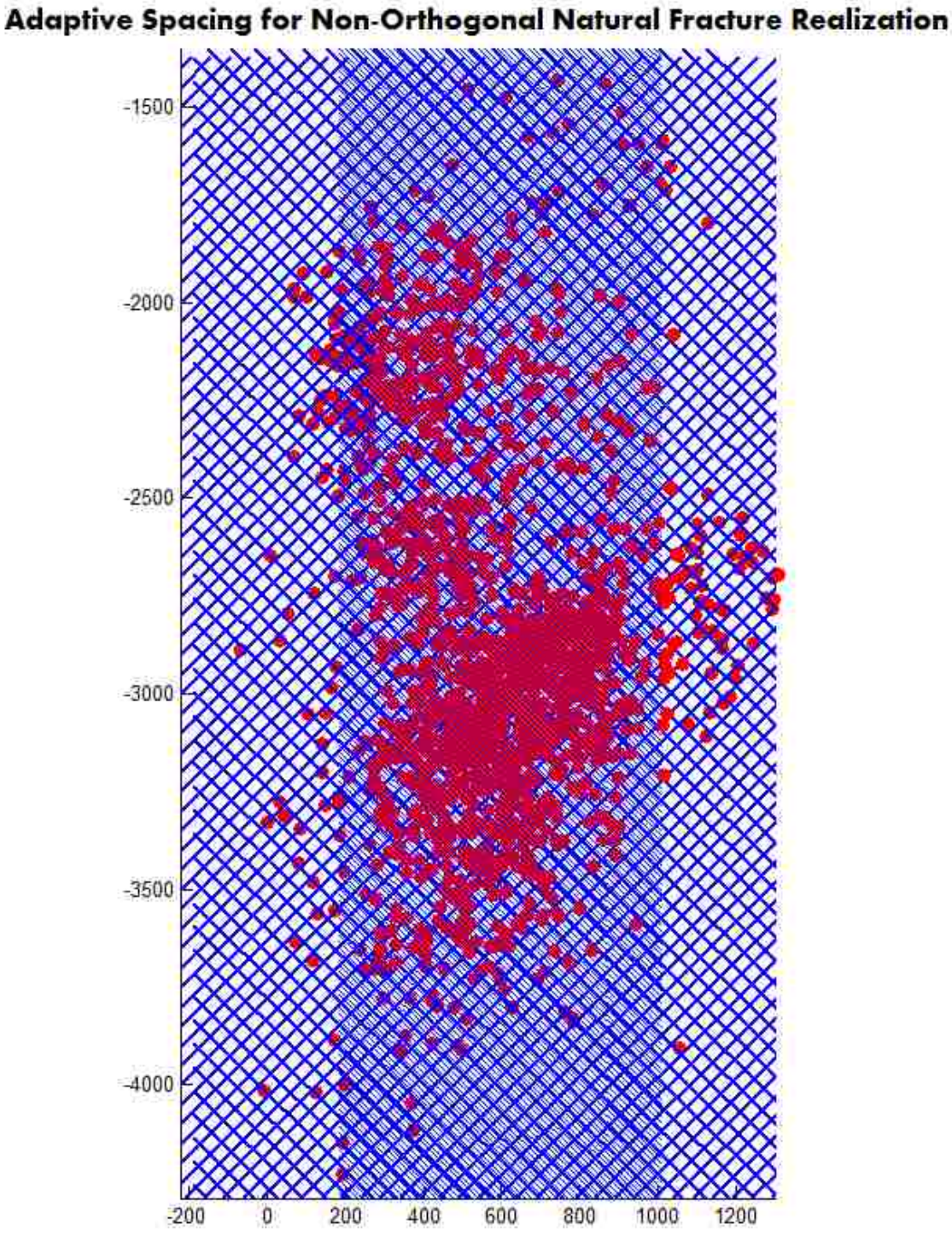

Figure 4.15. Adaptive spacing algorithm for non-orthogonal natural fractures, which also generated finer gridding systems and smaller overall squared error.

Similarly, natural fracture realizations with uniform spacing could be refined by removing part of the network that does not include any microseismic events. Therefore, a partial network of natural fractures will be formed based on the location of microseismic events. This could be achieved by establishing a cell array in MatLab with each element composed of coordinates of a small polygon and a identifier number. Sample refinement results are presented in Figure 4.16 and 4.17, which showed optimized partial networks of natural fractures for orthogonal case and non-orthogonal case. The overall squared error will remain the same during the refinement.

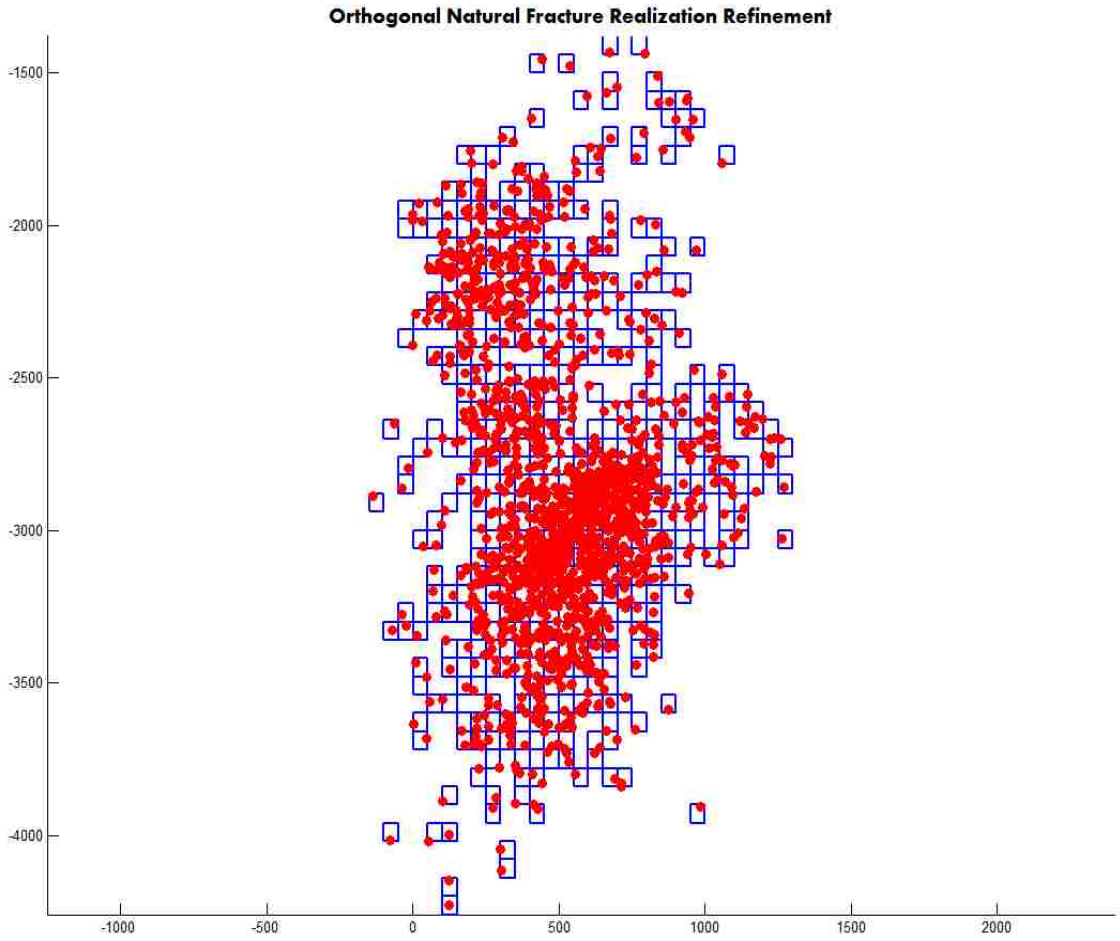

Figure 4.16. Refinement of orthogonal fracture network generated a partial network of natural fracture gridding system

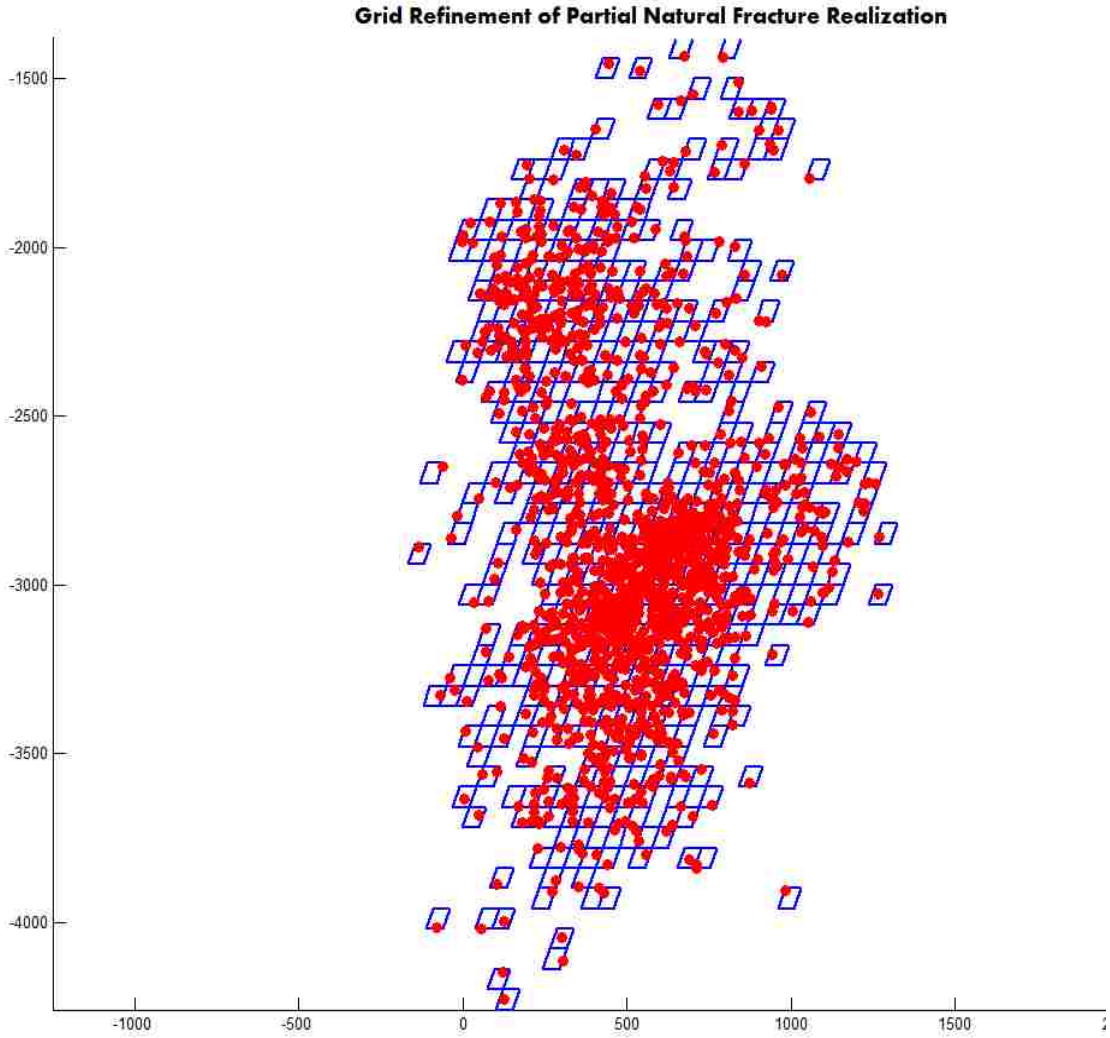

Figure 4.17. Grid refinement of non-orthogonal fracture network generated a partial network of natural fractures

4.6 Conclusion

During hydraulic fracturing, interaction between natural fractures and induced hydraulic fractures is an important design consideration in planning fracturing treatment. Accurate post treatment assessment of natural fracture distribution could allow for better reserve estimation, decline analysis, reservoir simulation and refract operations. Although outcrop and core studies provide a microscopic picture of the natural fracture system in hydrocarbon bearing formation,

large scale study of natural fracture system is not possible due to the limited access to the subsurface, and the fact that exact location or distribution of natural fractures are impossible to obtain with current technology. The optimization algorithm we propose in this chapter helps to fill this gap by using locations of large shear-type microseismic events to build a fracture grid that resembles the geometry of natural fracture system in the subsurface. In the next chapter, we will incorporate the natural fracture realizations into a numerical fracturing simulator to simulate fracturing treatment with discrete fracture network (DFN).

Chapter 5: Forward Modeling of Hydraulic Fracturing with Natural Fracture Distribution

In this chapter, we attempt to implement the methodologies described in the previous chapter for a field example and further evaluate the fitness of different natural fracture networks by matching the net pressure history from the simulation and the field data. A numerical fracturing simulator, StimPlan, will be used to model the reservoir which considers the Discrete Fracture Networks (DFNs) as potential propagation paths in fracturing simulation. Three stages of the treatment will be considered, and their net pressure responses from simulations will be quantitatively compared with field data to determine the degree of match of natural fracture networks. Preliminary analysis of the available information for the reservoir will be described first, which will allow for estimations of some petrophysical and reservoir properties needed for hydraulic fracturing models. Moreover, our forward modeling also considers properties of the natural fractures elaborated in the previous chapters and compare the differences in simulation results.

5.1 Preliminary Analysis

Due to the fact that the forward modeling with StimPlan requires an accurate and complete set-up of the well-reservoir-fracture system, it is essential to obtain all of the approximate petrophysical and mechanical properties of the reservoir, well and treatments. Although for confidentiality reasons, we were not provided all relevant data pertaining to this project, we rely on scientific estimations, empirical correlations and educated guesses for the rest of the parameters in our simulation model, and we were still able to infer some of the critical properties of the reservoir and treatments.

We have been provided the treatment history, well logs, well design and daily drilling reports, microseismic monitoring data, perforation designs, and fluid rheology from the operator. Of these information, well design and drilling report will allow us to construct the well path prior to conducting simulations. Microseismic data had previously been used in Chapter 4 for least square modeling in generating a number of natural fracture realizations. Treatment data, perforation design and fluid rheology information allows us to properly design the fracture system in StimPlan model, and their pressure information will allow for estimation of the closure pressure in the formation. Well logs will be used to estimate some of the petrophysical properties of the formation, including porosity, formation closure pressure, and Poisson's ratio. While all these model parameters can be estimated from documents released by the operator, during the history-matching process, they will be adjusted to match the net pressure of the actual treatment.

Density porosity logs and Neutron porosity logs were used to estimate the porosity and permeability of the formation. Separation of porosity logs were observed in the target interval due to the fact that the logging tool assumed a limestone formation and the actual formation it measured was shale formation. Considering the fact that this zone is a shale formation, we used porosity crossplots and estimated that the average porosity of the formation surrounding the well is about 4%, which is consistent with literatures on Barnett Shale properties (Gale et al, 2007).

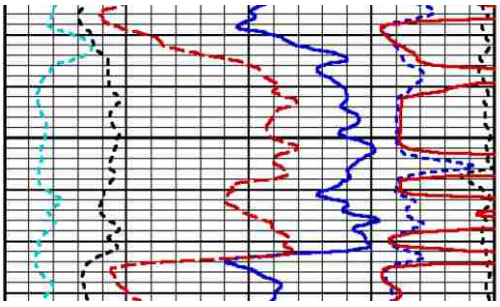

Figure 5.1 Porosity logs of the potential payzone

The Poisson's ratio of the shale payzone can be estimated from the empirical correlations developed by Al-Kattan and Al-Ameri (2012). It can be calculated by

$$\upsilon = 0.125q + 0.27 \tag{5.1}$$

where q is the shaliness index of the formation, which can be defined as

$$q = \frac{\phi_s - \phi_D}{\phi_s} \tag{5.2}$$

in which ϕ_D and ϕ_s is density porosity and sonic porosity. By analyzing the sonic log and density log of the formation, it's estimated that the Poisson's ratio of the formation is about 0.32.

Another important piece of information that we can obtain from the given data is the closure stress of the formation. An accurate estimation of this will allow for a better P_{net} estimation during the subsequent net pressure history matching process. The principle of step-rate injection test is used, in which the pump rate is plotted against bottomhole pressure to extrapolate a closure pressure value at q = 0. The initial pumping stages of stage 4 resembled the step-rate injection test, and it is concluded that the closure stress of the formation is around 7400 psi, as shown in Figure 5.2.

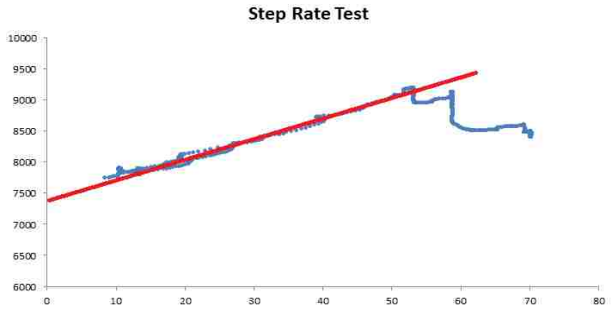

Figure 5.2 Step rate analysis showed a formation closure pressure of 7400 psi

The treatment data of the stimulation includes the time, bottomhole pressure history, treatment pressure, slurry rate and proppant concentration. Accordingly, we will be able to reproduce the treatment design of the original fracturing job. However, our forward modeling simulator only accepts a pre-defined, finite number of treatment stages, while our treatment data was recorded by seconds. To fill this gap, a MatLab script was developed to process the treatment data and generate the pump schedule that can be directly imported into the StimPlan. The processing interval was set to cover 500 seconds, or for the duration of the staged proppant concentration, whichever is smaller. As such, data was averaged in different intervals and its averages were automatically calculated and stored in a text file, which can be imported into the StimPlan pump schedule module directly.

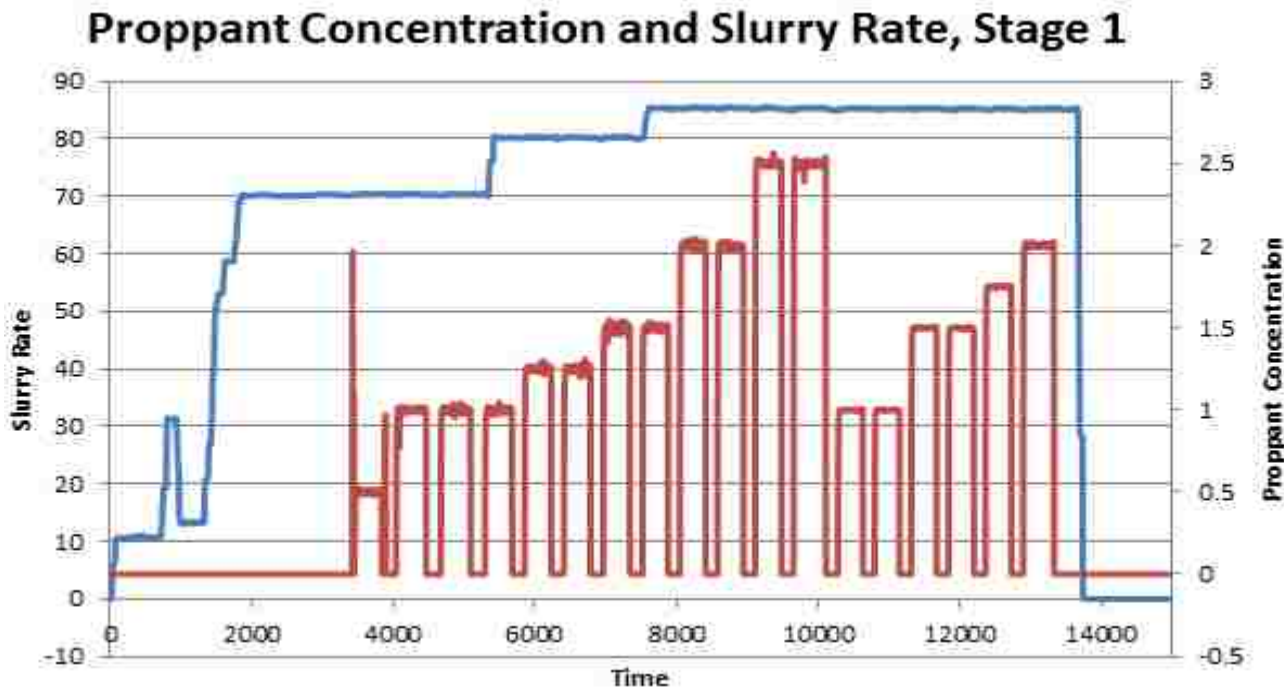

Figure 5.3: Slurry rate and proppant concentration for stage 1

5.2 StimPlan Simulation of Orthogonal Natural Fracture Realization

We use a commercial hydraulic fracturing simulator, called StimPlan, to simulate the hydraulic fracturing treatment for Well P1. StimPlan simulates the fracture treatments by dividing the treatment into small time steps and iteratively solves for parameters such as fracture geometries, pressures and fluid loss at each time step. The simulator is also capable of modeling fracturing treatments from simplified 1D model to complicated fully 3D model. For example, during the hydraulic fracturing treatment, the net pressure can be calculated as

$$p_{net} \approx \left[\frac{E'^3}{h_f^4} (K\mu q_i L) + p^4_{net-tip} \right]^{0.25} \tag{5.3}$$

where E′ is the modulus of the formation, K is formation toughness, h_f is fracture height, μ is the viscosity of the fracture fluid, q is the injection rate, and L is fracture length. The average induced fracture width for a Newtonian fracturing fluid can be calculated from:

$$\overline{w} = 3.27 \left[\frac{q_i \mu x_f}{E'} \right]^{0.25} \gamma \tag{5.4}$$

and

$$\overline{w} = 2.7 \left[\frac{q_i \mu x_f^{\ 2}}{E' h_f} \right]^{0.25} \left(\frac{\pi}{4} \right) \tag{5.5}$$

for PKN and KGD fracture model respectively, where q_i is the injection rate, μ is the apparent fracturing fluid viscosity, E′ is the formation plane strain modulus, h_f is the height of the fracture, x_f is the length of the fracture, and γ is the geometric factor. Induced fracture length can be approximated as

$$L = \frac{q_i t_p}{6C_L h_L \sqrt{t_p} + 4h_L S_p + 2\overline{w}h_f} \tag{5.6}$$

where q_i is the injection rate, t_p is the pumping time, C_L and S_p are fluid loss and spurt loss parameters, h_L is the permeable or fluid los height, h_f is the fracture height, and w is the fracture width. Fracture height can be estimated by knowing the induced fracture volume:

$$V_f = q_i t_i - \frac{2q_i \sqrt{t} K_L C_L r_p \sqrt{t_i}}{\pi C_L r_p} \tag{5.7}$$

where r_p is the ratio of net pay to fracture height, t_i is the injection time,q_i is the injection rate, C_L is the leakoff coefficient and K_L is the opening time distribution factor:

$$K_L = \frac{1}{2}\left[\frac{8}{3}\eta + \pi(1-\eta)\right] \tag{5.8}$$

By iteratively calculating these properties at each time step, it is possible to obtain a continuous dataset of induced fracture development, and the propagation of induced fractures can also be visualized by the simulator. However, those equations are only applicable in simulating the development of a symmetric bi-wing shape hydraulic fracture. The StimPlan will consider the pre-existing natural fracture network as potential paths of fluid flow and fracture growth, which will lead to asymmetric, complicated fracture growth pattern.

Our forward modeling models in StimPlan were set up with information including Well trajectories, original net pressure data, perforation design and pump schedule. Three layers of formation were established according to the geological settings of the well, in which Viola limestone is underneath the Barnett shale formation (Figure 5.4). Moreover, DFN option was

enabled, in which we were able to define the geometry, permeability of the natural fracture network (Figure 5.5).

Through net pressure matching, we mainly attempted to adjust the formation geomechanical properties, both for surrounding formations and our targeted formation where the horizontal wellbore is situated in. There were mainly 4 parameters that were turned out to be decisive in net pressure responses – modulus, fluid loss, toughness, and stress difference. As discussed before according to Economide (2000), the net pressure during the treatment can be approximated by

$$p_{net} \approx \left[\frac{E'^3}{h_f^4} (K\mu q_i L) + p^4_{net-tip} \right]^{0.25} \tag{5.9}$$

where E' is the modulus of the formation, K is formation toughness, h_f is fracture height μ is the viscosity of the fracture fluid, q is the pump rate, and L is fracture length. Therefore, the controllable variable during our simulation are E', K, L (related to fluid loss coefficient), and q. For example, if the overall simulated net pressure is below the measured value, we can increase the modulus and toughness of the formation to make net pressure higher. We may also reduce the fluid loss coefficient, so the length of the fracture will go up due to larger volume of fluid available for fracture propagation, and so will net pressure. On the other hand, net pressure discrepancies may occur locally instead of universally on the graph. If any region on the net pressure graph shows a local discrepancy, we may adjust the fluid properties or pump schedules for that specific treatment stage to locally alter the net pressure response of the simulation. For example, if net pressure is abnormally lower at certain point, we may discretize the pump

schedule by dividing that pumping stage to a faster one and a lower one. We may also increase the fracturing fluid viscosity of that stage to increase the net pressure response.

With these net pressure matching principles described above, we first conducted simulations for Stage 1,2 and 4 with a 90^{o} orthogonal natural fracture realization. The spacing and location of the natural fracture network were obtained from the optimization results in Chapter 4. Stage 3 treatment data from the operator were missing bottomhole pressure data, thus we were unable to generate the net pressure history of that stage and had to skip this stage. Net pressure matching results showed reasonable matches between the field data and measure data, as demonstrated below.

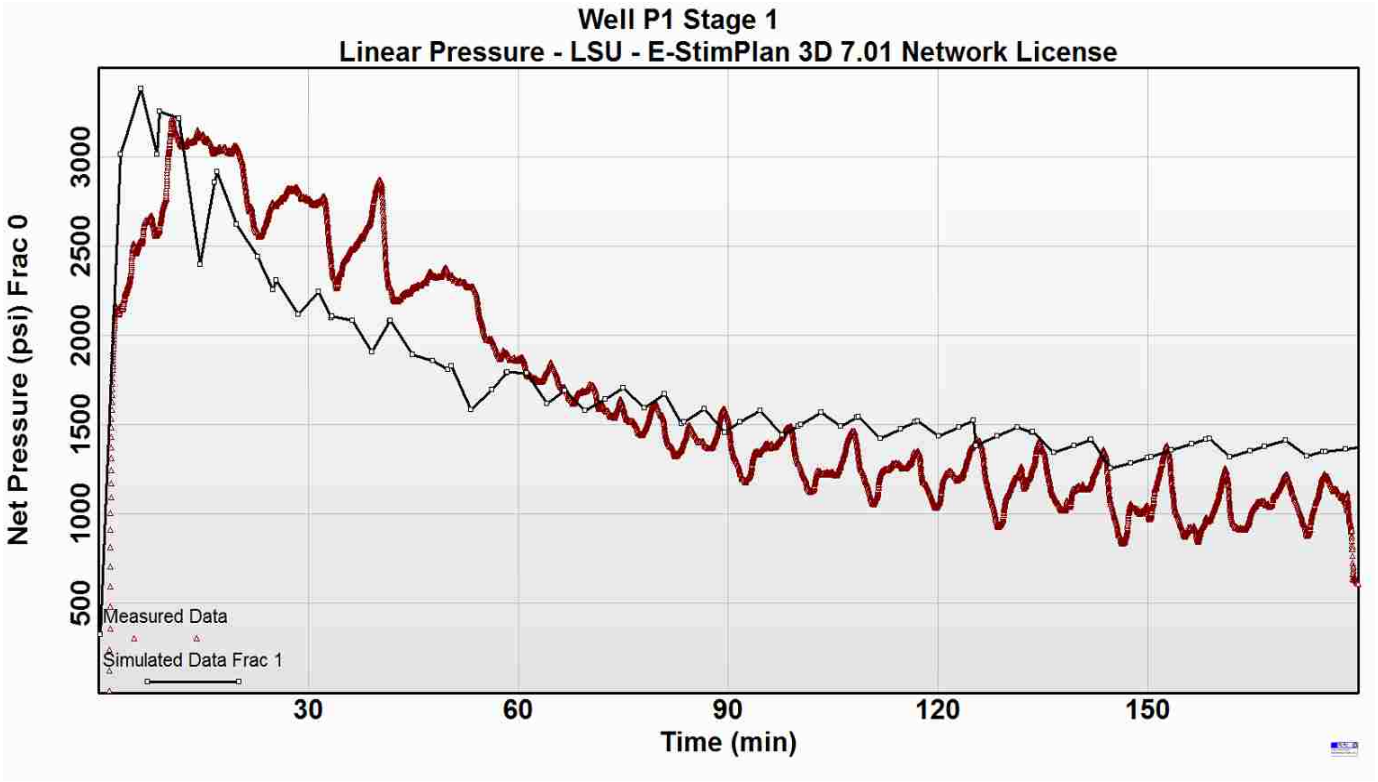

Figure 5.4a. Forward modeling of stage1of fracturing treatments with orthogonal natural fractures

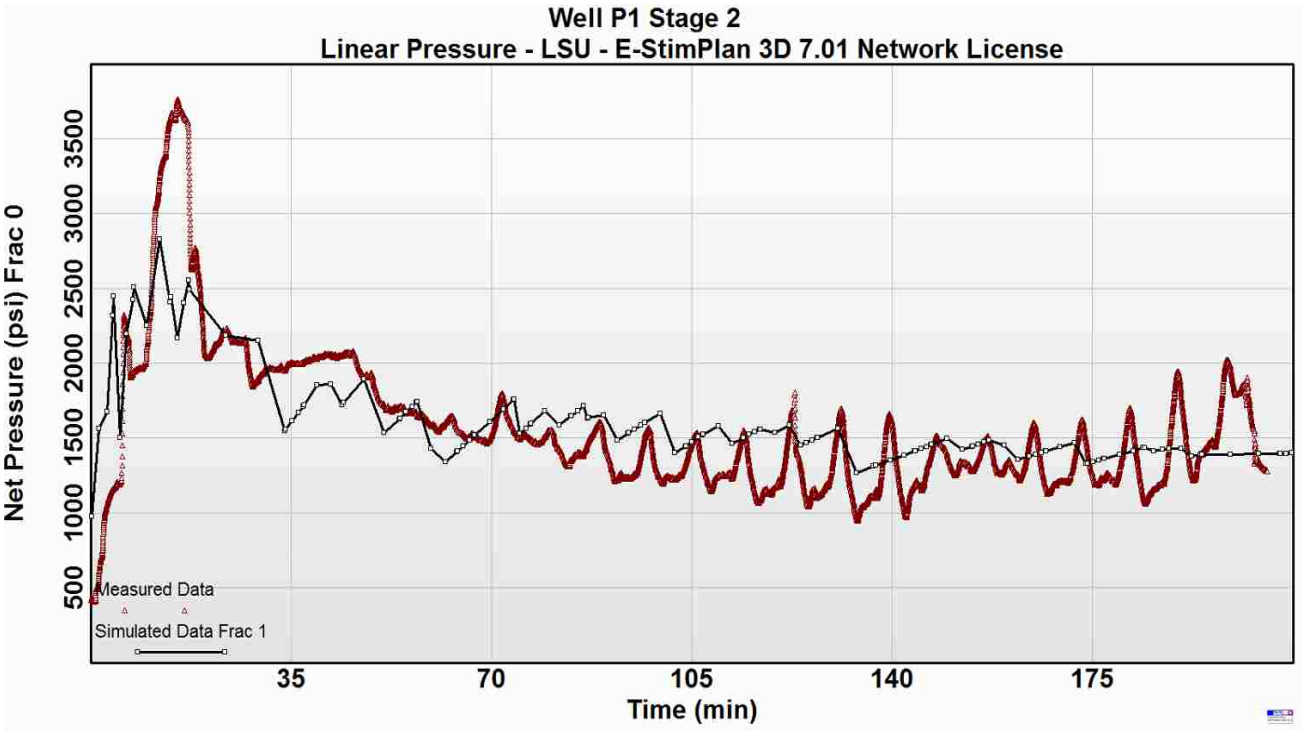

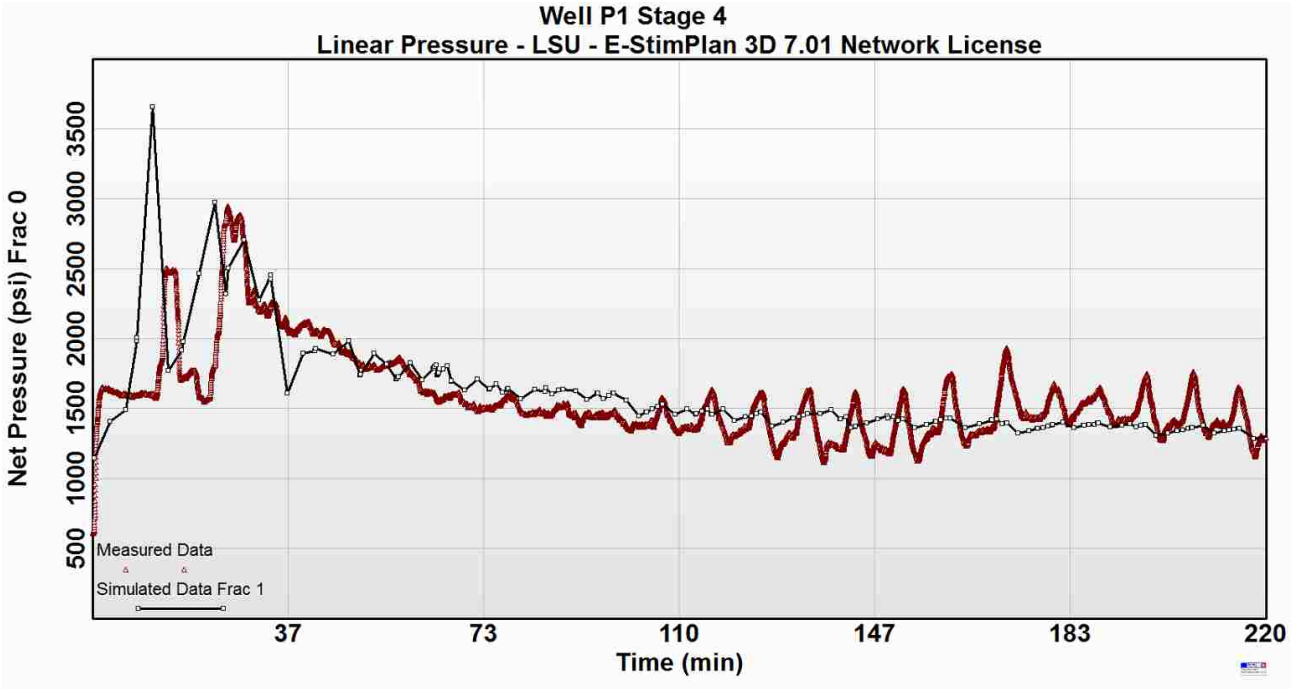

Figure 5.4b. Forward modeling of stage 2 and 4 of fracturing treatments with orthogonal natural fractures

5.3 StimPlan Simulation of Non-Orthogonal Natural Fracture Realization

We continued the forward modeling of hydraulic fracturing in this formation by incorporating non-orthogonal natural fracture realizations with StimPlan DFN functionality. We have modeled the non-orthogonal natural fracture networks in Chapter 4 and found that the total distance square between shear type microseismic events and natural fracture network is smaller by modeling a non-orthogonal fracture network. Here, we will build non-orthogonal DFN network and match the net pressure responses with the same principles described in 5.2. We first build a DFN case with the optimal non-orthogonal natural fractures, which is intersecting at approximately 46°. It can be observed that the net pressure response from simulations still showed a reasonable good match with field data, although deviations at the beginning of the treatments seems to be large due to the logarithm x axis.

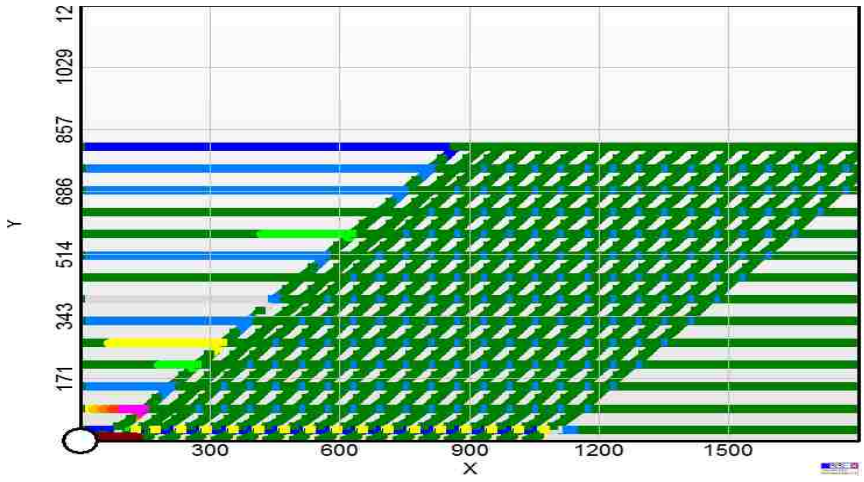

Figure 5.5. The non-orthogonal natural fracture network in the forward modeling of fracturing treatment. Colors in the network represent the fluid flow velocity in the natural fractures.

Lastly, we model the non-orthogonal natural fracture geometry with 60° intersection. It is noteworthy that although these fixed-angle intersecting natural fracture realizations may result in

better matches in net pressure responses, calculations in Chapter 4 have shown that the total distance square for these realizations are significantly larger than the optimized case. Therefore, to balance the fitness of both least square modeling and net pressure history-matching simultaneously, it is necessary to develop an integrated algorithm that could perform least-square modeling and forward modeling fracturing simulation in one centralized platform where results can be balanced, processed and compared together. Moreover, the matched net pressure responses must be quantitatively defined in order to compare their fitness among different cases. In the following section, we will develop corresponding MatLab algorithm for calculation net pressure deviations from treatments and forward modeling.

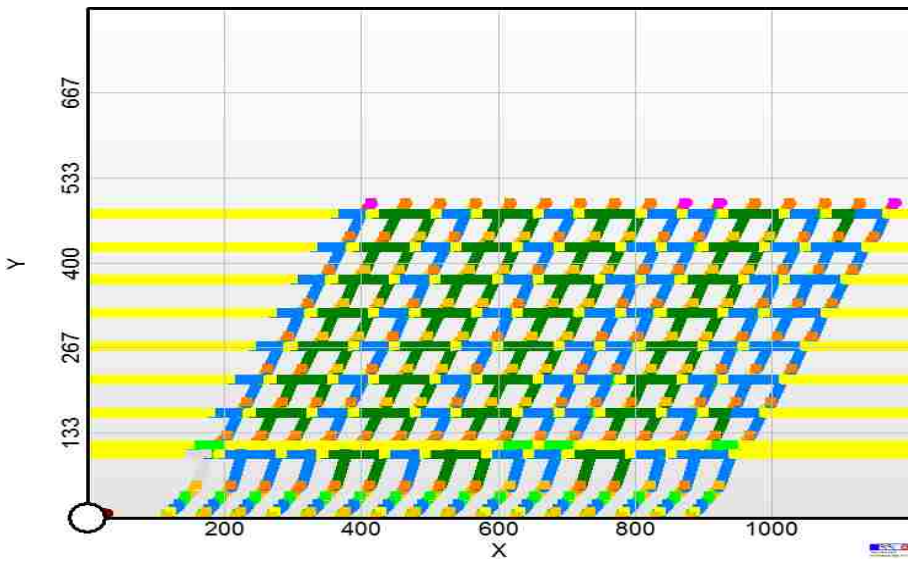

Figure 5.6. The 60 ^{o} intersecting natural fracture network during the forward modeling of fracturing treatment. Colors in the network represent the fluid flow velocity in the natural fractures.

Compared with the assumption of symmetric bi-wing induced fracture network (i.e. no natural fracture is considered), we've observed that under the same simulation parameters, the deviations between simulation and field data is larger, and net pressure response is generally higher than that of DFN cases (Figure 5.9). Moreover, due to the elimination of natural fracture

networks that may serve as significant potential source of leakoff, the treatment efficiency of DFN cases is smaller than the cases without natural fractures.

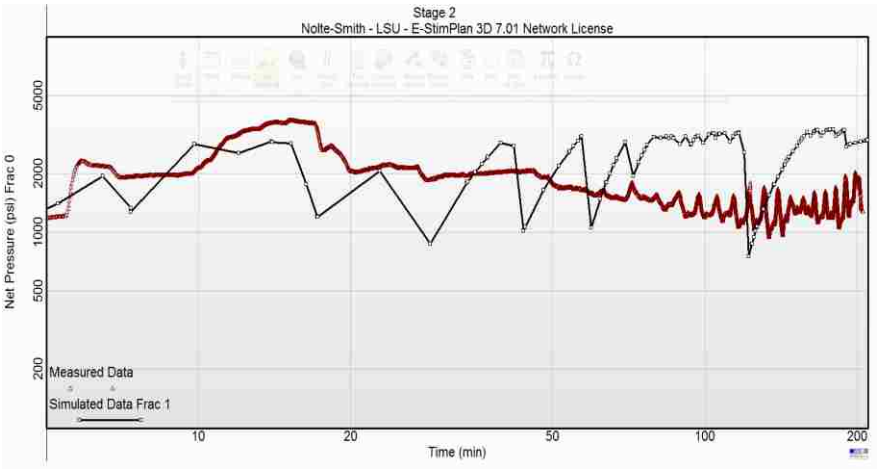

Figure 5.7. Simulations without natural fractures have higher net pressure responses and greater deviations from field data

5.4 Estimation of Net Pressure Deviations and Results Discussion

In this section, we will derive the formulation that could quantitatively define the deviation between measured net pressure history and simulated net pressure response from forward modeling. Although StimPlan itself doesn't provide such a functionality of calculating the average deviation between measured data and simulation data, the net pressure results from the simulation could be obtained by exporting the simulation data. Correspondingly, we can calculate its deviations from measurements at each time point, since the measurement data of the treatment was accurate up to seconds. We therefore define the following formula for pressure deviation at each point:

$$P_{dev}^{i} = \left(\frac{P_{msmt} - P_{sim}}{P_{msmt}} \right)^2 \tag{5.10}$$

where P_{dev}^{i} is the deviation between measurement and simulation at the i^{th} simulation step. P_{msmt} is the average measured net pressure around the i^{th} simulation time step, and P_{sim} is the simulated net pressure at the i^{th} simulation step. This term was squared to eliminate negative results and calibrate all deviations to positive values. Accordingly, the total deviation for a treatment is:

$$P_{dev}^{total} = \sum_{i=1}^{n} \left(\frac{P_{msmt} - P_{sim}}{P_{msmt}} \right)^2 \tag{5.11}$$

where n is the total number of simulation steps for each stage. The pressure deviation total for a specific natural fracture realization, therefore, could be calculated by adding up the pressure deviations for all three stages (Stage 1, 2 and 4). This calculation allows for a more direct and quantitative comparison of the different natural fracture realizations based on forward modeling results.

We've developed an algorithm in MatLab to perform this calculation for all stages with all natural fracture realizations. According to the formula above, we've computed the deviations for all stages of all realizations as follows

Table 5.1. Net Pressure Deviations Between Measurements and Simulations (Smaller is better)

NF Realizations	**Stage 1**	**Stage 2**	**Stage 4**	**Total**
Orthogonal	11.54	4.53	3.29	19.36
Non-Orthogonal	12.39	4.45	3.22	20.06
30^o Intersecting	10.61	4.42	3.25	18.28
35^o Intersecting	12.44	4.61	3.28	20.33
40^o Intersecting	9.24	4.25	3.22	16.71
45^o Intersecting	10.15	4.32	3.31	17.78
50^o Intersecting	11.09	4.52	3.30	18.91

55^o Intersecting	10.90	4.26	3.53	18.69
60^o Intersecting	9.75	4.28	3.47	16.84
65^o Intersecting	12.40	4.38	3.41	20.19
70^o Intersecting	10.07	4.37	3.39	17.83

As it's shown above, the 40^o intersecting natural fracture realization had the minimum overall deviations in forward modeling. However, it's noteworthy that this 40^o intersecting realization will not be the optimal natural fracture realization in least square modeling in Chapter 4. The total distance square of this realization was significantly higher than other realizations. Therefore, it's desirable to have a centralized simulation and optimization platform where forward modeling and least square modeling can be integrated into a single platform. As such, error analysis, optimization and result processing can be performed and leveraged within the same framework and could be more easily compared.

5.5 Conclusion

In this chapter, we conducted forward modeling and simulated the hydraulic fracturing treatments in Well P1 with different natural fracture geometries. The net pressure responses from simulations and field data was quantitatively compared to estimate the overall deviations, which could serve as an additional benchmark for determining the likelihood of having certain natural fracture geometries in the formation. In the next chapter, we will conduct numerical reservoir modeling with CMG and simulate the hydrocarbon production from Well P1, and we will show that the presence of natural fractures will impact both recovery rate and cumulative production of hydrocarbons in naturally fractured reservoirs.

Chapter 6: Numerical Simulation of Hydrocarbon Production with CMG

In this chapter, we use the numerical simulator CMG to simulate the hydrocarbon production from the well, and observe the effect of having hydraulic fractures or natural fracture networks on hydrocarbon recoveries and patterns of production rate decline. Reactivated natural fracture network not only serves as the flow paths for fracturing fluid during hydraulic fracturing, but produced hydrocarbon fluid may also flow through the natural fracture network, and thus the production of hydrocarbons may benefit from this behavior. This part of the research simulates the hydrocarbon production in such naturally fractured reservoirs, and therefore validates the effect of both hydraulic fractures and natural fracture networks on hydrocarbon production.

6.1 Model Setup

The mathematical model and flow equations of CMG are based on dual permeability flow equations in naturally fractured reservoirs. Dean and Lo (1988) have discussed the formulation of fluid flow equations in a naturally fractured reservoir by considering a dual-permeability formation, in which fractures and formations were considered to have different porosities and permeabilities. By using finite difference method, multiphase fluid flow in the reservoir/fracture system can be expressed as:

$$\Delta[T_{\alpha f}(\Delta p_{\alpha f} - g_{\rho\alpha f}\Delta D)] + T_a(p_{\alpha m} - p_{\alpha f}) + q_{\alpha f} = \frac{V_b}{\Delta t}\Delta_t\left(\frac{\varphi_f S_{\alpha f}}{B_{\alpha f}}\right) \tag{6.1}$$

and

$$\Delta[T_{gf}(\Delta p_{gf} - g_{\alpha gf}\Delta D)] + \Delta[R_{sf}T_{of}(\Delta p_{of} - g_{\rho of}\Delta D)] + T_g(p_{gm} - p_{gf}) + R_s T_o(p_{om} - p_{of}) + q_{gf}) \tag{6.2}$$
$$\frac{V_b}{\Delta t}\Delta_t\left(\frac{\varphi_f S_{gf}}{B_{gf}} + \frac{\varphi_f R_{sf} S_{of}}{B_{of}}\right)$$

for water/oil–fracture system and gas-fracture system, respectively. Similarly, flow equations in rock matrix are also formulated as:

$$\Delta[T_{\alpha m}(\Delta p_{\alpha m} - g_{\rho \alpha m}\Delta D)] - T_{\alpha}(p_{\alpha m} - p_{\alpha f}) = \frac{V_b}{\Delta t}\Delta_t(\frac{\varphi_m S_{\alpha m}}{B_{\alpha m}}) \tag{6.3}$$

and

$$\begin{aligned}&\Delta[T_{gm}(\Delta p_{gm} - g_{\rho gm}\Delta D)] + \Delta[R_{sm}T_{om}(\Delta p_{om} - g_{\rho om}\Delta D)] - T_g(p_{gm} - p_{gf}) \\ &+ R_s T_o(p_{om} - p_{of}) + q_{gf}) = \frac{V_b}{\Delta t}\Delta_t(\frac{\varphi_m S_{gm}}{B_{gm}} + \frac{\varphi_m R_{sm} S_{om}}{B_{om}})\end{aligned} \tag{6.4}$$

for water/oil-matrix system and gas-matrix system, respectively. T is the matrix transmissibility, which can be calculated as:

$$(T_{wf})_x = 0.001127\left(\frac{k_x k_{rw}}{B_w \mu_w}\right)\frac{\Delta y \Delta z}{\Delta x} \tag{6.5}$$

for water transmissibility in the x direction. Transmissibility for other phases in other directions may also be calculated in a similar pattern. These equations are solved simultaneously in CMG by finite difference method to obtain flow rates for each phase at each time step.

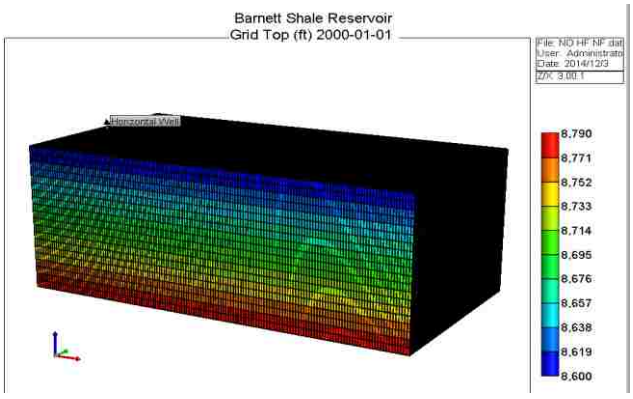

Figure 6.1. GEM-type reservoir model in CMG

The CMG model was established based on the actual well design and reservoir conditions discussed in Chapter 2, and will consider either oil or gas as reservoir fluid (i.e. either oil-water system or gas-water system). The shale reservoir was modeled with a 150*80*20 block unit, in which I and J direction was sized at 10 ft per block, and K direction (vertical direction) was 5 ft per block. Therefore, the size of the reservoir model is 1500 ft and 800 ft in I and J directions, and 100 ft in K direction (Figure 6.1). The reservoir model was created in CMG Builder using GEM module with a dual permeability (DUALPERM) system. The horizontal section of the well was estimated to span approximately 1400 ft in the reservoir.

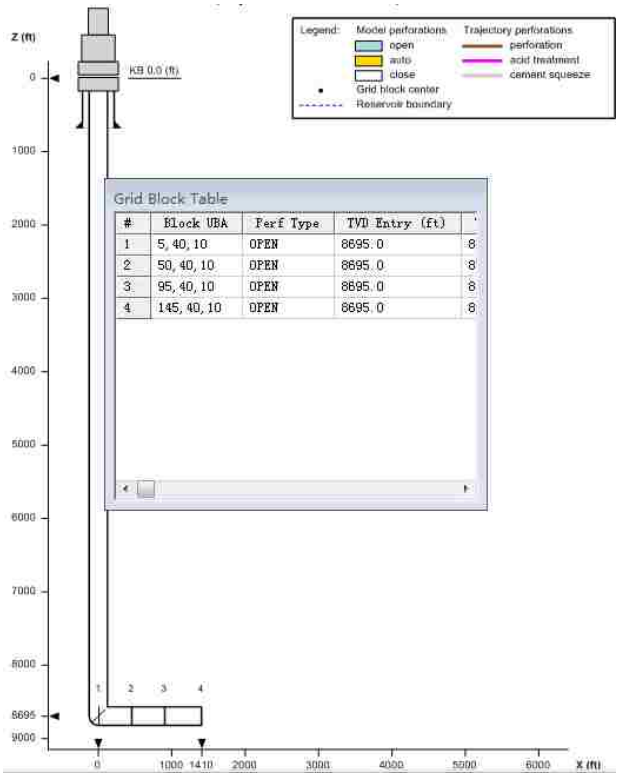

Figure 6.2. Well schematic in the reservoir model

Therefore, the horizontal well was determined to occupy about 140 grid blocks in I direction. We've also placed the well in the center of the reservoir. As such, the well was constructed in the

model such that it spanned 140 blocks in I direction, and was situated in the 10th layer in K direction. According to the well trajectory, distance between the first perforation and the 4th perforation was about 1400 ft, and we have reproduced this scenario in the model as well. The full schematic of the well in this reservoir model was shown in Figure 6.2.Moreover, we have assumed a two phase system in this reservoir model – gas (CH_4)-water or oil-water, and the water-gas/water-oil contact was approximately 400 ft below the well. Gas absorption by shale was modeled using Langmuir's Absorption correlation. Other properties of the reservoir are presented below in Table 6.1.

Table 6.1: Reservoir Properties used in the CMG Model

Property	**Value**
Matrix Porosity	0.03
Fracture Porosity	0.002
Matrix Permeability (All Directions)	0.0001 md
Fracture Permeability (I and J)	0.00002 md
Fracture Permeability (K)	0.00004 md
Langmuir Absorption Constant (CH_4)	0.002
Langmuir Absorption Constant (CH_4 in Fractures)	0
Maximal Absorbed Mass (CH_4)	0.1
Maximal Absorbed Mass (CH_4 in Fractures)	0
Rock Density	120 lb/ft^3

To model hydraulic fractures, we conducted a Local Grid Refinement (LGR) on the model, which modified the grid-block properties on the fracture path to reflect the presence of hydraulic fractures. We've modeled 0.1 in hydraulic fractures and 1 mm secondary fractures in the model, in which permeabilities were 10000 md and 0.3 md, respectively. Hydraulic fractures were modeled to be perpendicular to the horizontal wellbore, and their half-length was 300 ft.

Moreover, we've assumed that hydraulic fractures will only grow 1 grid-block (5 ft) in upper and lower directions (Figure 6.4).

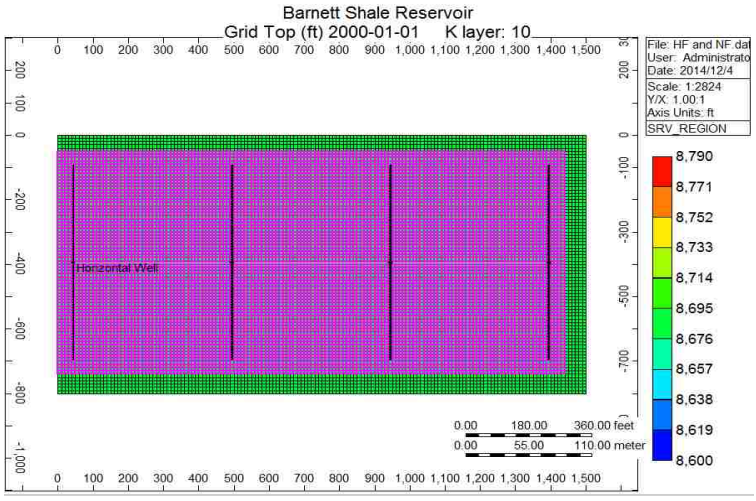

Figure 6.3. Adding a Stimulated Reservoir Volume (SRV) reflects the presence of natural fracture network while retaining hydraulic fractures previously modeled

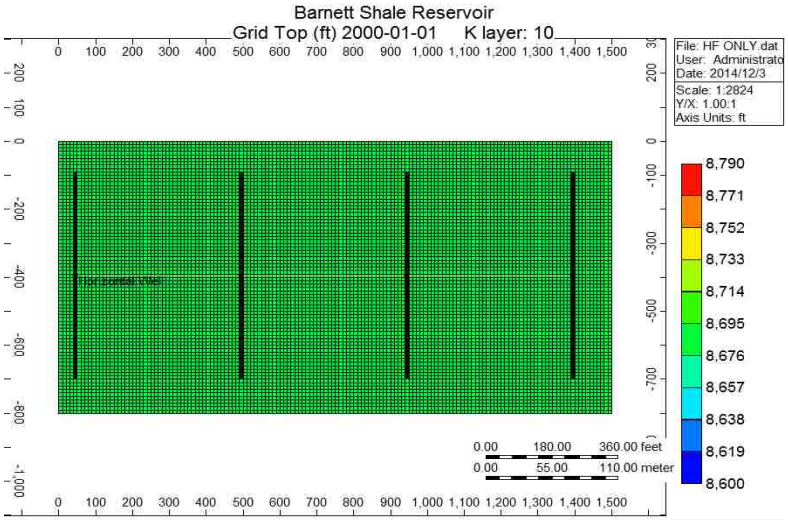

Figure 6.4. Hydraulic fractures were generated using Local Grid Refinement (LGR) technique in the reservoir model

To model natural fracture networks, we've added a Stimulated Reservoir Volumn (SRV) to the model. This SRV functionality models the fluid flow into a network of fractures connected to either vertical or horizontal wells. By adding a SRV to the model, scenarios in

which the well was surrounded by a network of natural fractures could be simulated. In our model, we've established a SRV in which fracture spacing was 200 ft and 201.11 ft in I and J direction respectively – a reproduction of the least square modeling results for optimal orthogonal natural fracture realizations. Therefore, this model became an integrated reservoir model in which both natural fracture networks and hydraulic fractures are being modeled.

6.2 Simulation Results and Discussion

Our CMG models considered 4 year of gas production from 01/01/2000 to 01/01/2004, simulated on a semi-monthly basis. Moreover, both production rate of hydrocarbons and cumulative hydrocarbon production will be evaluated. First, productions were compared between hydraulically fractured well and un-stimulated well. It can be observed from the production history below that adding hydraulic fractures significantly improved both production rate of the well and the cumulative gas production of the reservoir.

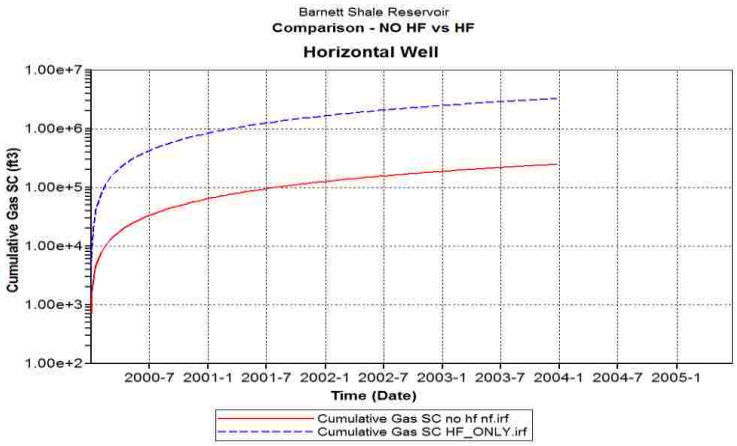

Figure 6.5. Hydraulic fracturing leads to a significant increase in cumulative production in the reservoir

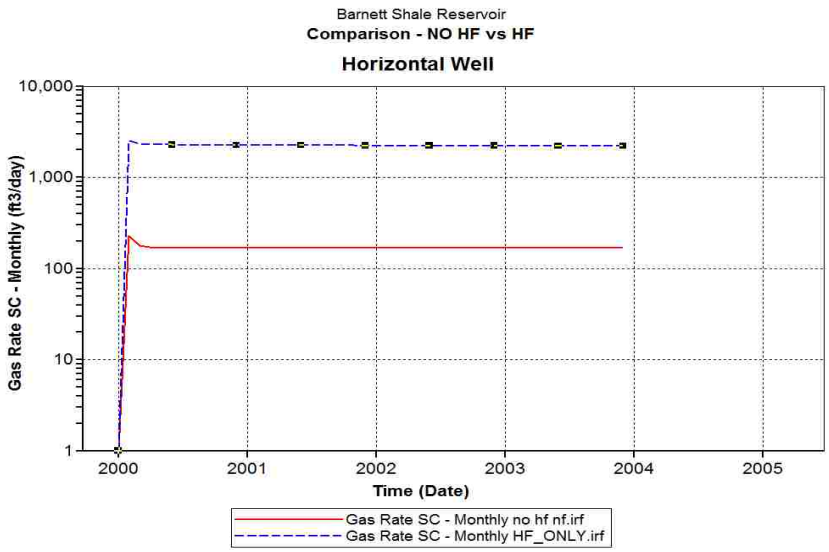

Figure 6.6. Production rate was improved when the well was hydraulically

Next, production from naturally fractured reservoir was compared with the one being hydraulically fractured only. According to Figure 5.8 and 5.9, the presence of natural fracture network will slightly improve both production rate and cumulative production. This is due to the fact that natural fractures in such cases usually have much lower permeability than hydraulic fractures. Therefore, production enhancements from naturally fractured reservoirs are less evident.

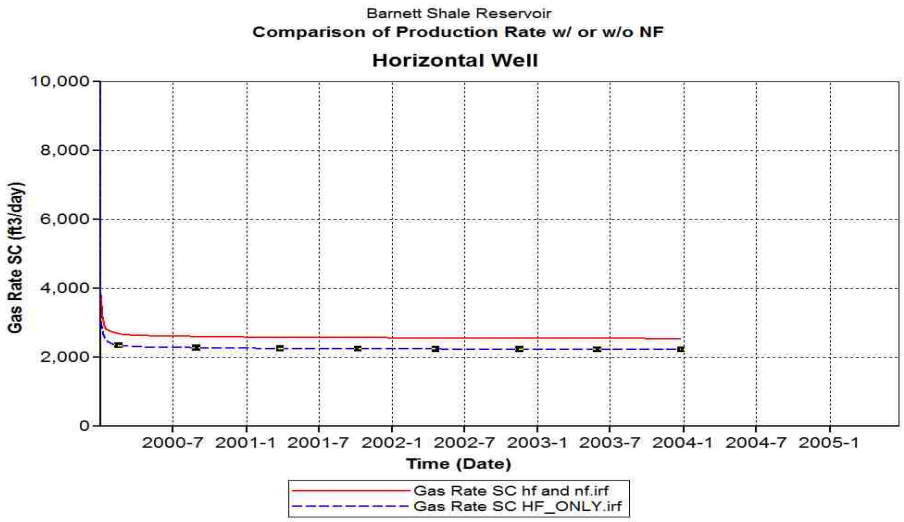

Figure 6.7. Production rate was slightly improved in naturally fractured reservoirs

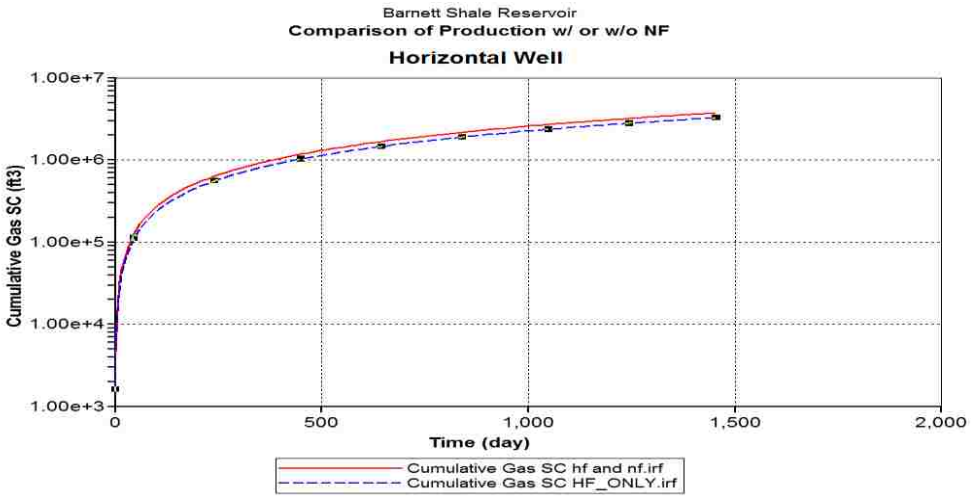

Figure 6.8. Production enhancement was also observed in naturally fractured reservoirs

In summary, our simulation results showed that gas production from this reservoir could be improved by stimulating the well with hydraulic fracturing and by the presence of natural fracture network. Production enhancement was significant when the well was stimulated by 4 transverse hydraulic fractures, while the presence of natural fracture network only slightly improved the gas production of the well.

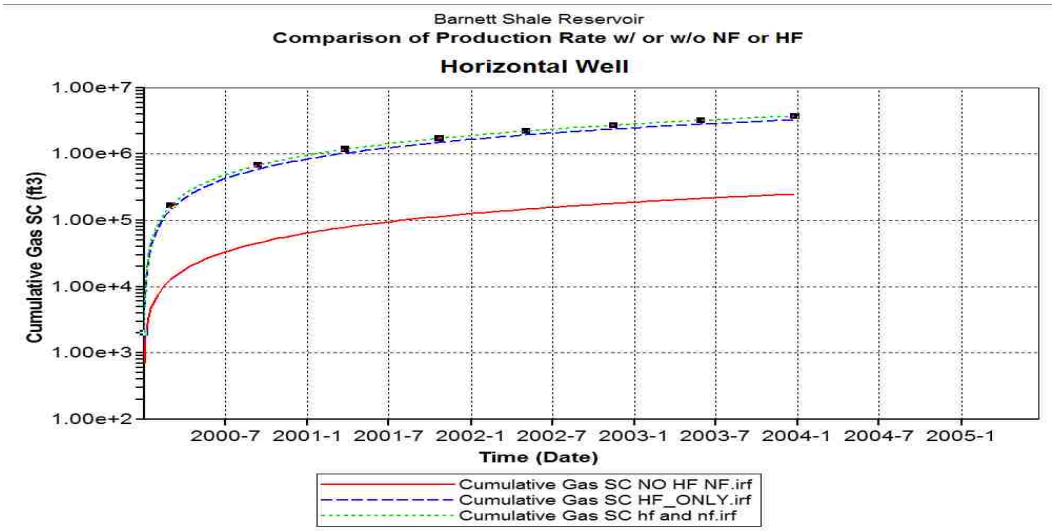

Figure 6.9 Production enhancements from hydraulic fracturing and natural fractures for shale gas reservoir

Similar production enhancements were also observed when we model the reservoir as a shale oil reservoir. Production histories over the same 4-year period have shown that oil production from the tight oil reservoir was also benefited from the presence of natural fracture network or hydraulic fracturing (Figure 6.10). It is also noteworthy that oil production without hydraulic fracturing was extremely low in our shale oil simulation; therefore, without reservoir stimulation, it will not be economically viable to produce hydrocarbons from such low permeability shale reservoirs.

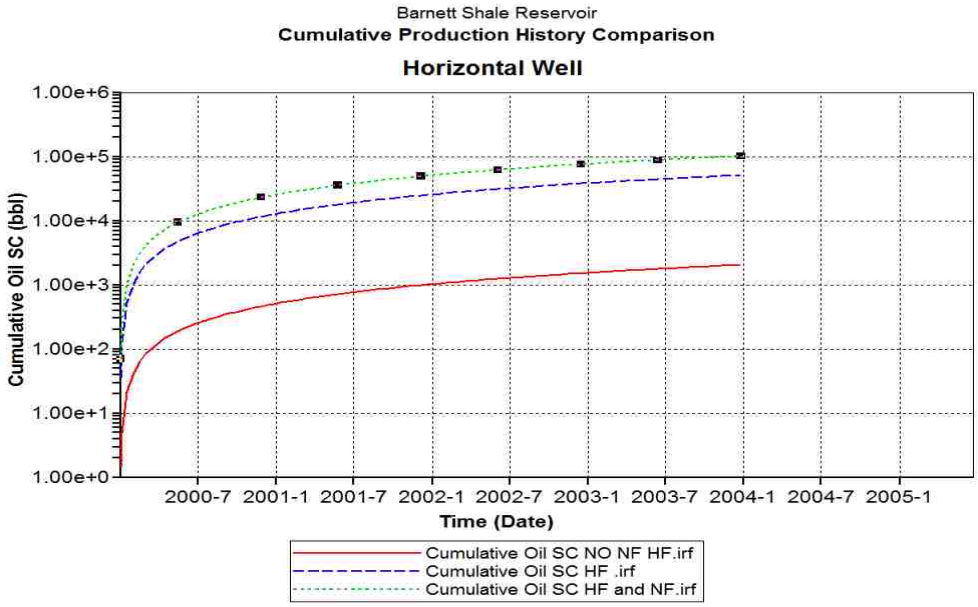

Figure 6.10. Production enhancements from hydraulic fracturing and natural fractures for shale oil reservoir

In conclusion, we have shown through simulation study that hydrocarbon recoveries from low permeability shale reservoirs can be severely impacted by inadequate reservoir productivity in such reservoirs, thus it's not economically feasible to develop such shale reservoirs without conducting reservoir stimulation. We have shown that through hydraulic fracturing, the hydrocarbon recovery rate as well as the cumulative recovery of the well could be significantly

improved. Furthermore, our simulation studies have shown that the presence of natural fracture network also leads to production enhancements in shale reservoirs, although less significant than those of hydraulic fracturing.

6.3 Conclusion

In this chapter, we have conducted numerical reservoir modeling with CMG and simulated the hydrocarbon recovery with reservoir stimulation by hydraulic fracturing and the presence of natural fractures. We showed that both natural fractures and hydraulic fracturing may significantly improve both recovery rate and cumulative recovery of hydrocarbons in naturally fractured reservoirs. In the next chapter, the entire thesis will be summarized and concluded, and recommendation for future work will also be provided.

Chapter 7: Conclusions and Recommendation for Future Work

In this research, we have developed an integrated modeling workflow to estimate the most likely geometry of natural fracture network based on formation evaluations, microseismic data, treatment history and production history. Least-square modeling first find natural fracture gridding systems that result in smaller overall squared error between fracture networks and double couple microseismic events. Forward modeling that incorporates Discrete Fracture Network will subsequently be used to simulate hydraulic fracturing treatments, and the net pressure responses from simulations and field measurements will be quantitatively compared to screen out candidate natural fracture geometries. Reservoir simulation tools will also be used thereafter to simulate the production of hydrocarbon from such naturally fractured reservoirs, and the production history from simulations and the actual well will be compared to further evaluate the fitness of natural fracture realizations. This workflow is able to integrate scientific data from multiple aspects of the reservoir development process, and results from this workflow will provide both geologist and reservoir engineers an innovative assessment tool for evaluating and modeling naturally fractured reservoirs.

Recommendations for future work include

1) Further investigate and collect the information about the stress field in this reservoir, and determine the most likely directions of the present day in-situ stress and paleostress field. Having such information will help to more accurately estimate the most likely orientations of natural fractures at present time.

2) Conduct complete reservoir study to gather detailed information about the reservoir and the production history, which will allow for more accurate reservoir modeling in simulating hydrocarbon recoveries.

3) Develop a centralized simulation platform or integrate different modeling softwares through automation. This will allow for faster and smooth modeling and optimization, and different fitting criteria of natural fracture geometries can be integrated and weighted to achieve a more reliable conclusion.

References

Ali Daneshy, A., 1973, Experimental Investigation of Hydraulic Fracturing Through Perforations, SPE Journal of Petroleum Technology, Issue 10, Vol. 25, pp. 1201 – 1206.

Al-Haddad, S.M., and Crafton, J.W., 1991, Productivity of Horizontal Wells, paper SPE 21868 presented at SPE Low Permeability Reservoirs Symposium, 15-17 April, Denver, Colorado.

Al-Katta, W., and Al-Ameri N.J., 2012, Estimation of the Rock Mechanical Properties Using Conventional Log Data in North Rumaila Field, Iraqi Journal of Chemical and Petroleum Engineering, Vol.13 No.4 (December 2012) 27- 33

Baig, A.M., and Prince, M., 2010, Microseismic Moment Tensors: A Path to Understanding Growth of Hydraulic Fractures, paper SPE 137771 presented at the Canadian Unconventional Resources & International Petroleum Conference, Calgary, Canada.

Becker, G.F., 1893, Finite Homogeneous Strain, Flow and Rupture of Rocks, Geological Society of America Bulletin, v.2, p. 49-74

Bedayat, H., & Dahi Taleghani, A. (2014). Interacting double poroelastic inclusions. Mechanics of Materials, 69(1), 204–212. doi:10.1016/j.mechmat.2013.10.006.

Blanton, T.L., 1982, An Experimental Study of Interaction Between Hydraulically Induced and Pre-Existing Fractures, paper SPE 10847 presented at the SPE/DOE unconventional gas recovery symposium, Pittsburg, Pennsylvania, USA

Bonnet, E., O. Bour, N.E. Odling, P. Davy, I. Main, P. Cowie and B.Berkowitz, 2001, Scaling of fracture systems in geological media: Rev. Geophys., v.39, p. 347-383

BP Statistical Review of World Energy 2013, British Petroleum Publishing, London, United Kingdom.

Cho, Y., Ozkan, E., & Apaydin, O. G. (2013, May 1). Pressure-Dependent Natural-Fracture Permeability in Shale and Its Effect on Shale-Gas Well Production. Society of Petroleum Engineers. doi:10.2118/159801-PA

Dahi Taleghani. A., and Olson, J.E., How Natural Fractures Could Affect Hydraulic Fracture Geometry, Paper SPE 167608 published in SPE Journal, August 2013.

Dahi Taleghani. A., and Olson, J.E., How Natural Fractures Could Affect Hydraulic Fracture Geometry, Paper SPE 167608 published in SPE Journal, August 2013.

Dahi Taleghani, A., Olson, J.E., and Wang, W., 2013, Thermal Reactivation of Microfractures and its Potential Impact on Hydraulic Fractures Efficiency, Paper SPE 163872 presented in the SPE Hydraulic Fracturing Technology Conference, The Woodlands, Texas.

Dahi Taleghani. A., and Olson, J.E., 2013, How Natural Fractures Could Affect Hydraulic Fracture Geometry, Paper SPE 167608 published in SPE Journal, August 2013.

Dahi Taleghani, A., and Olson, J.E., 2011, Numerical Modeling of Multi-Stranded Hydraulic Fracture Propagation: Accounting for the Interaction Between Induced and Natural Fractures, paper SPE 124884 presented at the SPE Annual Technical Conference and Exhibition, New Orleans, LA, USA

David, C., 2013, Environmental Regulation of Hydraulic Fracturing in Queensland, paper 166146 presented at SPE Annual Technical Conference and Exhibition, New Orleans, Louisiana.

Dean, R. H., & Lo, L. L.,1988, Simulations of Naturally Fractured Reservoirs. Society of Petroleum Engineers. doi:10.2118/14110-PA

Economides, M.J., and Nolte, K.G., 2000, Reservoir Stimulation, John Wiley & Sons Publishing, New York City, New York.

Engelder, T., and Lacazette, A., 1990, Natural Hydraulic Fracturing, Barton, N., and Stephansson, O., eds., Rock Joints, A.A. Balkema, Rotterdam, p.35-44

Fan, L., Martin, R. B., Thompson, J. W., Atwood, K., Robinson, J. R., and Lindsay, G. J., 2011, An Integrated Approach for Understanding Oil and Gas Reserves Potential in Eagle Ford Shale Formation. Society of Petroleum Engineers. doi:10.2118/148751-MS

Fisher, M. K., Heinze, J. R., Harris, C. D., Davidson, B. M., Wright, C. A., & Dunn, K. P. (2004, January 1). Optimizing Horizontal Completion Techniques in the Barnett Shale Using Microseismic Fracture Mapping. Society of Petroleum Engineers. doi:10.2118/90051-MS

Flagg, A.H., Myers, J.P., Campbell, J.L., Terry, J.M., and Mardock, E.S., 1955, Radioactive Tracers in Oil Production Problems, paper SPE 424-G presented at Petroleum Branch Fall Meeting, San Antonio, Texas.

Friedman. M., and McKiernan, D.E., 1995, Extrapolation of Fracture Data from Outcrops of the Austin Chalk in Texas to corresponding Petroleum Reservoirs at Depth, the Journal of Canadian Petroleum Technology, Volume 34, No.8 pp 43-49, October 1995.

Friedrich, M., & Milliken, M. (2013, August 12). Determining the Contributing Reservoir Volume from Hydraulically Fractured Horizontal Wells in the Wolfcamp Formation in the Midland Basin. Society of Petroleum Engineers. doi:10.1190/URTEC2013-149

Garcia, A., and Mohaghegh, S.D., 2004, Forecasting US Natural Gas Production into year 2020: a Comparative Study, paper 91413 presented at SPE Eastern Regional Conference and Exhibition, Charleston, West Virgina.

Gidley, J.L., Holditch, S.A., Nierode, D.E., and Veatch, R.W., 1990, Recent Advances in Hydraulic Fracturing, p.138 of SPE Monograph Vol.12, Society of Petroleum Engineers, Richardson, Texas.

Gomaa, A.M., Qu, Q., Maharidge, R., Nelson, S., and Reed, T., 2014, New Insights into Hydraulic Fracturing of Shale Formations, paper IPTC 17594 presented at International Petroleum Technology Conference, Doha, Qatar.

Grebe, J.J., and Stoesser, M., 1935. Increasing Crude Production 20,000,000 bbl from Established Fields, page 47382 presented in World Petroleum Journal, August 1935.

Griffith, A. A. (1921), "The phenomena of rupture and flow in solids",Philosophical Transactions of the Royal Society of London, A 221: 163–198,doi:10.1098/rsta.1921.0006.

Heffer, K.J., and Bevan, T.G., 1990, Scaling Relationship in Natural Fractures: Data, Theory, and Application, Paper SPE 20981 presented at Europec 90, the Hague, Netherlands,1990.

Hopkins, C. W., Frantz, J. H., Hill, D. G., & Zamora, F. (1995, January 1). Estimating Fracture Geometry in the Naturally Fractured Antrim Shale. Society of Petroleum Engineers. doi:10.2118/30483-MS

Hons, M., Stewart, R., Lawton, D., and Bertram, M., 2007, Ground Motion Through Geophones And MEMS Accelerometers: Sensor Comparison In Theory, Modeling and Field Data, paper 2007-0011 presented at SEG Annual Meeting, San Antonio, Texas

Huang, J., Griffiths, D. V., & Wong, S.-W. (2011, March 1). Characterizing Natural-Fracture Permeability From Mud-Loss Data. Society of Petroleum Engineers. doi:10.2118/139592-PA

Hubbert, M.K., and Willis, D.G., 1957, Mechanics of Hydraulic Fracturing, Paper T.P.4597, Vol. 210 of AIME Petroleum Transactions presented at AIME Petroleum Branch Fall Meeting, Los Angeles, California.

Hulsey, B.J., Cornette, B., and Pratt, D., 2010, Surface Microseismic Mapping Reveals Details of the Marcellus Shale, paper 138806 presented at SPE Eastern Regional Meeting, Morgantown, West Virginia.

James, A.V.G., 1920, Factors Producing Columnar Structure in Lavas and its Occurrence near Melbourne, Australia, Journal of Geology, v. 28, p. 458 – 469

Kelldorf, W.N., 1970, Radioactive Tracer Surveying: A Comprehensive Report, paper SPE 2413 in Journal of Petroleum Technology Issue 06, Vol. 22, pp 661-669.

Kumar, T.A.,Majors,P., and Rossen, W.,1997, Measurement of Aperture and Multiphase Flow in Fractures with NMR Logging, SPE Journal of Formation Evaluation, June 1997.

Lamont, N., and Jessen, F., 1963, The Effect of Existing Fractures in Rocks on the Extension of Hydraulic Fractures, JPT 203-209, February 1963.

Langenbruch, C., & Shapiro, S. A. (2014, October 29). Probability of Brittle Rock Failure During Hydraulic Fracturing of Conventional and Unconventional Reservoirs. Society of Exploration Geophysicists.

Laubach, S.E., Olson, J.E., and Gale, J.F.W., 2004, Are Open Fractures Necessarily Aligned with Maximum Horizontal Stress? Journal of Earth and Planetary Science Letters, February 2004.

Ma, X., Plaksina, T., & Gildin, E. (2013, August 12). Optimization of Placement of Hydraulic Fracture Stages in Horizontal Wells Drilled in Shale Gas Reservoirs. Society of Petroleum Engineers. doi:10.1190/URTEC2013-151

Marrett, R., O.J. Ortega, and C.M.Kelsey, 1999, Extent of Power-law Scaling for Natural Fractures in Rocks, Geology 27(9):799-802.

Miller, B. A., Paneitz, J. M., Mullen, M. J., Meijs, R., Tunstall, K. M., & Garcia, M. (2008, January 1). The Successful Application of a Compartmental Completion Technique Used To Isolate Multiple Hydraulic-Fracture Treatments in Horizontal Bakken Shale Wells in North Dakota. Society of Petroleum Engineers. doi:10.2118/116469-MS

Montgomery, C.T., and Smith, M.B., 2010, Hydraulic Fracturing: History of an Enduring Technology, SPE Journal of Petroleum Technology, December 2010.

Nelson, R.A., 2001, Geologic Analysis of Naturally Fractured Reservoirs.

Nolte, K.G., and Smith, M.B., 1981, Interpretation of Fracturing Pressures, paper SPE 8297 in Journal of Petroleum Technology Issue 09, Vol. 33, pp 1767-1775.

Odling, N. E., Network properties of a two-dimensional fracture pattern, Pure Appl. Geophys., 138, 95–114, 1992.

Olson, J., and Pollard, D. D. (1988, January 1). Inferring Stresstates From Detailed Joint Geometry. American Rock Mechanics Association.

Olson, J.E., 1993, Joint pattern development: effect of subcritical crack growth and mechanical crack interaction, Journal of geophysical research, 98, pages: 12251-12265.

Olson,J.E.,2003, Sublinear scaling of fracture aperture versus length: An exception or the rule?, Journal of Geophysical Research, VOL. 108, NO. B9, 2413, doi:10.1029/2001JB000419.

Papazis, P. K., 2005, Petrographic characterization of the Barnett Shale, Fort Worth Basin, Texas: M.S. thesis, University of Texas at Austin, Austin, Texas, 142 p. and appendices

Patel, H., Johanning, J., and Fry, M., 2013, Borehole Microseismic, Completion and Production Data Analysis to Determine Future Wellbore Placement, Spacing and Vertical Connectivity, Eagle Ford Shale, South Texas, Paper SPE 168875 presented in Unconventional Resources Technology Conference, 12-14 August 2013, Denver, Colorado, USA

Pollard, D.D., and Aydin, A., 1988, Progress in Understanding Jointing Over the Past Century, Geological Society of America Bulletin v.100, p.1181-1204.

Pommer, L., Gale, J. F. W., Eichhubl, P., Fall, A., & Laubach, S. E., 2013, Using Structural Digenesis to Infer the Timing of Natural Fractures in the Marcellus Shale. Society of Petroleum Engineers. doi:10.1190/URTEC2013-167

Pongratz, R., Kuvshinov, I.K., and Latkin, K.E., 2008, Evolution of Hydraulic Fracturing in Russia, paper SPE 114876 presented at SPE Russian Oil and Gas Technical Conference and Exhibition, Moscow, Russia

Price, N., 1959, Mechanics of Jointing in Rocks, Geology Magazine, v. 96, p. 149 – 167.

Priest, S. D., and J. A. Hudson, Estimation of discontinuity spacing and trace length using scanline surveys, Int. J. Rock Mech. Min. Sci. Geomech. Abstr., 18, 183–197, 1981.

Rouleau, A., and J. E. Gale, Statistical characterization of the fracture system in the Stripa granite, Sweden, Int. J. Rock Mech. Min. Sci. Geomech. Abstr., 22, 353–367, 1985.

Shah, K., Shelley, R. F., Gusain, D., Lehman, L. V., Mohammadnejad, A., & Conway, M. T. (2013, February 4). Development of the Brittle Shale Fracture Network Model. Society of Petroleum Engineers. doi:10.2118/163829-MS

Sheldon, P., 1912, Some Observations and Experiments on Joint Planes, Journal of Geology, v. 20, p. 53 – 79, 164 – 183.

Smith, M. B. (2006, January 1). Hydraulic Fracturing: "THE" Multidisciplinary Technology. Society of Petroleum Engineers.

Stearns, D.W., and Friedman, M., 1972, Reservoirs in Fractured Rocks: Geologic Exploration Methods , American Association of Petroleum Geology, 16, 82 – 106.

Tinker, S.J., Baycroft, P.D., Ellis, R.C., and Fitzhugh, E., 1997, Mini-Frac Tests and Bottomhole Treating Pressure Analysis Improve Design and Execution of Fracture Stimulations, paper SPE 37431 presented at SPE Production Operations Symposium, Oklahoma City, Oklahoma

Thornton, M., and Eisner, L., 2011, Uncertainty in Surface Microseismic Mapping, paper 2011-1524 presented at SEG Annual Meeting, San Antonio, Texas.

U.S Environmental Protection Agency, http://www.epa.gov

Valko, P. P., & Economides, M. J. (1999, May 1). Fluid-Leakoff Delineation in High-Permeability Fracturing. Society of Petroleum Engineers. doi:10.2118/56135-PA

Valencia, K. J. L., Chen, Z., Hodge, M. O., and Rahman, S. S., 2005, Optimizing Stimulation of Coalbed Methane Reservoir Using Multi-Stage Hydraulic Fracturing Treatment and Integrated Fracture Modeling.paper 93245 presented at SPE Asia Pacific Oil and Gas Conference and Exhibition, Jakarta, Indonesia.

Van Hise, C.R., 1896, Principles of North American Pre-Cambrian Geology, U.S. Geological Survey 16th Annual Report, p 581 – 874.

Vermylen, J., and Zoback, M.D., 2011, Hydraulic Fracturing, Microseismic Magnitudes, and Stress Evolution in the Barnett Shale, Texas, USA, paper 140507 presented at SPE Hydraulic Fracturing Technology Conference, The Woodlands, Texas.

Warpinski, N.R., and Teufel, L.W., 1987, Influence of Geologic Discontinuities on Hydraulic Fracture Propagation, SPE Journal of Petroleum Technology, Volume 39, Number 2, February 1987.

Warpinski, N., Kramm, R. C., Heinze, J. R., & Waltman, C. K. (2005, January 1). Comparison of Single-and Dual-Array Microseismic Mapping Techniques in the Barnett Shale. Society of Petroleum Engineers. doi:10.2118/95568-MS

Williams, B.B., and Nierode, D.E., 1972, Design of Acid Fracturing Treatments, SPE paper 3720 in Journal of Petroleum Technology Issue 07, Vol. 24, pp 849 – 859.

Wiliams, R.L., and McCarthy, J.T., 1987, Using Multiple Radioactive Tracers to Optimize Stimulation Designs, paper SPE 16383 presented at SPE California Regional Meeting, Ventura, California

Woodworth, J.B., 1896, On the Fracture System of Joints with Remarks on Certain Great Fractures, Boston Society of Natural Historical Proceedings, v. 27, p. 163 – 183.

Zhao, G. (2013, November 5). Modeling Complex Natural Fracture Network in Heterogeneous Tight Formations Using Semi-Analytical Strategy. Society of Petroleum Engineers. doi:10.2118/167127-MS

Vita

Ping Puyang was from Haikou, Hainan province of the People's Republic of China. He attended the Westbrook-Walnut Grove Senior High School in Westbrook, MN in 2005 as an exchange student nominated by the Ministry of Education of the People's Republic of China, and this experience motivated him to pursue higher education in United States. He returned to U.S. in 2008 with a full tuition-waiver scholarship to attend the Louisiana State University, and finished his bachelor's degree in Petroleum Engineering with Latin honor in May, 2012. He continued to the graduate program at LSU with the same major, focused his research on hydraulic fracturing in naturally fractured reservoirs, and is expected to receive his degree in May, 2015.